AWARD NUMBER: W81XWH-18-1-0160

TITLE: Dual PET/Fluorescence Imaging of Glioma with an MMP-14-Activatable Peptide Probe

PRINCIPAL INVESTIGATOR: Jason Warram, PhD

CONTRACTING ORGANIZATION: University of Alabama, Birmingham, AL

REPORT DATE: June 2022

TYPE OF REPORT: Final

PREPARED FOR: U.S. Army Medical Research and Development Command
Fort Detrick, Maryland 21702-5012

REPORT DOCUMENTATION PAGE

Form Approved
OMB No. 0704-0188

1. REPORT DATE	2. REPORT TYPE	3. DATES COVERED
June 2022	Final	01Sep2018-28Feb2022

4. TITLE AND SUBTITLE

Dual PET/Fluorescence Imaging of Glioma with an MMP-14-Activatable Peptide Probe

5a. CONTRACT NUMBER

5b. GRANT NUMBER
W81XWH-18-1-0160

5c. PROGRAM ELEMENT NUMBER

6. AUTHOR(S)
Jason Warram, PhD

E-Mail:

5d. PROJECT NUMBER

5e. TASK NUMBER

5f. WORK UNIT NUMBER

7. PERFORMING ORGANIZATION NAME(S) AND ADDRESS(ES)

University of Alabama at Birmingham
AB1170
1720 2nd Avenue South
Birmingham, AL 35294-0111

Stanford University
1201 Welch Road
Stanford, CA 94305-2004

8. PERFORMING ORGANIZATION REPORT NUMBER

9. SPONSORING / MONITORING AGENCY NAME(S) AND ADDRESS(ES)

U.S. Army Medical Research and Development Command
Fort Detrick, Maryland 21702-5012

10. SPONSOR/MONITOR'S ACRONYM(S)

11. SPONSOR/MONITOR'S REPORT NUMBER(S)

12. DISTRIBUTION / AVAILABILITY STATEMENT

Approved for Public Release; Distribution Unlimited

13. SUPPLEMENTARY NOTES

14. ABSTRACT

The purpose of the project is to develop and test, in preclinical models, a sensitive, specific imaging peptide probe to distinguish GBM tissue from healthy tissue. The novel imaging probe targets a cell-surface marker, matrix metalloproteinase 14 (MMP-14) that is expressed to a much greater degree in GBM cells than in healthy cells. Upon binding to MMP-14, a dual-modality fluorescent tag is activated. This tag is detectable by positron emission tomography (PET) for pre-operative tumor assessment, and by near infrared fluorescence (NIRF) imaging for real-time surgical guidance in distinguishing tumor cells from healthy cells. Results from the project indicate that GBM cells with MMP-14 activity showed activation and retention of NIRF signal from the cleaved peptide probes. Resected mouse brains with patient derived xenograft (PDX) GBM tumors showed tumor-tobackground NIRF ratios of 7.6-11.1 at 4 h after *i.v.* injection of the peptides. PET images showed localization of activity in orthotopic PDX tumors after *i.v.* injection of radiolabeled peptide probes; uptake of the radiolabeled probes in tumors was significantly reduced ($p<0.05$) by blocking with the non-labeled peptide. PET and NIRF signals correlated linearly in the orthotopic PDX tumors. Immunohistochemistry showed co-localization of MMP-14 expression and NIRF signal in the resected tumors.

15. SUBJECT TERMS
Glioma, GBM, molecular imaging, peptide, PET, NIRF, preclinical, MMP-14 dual modality

16. SECURITY CLASSIFICATION OF:			17. LIMITATION OF ABSTRACT	18. NUMBER OF PAGES	19a. NAME OF RESPONSIBLE PERSON
a. REPORT	b. ABSTRACT	c. THIS PAGE			USAMRDC
Unclassified	Unclassified	Unclassified	Unclassified	51	19b. TELEPHONE NUMBER *(include area code)*

TABLE OF CONTENTS

1. **INTRODUCTION:** Malignant glioma (GBM) is the most common brain tumor that occurs in adults, yet the 5-year survival rate is only 5%, with the majority of patients surviving less than 14 months after diagnosis. It is a rapidly growing, aggressive tumor that grows diffusely into neighboring areas of the brain. Exposure to ionizing radiation is the main external risk factor associated with GBM, and individuals exposed to nuclear weapons testing or other types of ionizing radiation are at an increased risk of developing GBM compared to the general population. There are known survival benefits associated with surgical removal of the GBM tumor. However, the diffuse growth of the tumor makes it difficult for a surgeon to clearly distinguish tumor cells from adjacent, healthy cells. As a result, GBM cells remain in the brain post-surgery, leading to tumor recurrence and the death of the patient. Therefore, there is an urgent need for novel tools that improve tumor detection and the prognosis for individuals diagnosed with GBM. The purpose of the project is to develop and test, in preclinical models, an imaging probe that is both sensitive and specific in distinguishing GBM tissue from healthy tissue. The novel imaging probe will target a cell-surface marker, matrix metalloproteinase 14 (MMP-14) that is expressed to a much greater degree in GBM cells than in healthy cells. Upon binding to its target, a dual-modality fluorescent tag will be activated. This tag will be both detectable by positron emission tomography (PET) to allow for pre-operative assessment of tumor burden and localization, and by near infrared fluorescence (NIRF) imaging to allow for real-time surgical guidance in distinguishing tumor cells from healthy cells. Once developed, the use of this probe will be validated in mouse models of GBM to determine *in vivo* pharmacokinetics, biodistribution, signal retention, sensitivity, and specificity for imaging the GBM tumors. The successful development of this innovative tool will provide a crucial foundation to address a critical gap in managing GBM patient care.

2. **KEYWORDS:** Glioma, GBM, molecular imaging, peptide, PET, NIRF, preclinical, MMP-14, dual modality

3. **ACCOMPLISHMENTS:**

   - **What were the major goals of the project?**

Specific Aim 1: Design and characterize an MMP-14 activatable dual PET/NIRF peptide probe.
Major goal 1: Develop novel MMP-14 activatable peptide probes.
Milestone achieved: Identification of initial candidate MMP-14 peptide probes at Stanford and shipment to UAB.
Target completion from SOW: February 2019
Actual completion date: Prior to July 2018

Specific Aim 2: Establish the sensitivity and specificity of the MMP-14 activatable dual PET/NIRF peptide probe for in vivo imaging of GBM models.
Major goal 2: Perform in vivo studies (using the peptides in mice with GBM tumors) to identify a lead peptide probe.
Milestone to achieve: Identify a lead substrate-peptide conjugate for further in vivo studies. Criteria for identification will be: candidate with highest tumor uptake with lowest background tissue accumulation.
Target completion from SOW: August 31, 2019
Percentage of completion as of August 1, 2021: 90%

Major goal 3: Determine the optimal dose and imaging time points for *in vivo* imaging with the lead peptide probe, with corresponding sensitivity and specificity metrics.
Milestone to achieve: Identification of optimal dose and imaging time point for the lead peptide probe.
Target completion from SOW: November 31, 2019
Percentage of completion as of August 1, 2021: 50%

Milestone to achieve: Sensitivity, specificity, PPV (positive predictive value), NPV (negative predictive value) of lead peptide probe determined.
Target completion from SOW: December 31, 2019
Percentage of completion as of August 1, 2021: 70%

Major goal 4: Test lead peptide probe in a panel of GBM models *in vivo.*
Milestone to achieve: Global sensitivity, specificity, PPV, NPV of lead peptide probe determined across multiple PDX models.
Target completion from SOW: June 30, 2020
Percentage of completion as of August 1, 2021: 25%

Milestone to achieve: Submit additional extramural research proposals (DOD, NIH) for subsequent stages of investigation (surgical resection in mice with PDX tumors).
Target completion from SOW: August 31, 2020
Percentage of completion as of August 1, 2021: 25%

- **What was accomplished under these goals?**

New accomplishments since the prior reporting period:

Major activity: Dr. Jianghong Rao at Stanford has synthesized and characterized additional, novel MMP-14 activatable peptide and binding peptide probes for the project. The objective is to utilize the same core peptide sequence and components for NIRF and PET imaging as the initial lead peptide constructs, while using a different linker component for incorporating the metal-binding chelate NOTA (used for radiolabeling). Methods have included a combination of solid phase peptide synthesis and solution phase chemistry to produce the peptides, followed by standard chemical characterization techniques (high performance liquid chromatography and mass spectrometry). Radiolabeling experiments with ^{64}Cu to generate the peptides for PET imaging have been performed. Major accomplishments: The synthesis route and linker, formed by a thiol-cyanobenzothiazole reaction, allows the chelate to be joined to the peptide after the Cu-mediated cycloaddition reaction between the azide and alkyne moieties present on the separate binding and substrate peptides. These new peptides and method of production avoid potential binding of Cu ions to the chelate during the cycloaddition reaction to form the final MMP-14 peptide probe. Characterization of the products indicate successful production of the desired peptides (Figures AA and AB below). The new ^{64}Cu-labeled MMP-14 activatable+binding peptide product has been obtained in produced at >99% radiochemical purity as determined by radioactive HPLC (Figure AC below). The new ^{64}Cu-labeled binding peptide has also been produced at very low peptide concentrations (less than $1x10^{-7}$ M peptide concentration in the labeling reaction) during initial radiolabeling studies.
Key outcome achieved: additional, novel MMP-14 peptide probes have been successfully produced to fulfill Major Goal 1 above.

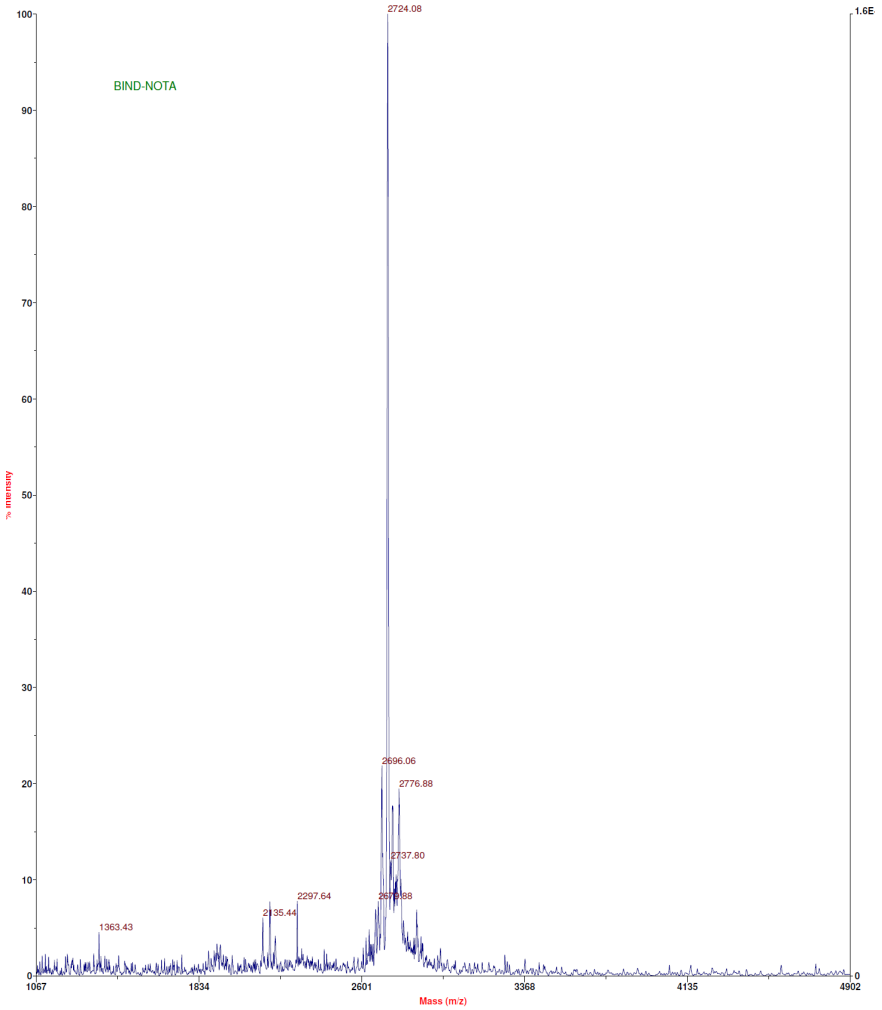

Figure AA. Mass spectrometry characterization of the novel binding peptide. Anticipated mass: 2719.2 m/z; observed mass: 2724.1 m/z

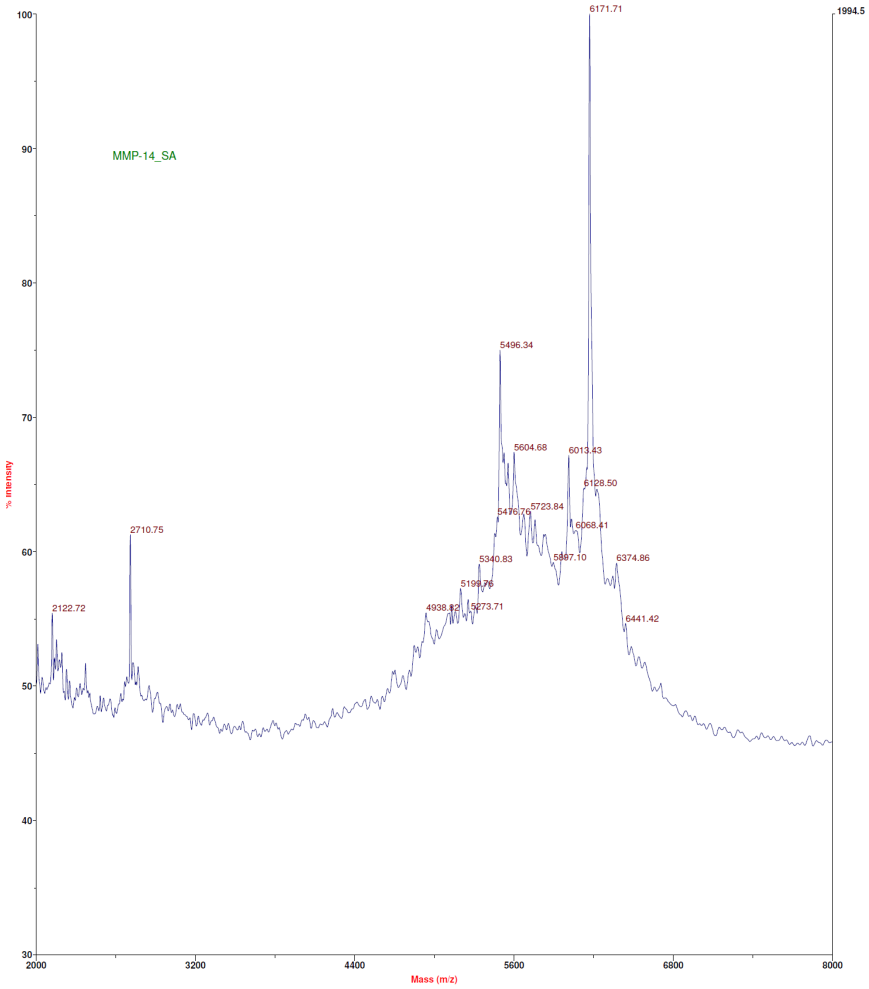

Figure AB. Mass spectrometry characterization of the novel MMP-14 peptide. Anticipated mass: 6171.3 m/z; observed mass: 6171.7 m/z.

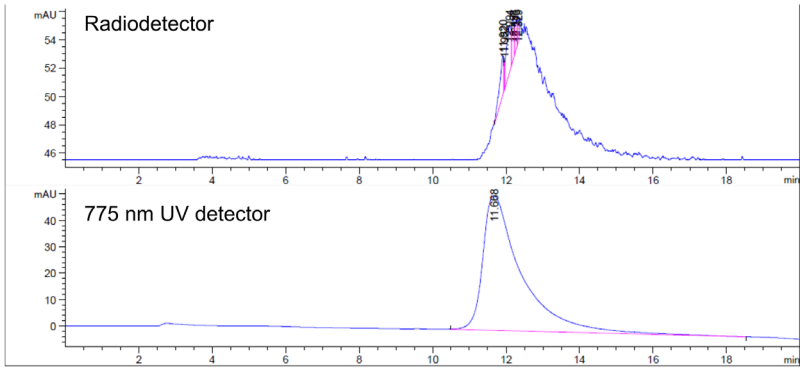

Figure AC. Radiodetector and UV detector HPLC characterization of the novel ^{64}Cu-labeled MMP-14 peptide.

Major activity: Characterized MMP-14 expression and activity in several patient derived xenograft (PDX) glioma tumor models. The objective was to validate the overexpression, relative expression levels, and activity of MMP-14 in glioma tumor models that mimic the characteristics of human glioma. This information is essential to select tumor models that have varying levels of active MMP-14 for studies in Major goal 4 of the project (testing the peptide probes in a panel of GBM models *in vivo*. Methods included Western blot analyses of MMP-14 expression in lysates from PDX GBM tumor lines passaged in athymic mice; and gel zymography analyses of MMP-2 activity in lysates from PDX GBM tumor lines passaged in athymic mice. Major results: Western blot analyses indicated human PDX GBM tumor lines passaged in athymic mice show varying levels of MMP-14 based on the tumor line (Figure AD below). Similarly, activity of MMP-14 as derived from the amount of active MMP-2 in tumor lysates varies across different PDX GBM tumors, where the tumors show measurable amounts of enzyme activity (Figure AE below). Candidate models with “high” and “low” levels of MMP-14 activity have been identified for use in future studies.

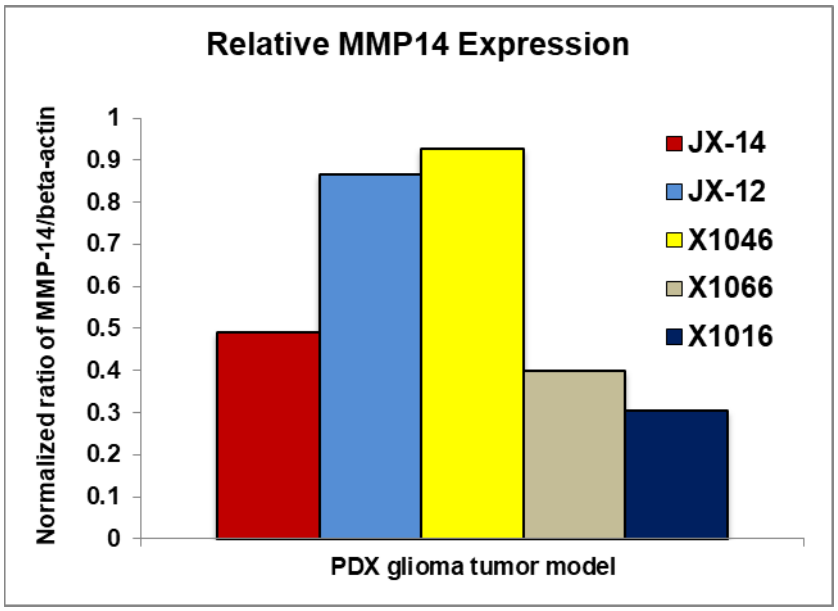

Figure AD. Quantified respective blot intensities (determined by Western blot) of MMP-14 relative to beta-actin from lysates of PDX glioma tumors grown in mice.

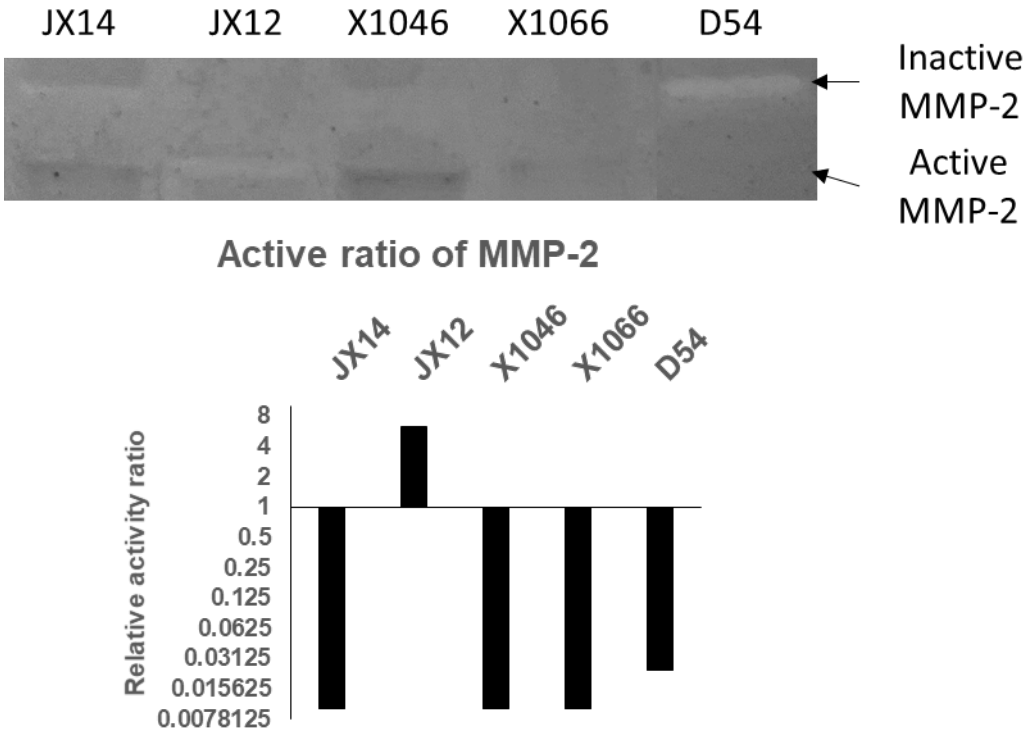

Figure AE. MMP-2 gel zymography (top) and quantification of relative active/latent band intensity (bottom, shown in logarithmic scale) of lysates of PDX glioma tumors grown in mice (JX14, JX12, X1046, X1066) and adherent GBM cells grown in vitro (D54).

Major activity: Fluorescence imaging with 5-ALA and an alternative NIRF imaging agent was performed in mice bearing orthotopic PDX GBM tumors. The objective is to utilize established imaging agents to validate imaging and quantitative measurement techniques for use in the planned studies with the MMP-14 peptide probes, in direct comparison to the FDA approved imaging agent 5-ALA. Methods have included fluorescence imaging studies performed in mouse tissues resected after i.v. injection of 5-ALA or IRDye800-labeled anti-EGFR antibody in mice with orthotopic (intracranial) PDX) GBM tumors; immunohistochemical analyses of target protein expression in the resected tumor tissues; and quantitative comparison of accuracy for the imaging agents. The spatial overlap, imaging intensity, sensitivity, and specificity of the respective fluorescence signals were compared to determine tumor-to-background

ratios in regions of the tumor and normal brain that are relevant to clinical surgical resection techniques in human patients. Major results: As shown in our recent *Mol Cancer Ther* publication Figure 1 (see appendix), fluorescence signals of imaging agents varies based on location within and adjacent to the tumor. Our quantified measurements indicate that fluorescence tumor-to-background (TBR) ratios in the PDX GBM tumor core and margins are significantly higher for the NIRF imaging agent relative to the clinically approved imaging agent 5-ALA (appendix Figures 2, 3, and 4 from *Mol Cancer Ther* 2020;19:1922–9 publication). Mice that received both 5-ALA and the IRDye800-labeled antibody showed a core tumor TBR of 8.11 ± 1.489 and 51. 46 ± 25.30 for 5-ALA and the IRDye800 signals, respectively, while the tumor margin TBR was 7.32 ± 1.66 and 32.77 ± 19.79 for the 5-ALA and IRDye800-antibody signals, respectively (appendix Figure 5C from *Mol Cancer Ther* 2020;19:1922–9 publication). There was a higher variation, as determined by the imaging signal standard deviation, for 5-ALA relative to the IRDye800-antibody signal in the tumor core and margin regions of the tissues (appendix Figure 6A from *Mol Cancer Ther* 2020;19:1922–9 publication). Both 5-ALA and IRDye800-antibody signals had 100% sensitivity for detecting tumor core and margin relative to normal background tissue, although the specificity and area under the curve (AUC) values were significantly higher for IRDye800-antibody signals relative to 5-ALA (appendix Figure 6B,C and Table 2 from *Mol Cancer Ther* 2020;19:1922–9 publication). These results support the rationale for targeted molecular NIRF imaging of GBM.

The following accomplishments were part of the prior reporting period:

Major activity: Dr. Jianghong Rao at Stanford has been synthesizing and characterizing the novel MMP-14 activatable peptide probes for the project. The objective is to produce MMP-14 activatable peptide probes that could be used for both NIRF and PET imaging of MMP-14 activity and expression (see Figure 1 of the attached manuscript, *Eur J Nucl Med Mol Imaging* (2020) 47:1412–1426, in the appendix). Methods have included a combination of solid phase peptide synthesis and solution phase chemistry to produce the peptides, followed by standard chemical characterization techniques (high performance liquid chromatography and mass spectrometry). Major accomplishments: As shown in Supplementary Figures S2, S3, S4, S5, S6, and S7 (see attached Supplementary Material in the appendix, for manuscript *Eur J Nucl Med Mol Imaging* (2020) 47:1412–1426), their work has generated an MMP-14 activatable "substrate peptide" that can be used for NIRF imaging, an MMP-14 "binding peptide" that can be used for PET imaging, and a "substrate-binding peptide" (a covalently joined construct of the substrate and binding peptide moieties) that can be used for both NIRF and PET imaging. These peptides have been sent to Dr. Jason Warram at UAB and used in the following in vitro and in vivo experiments.

Key outcome achieved: an initial series of novel, MMP-14 peptide probes has been successfully produced to fulfill Major Goal 1 above.

Major activity: Characterized MMP-14 expression and activity in several human glioma tumor tissues and cells lines. The objective was to validate the overexpression of MMP-14 in glioma and glioma cell lines that would be suitable in assays that employ peptide probes as enzymatic substrates for MMP-14. Methods have included immunofluorescence staining of a human glioma tissue microarray, GBM cell lines cultured in vitro, and GBM tumor xenografts grown in athymic nude mice in vivo; Western blot analyses of MMP-14 and MMP-2 expression in GBM cell lines cultured in vitro; and gel zymography analyses of soluble MMP-2 activity of GBM cell lines cultured in vitro. Major results: Human glioma tissues, GBM xenografts, and GBM cell lines express MMP-14 on the cell surface, and expression levels are significantly higher in GBM tissues relative to normal brain tissue ($p<0.05$). Different GBM cell lines display different levels of MMP-14 expression and activity (see Figure 2 of the attached manuscript, *Eur J Nucl Med Mol Imaging* (2020) 47:1412–1426, in the appendix, and Supplementary Figure S1 of the attached Supplementary Material in the appendix), and are suitable for assays with novel MMP-14 peptide probes.

Major activity: Determine peptide probe binding, cleavage, and NIRF signal activation in vitro with MMP-14 enzyme, GBM cell lines. The objective is to determine that the novel peptides are substrates for MMP-14 to activate the NIRF signal, and that GBM cells show retention of the NIRF and PET signals from the peptides. Methods have included NIRF activation and microscopy studies using the peptides and recombinant MMP-14 enzyme or GBM cell lines cultured in vitro, and binding assays with the radiolabeled binding peptide or substrate-binding peptide and GBM cell lines cultured as adherent monolayers in vitro. Major results: Both the substrate peptide and substrate-binding peptides showed NIRF signal activation within the first several minutes and up to 2 h after incubation with MMP-14 enzyme or with GBM cells. GBM cells incubated for 4 h with the substrate-binding peptide showed significantly more cell-associated NIRF signal than cells incubated for 4 h with the substrate peptide ($p<0.05$) (see Figure 3 of the attached manuscript, *Eur J Nucl Med Mol Imaging* (2020) 47:1412–1426, in the appendix). These results are consistent with the anticipated mechanism of the substrate-binding peptide, where the MMP-14 binding moiety mediates cellular retention of the residual fluorophore-containing product following cleavage of the substrate sequence by MMP-14. Ongoing studies with the peptides are being performed to determine the enzyme selectivity and kinetics of peptide cleavage in the presence of MMP inhibitors. Cell binding studies showed that the radiolabeled ^{64}Cu-binding peptide binds to GBM cells cultured in vitro, with increased cell-associated activity present at 2 h than at 30 min (Figure A). As expected, lower activity was associated with the cells when the non-labeled binding peptide was used to block MMP-14 binding sites. Separate studies showed that the radiolabeled ^{64}Cu-substrate-binding peptide also bound to GBM cells cultured in vitro in a temperature-dependent manner, where more activity was present following incubation at 37 °C relative to 4 °C (Figure B). This result is consistent with internalization of the radiolabeled peptide after binding to MMP-14 on the cell surface. Ongoing studies with the radiolabeled peptides are being performed to determine the affinities and further define the specific binding of the peptides to MMP-14 on GBM cells cultured in vitro.

Key outcomes achieved: MMP-14 and human GBM cells are capable of cleaving the novel peptide substrates in vitro to activate the NIRF signal. The cell-associated NIRF and PET signals from the peptides indicate that the peptides bind to the GBM cell lines.

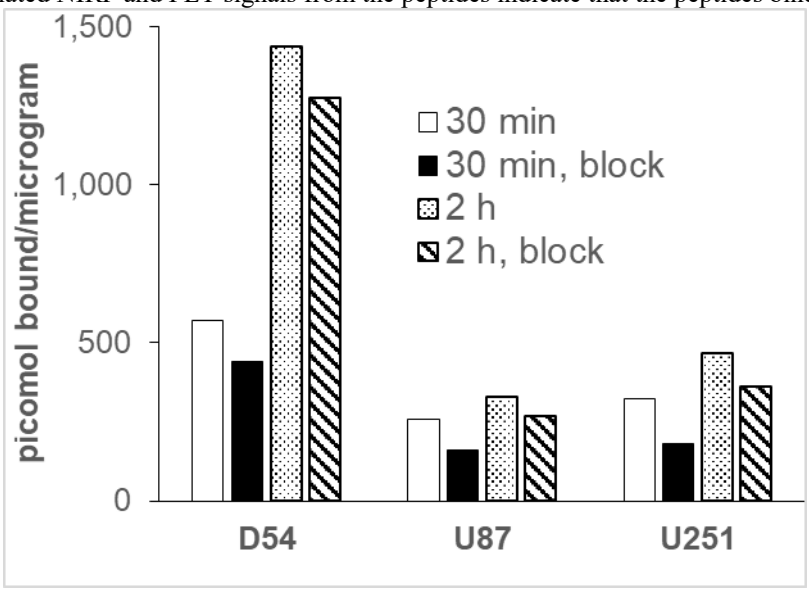

Figure A. Radiolabeled binding peptide binds to human GBM cells in vitro. Adherent GBM cells in 24-well plates (0.4 million cells/well) were incubated at 37 °C for 30 min or 2 h with 46 nM ^{64}Cu-binding peptide. Excess non-labeled binding peptide (1 μM) was added as a block to selected wells. Following incubation, cells were rinsed with PBS and lysed with 1 M NaOH, and the solution was counted on a gamma counter to calculate the cell-associated ^{64}Cu-binding peptide signal, expressed as picomol bound per microgram of protein present in the lysed cell solution.

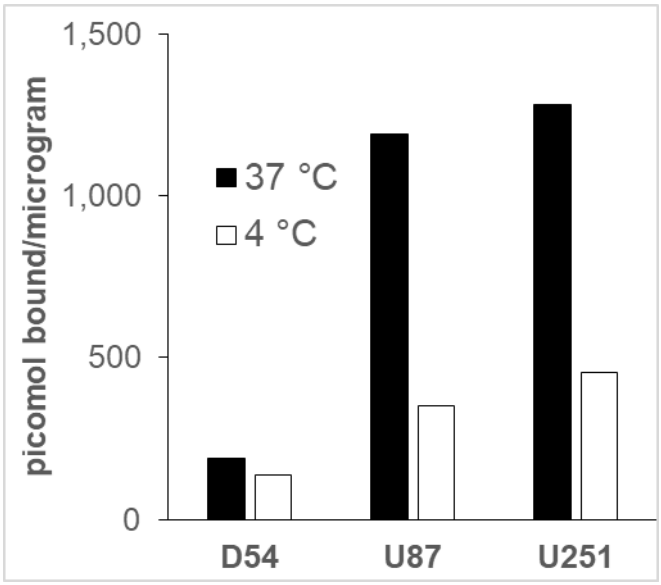

Figure B. Radiolabeled substrate-binding peptide binds to human GBM cells in vitro. GBM cells in suspension (0.5 million cells/tube) were incubated at 37 °C or 4 °C for 10 h with 20 nM ^{64}Cu-substrate-binding peptide. Following incubation, cells were rinsed with PBS, then cell surface-bound activity was collected by rinsing the cells with pH 4 buffer for 10 min. The cells were then lysed with 1 M NaOH, and the collected solutions were counted on a gamma counter to calculate the cell-associated ^{64}Cu-substrate-binding peptide signal, expressed as picomol bound per microgram of protein present in the collected solutions.

Major activity: Perform NIRF imaging and PET/CT pharmacokinetic and biodistribution studies with the first candidate substrate, binding, and substrate-binding peptide probes in mice with orthotopic PDX GBM tumors (one xenoline). The objective is to characterize the GBM xenograft tumor uptake, specificity and pharmacology of the imaging candidates in mice. Methods have included NIRF imaging studies performed 1-24 h after i.v. injection of the peptides in mice with subcutaneous (s.c.) flank xenografts of GBM cell lines, or in mice with orthotopic (intracranial) patient-derived xenograft (PDX) GBM tumors. PET/CT imaging and biodistribution studies with the peptides have been performed 1-6 h after i.v. injection of the radiolabeled peptides in mice with orthotopic PDX GBM tumors. Major results: At 24 h after *i.v.* injection of the substrate-binding peptide, *in vivo* NIRF imaging showed a low tumor-to-background ratio (TBR, 1.3±0.2 relative to muscle) in s.c. D54 tumors and significantly higher TBR in s.c. U87 tumors (2.2±0.4; $p<0.001$) (see Figure 4A,B of the attached manuscript, *Eur J Nucl Med Mol Imaging* (2020) 47:1412–1426, in the appendix). Low NIRF signal was observed in all normal tissues except the kidneys, indicating predominantly renal clearance of

the peptide. Subcutaneous U87 tumors from groups of mice injected *i.v.* with either the substrate peptide or the substrate-binding peptide showed no significant difference in TBR or mean NIRF intensity at the 24 h time point (see Supplementary Figure S8 of the attached Supplementary Material in the appendix). These initial studies demonstrated that glioma tumors show uptake of NIRF signal after administering the quenched peptide substrates.

High contrast of the NIRF signal in orthotopic PDX JX12 tumors relative to adjacent normal brain was apparent in gross slices of resected brains at 1, 4, and 24 h after *i.v.* injection of either the substrate peptide (see Figure 4C of the attached manuscript, *Eur J Nucl Med Mol Imaging* (2020) 47:1412–1426, in the appendix) or the substrate-binding peptide (see Figure 4D of the attached manuscript, *Eur J Nucl Med Mol Imaging* (2020) 47:1412–1426, in the appendix). NIRF analyses of gross brain slices from the 4 and 24 h time points (see Table 1 of the attached manuscript, *Eur J Nucl Med Mol Imaging* (2020) 47:1412–1426, in the appendix) showed significantly higher ($p<0.001$) mean NIRF signal in the tumor relative to adjacent normal brain from mice given the substrate-binding peptide. While the NIRF mean tumor signals and TBRs were higher in mice given the substrate-binding peptide relative to the substrate peptide (see Table 1 of the attached manuscript, *Eur J Nucl Med Mol Imaging* (2020) 47:1412–1426, in the appendix), the TBRs were not significantly different at the time points examined ($p>0.05$, ANOVA). NIRF microscopy showed dispersion of the activated NIRF signal from the peptides throughout the tumors, including near the leading edge of tumor progression (see Figure 4C, D of the attached manuscript, *Eur J Nucl Med Mol Imaging* (2020) 47:1412–1426, in the appendix). Both peptides also yielded positive NIRF signals in regions of diffuse glioma cell growth beyond the bulk tumor. Comparing histological tissue sections with confirmed glioma growth by H+E to NIRF signals measured in tissue sections yielded sensitivities above 83% for the substrate peptide and above 85% for the substrate-binding peptide (see Supplementary Table S1 of the attached Supplementary Material in the appendix) at the 4 h and 24 h time points. These results confirmed that the novel MMP-14 peptides could be used for NIRF imaging of orthotopic models of human glioma.

A preliminary study was performed using the binding peptide labeled with ^{68}Ga (^{68}Ga-binding peptide) in mice with orthotopic PDX JX12 tumors. At 2 h after i.v. dosing, the tumors were visible during PET/CT imaging while normal brain showed low uptake of activity (see Figure 5A of the attached manuscript, *Eur J Nucl Med Mol Imaging* (2020) 47:1412–1426, in the appendix). *Ex vivo* biodistribution analyses indicated significantly more uptake of radioactivity in brains of mice injected with ^{68}Ga-binding peptide (0.16±0.02 %ID/g) compared to brains of mice injected with ^{68}Ga-binding peptide and 60-fold excess non-labeled binding peptide as a blocking agent (0.07±0.02 %ID/g, $p<0.01$) (see Figure 5B of the attached manuscript, *Eur J Nucl Med Mol Imaging* (2020) 47:1412–1426, in the appendix), thus supporting the specific retention of the radiolabeled peptide in the PDX tumors. The amount of ^{68}Ga in resected brains correlated with qualitative tumor burden determined by H+E tissue analyses (see Supplementary Figure S10 of the attached Supplementary Material in the appendix). PET images and *ex vivo* biodistribution analyses showed high accumulation of activity in the liver, spleen, and kidneys (see Supplementary Figure S11, S12 of the attached Supplementary Material in the appendix), which was likely due to the relative hydrophobicity of the peptide at physiological pH. A separate cohort of mice bearing orthotopic PDX JX12 tumors were used for PET imaging and biodistribution analyses with ^{64}Cu-labeled substrate-binding peptide (^{64}Cu-substrate-binding peptide). At 4 h after i.v. dosing, PET/CT imaging showed significant contrast in the tumor relative to normal brain (see Figure 5C of the attached manuscript, *Eur J Nucl Med Mol Imaging* (2020) 47:1412–1426, in the appendix), yielding a standardized uptake value ratio (SUVR: ratio of tumor SUV_{mean} to normal brain SUV_{mean}) of 3.9±0.5. The SUVR was lower in a group of tumor-bearing mice (2.5±1.3) that had been co-injected with 80-fold excess of the non-labeled binding peptide as a blocking agent, although the difference between the two groups of mice was not significant ($p=0.056$). The activity present in whole resected brains from mice in the ^{64}Cu-substrate-binding peptide group (0.43±0.13 %ID/g) was significantly higher than that in the blocked group (0.23±0.07 %ID/g; $p<0.05$) (see Figure 5D of the attached manuscript, *Eur J Nucl Med Mol Imaging* (2020) 47:1412–1426, in the appendix). This result suggests that the binding peptide is able to partially block binding of the substrate-binding peptide to PDX glioma tumors *in vivo*. Biodistribution analyses of resected tissues was consistent with the PET images, indicating predominantly hepatobiliary accumulation of activity (see Supplementary Figure S14, S15 of the attached Supplementary Material in the appendix). Future studies planned include pharmacology studies of the radiolabeled substrate-binding peptide from 0-6 h after i.v. injection in mice with orthotopic PDX GBM tumors.

Key outcomes achieved: The first candidate peptide probes show specific localization and favorable retention of the NIRF and PET signals in a human PDX GBM tumor model in vivo.

Major activity: Perform histological and zymography analyses of MMP-14 in resected tumors and brain sections from biodistribution studies. The objective is to correlate MMP-14 target expression and probe signal accumulation. Methods include NIRF imaging, histology, MMP-14 immunofluorescence staining, and gel zymography of resected tissues from orthotopic PDX tumor-bearing mice injected with the radiolabeled peptide probes. Correlations between PET, NIRF, and MMP-14 levels in the tumors will be generated and compared to values obtained from normal tissues. Major results: The resected brains from mice injected with the ^{64}Cu-substrate-binding peptide in the above studies were sectioned and used for NIRF analyses. Gross imaging showed high contrast between the NIRF signal in PDX tumor regions compared to contralateral normal brain, yielding a TBR of 7.2±1.3 ($p<0.001$). The summed NIRF signal from tumor regions in these tissue sections correlated linearly ($R^2=0.84$, $p<0.0001$) with the *in vivo* PET %ID/cm^3 signal present in the tumor-bearing brain regions (see Figure 6A of the attached manuscript, *Eur J Nucl Med Mol Imaging* (2020) 47:1412–1426, in the appendix). Microscopic imaging of hematoxylin and eosin (H+E) stained tissue sections confirmed that the NIRF signal co-localized in the PDX glioma tumors, which showed high expression of MMP-14 relative to normal brain (see Figure 6B-G of the attached manuscript, *Eur J Nucl Med Mol Imaging* (2020) 47:1412–1426, in the appendix). These results support the hypothesis that the NIRF signal from the cleavable peptide was specifically retained in the PDX glioma tumors due to the expression of MMP-14 in the tumors. Future studies will compare tissue MMP activity (as determined by gel zymography) and quantified MMP-14 expression with the PET and activated NIRF signals in the tissues.

Key outcomes achieved: The PET and NIRF signals from the first candidate peptide probes show a positive, linear correlation in

tumor tissues. Signals from the probes show high spatial congruity with MMP-14 expression in tumor tissues. Based on the cumulative results, the initial candidate peptides meet criteria as "lead" probes for the remaining studies.

- **What opportunities for training and professional development has the project provided?**

A graduate student (Logan Stone) has begun working significantly on the project; due to his involvement, he is receiving mentoring in designing and executing multi-modality imaging experiments, NIRF image processing, PET image processing, histological analyses, tumor biology, writing scientific research grants, and manuscript preparation.

The following were included in the last reporting period: Two different postdoctoral scholars (Benjamin Kasten and Hailey Houson) have worked significantly on the project under the mentorship of Dr. Jason Warram and other senior investigators at UAB. Training activities resulting from the project have provided these postdoctoral scholars with greater proficiency in designing and executing multi-modality imaging experiments, NIRF image processing, PET image processing, histological analyses, tumor biology, writing scientific research grants, and manuscript preparation. Their professional development activities have included the opportunity to attend and present at annual scientific conferences (as specified further below). Four different medical students (Aditi Jani, Denzel Cole, Andrew Prince, Neha Udayakumar) completed a 2-4 month mentored scholarly research activity rotation in Dr. Warram's laboratory. Three different undergraduate students (Savannah Ferch, Himani Modi, Morgan Richardson) also participated in directed research activities in Dr. Warram's laboratory as part of their degree credits. These individuals received training in techniques related to the project, including cell assays, histological tissue processing and analyses, and fluorescence imaging.

- **How were the results disseminated to communities of interest?**

Initial results from the project have been disseminated to the scientific research community through presentation at an annual, national meeting (Society of Nuclear Medicine and Molecular Medicine, 2019 Annual Meeting, from prior reporting period), and through publication of a manuscript in a peer-reviewed journal (*Eur J Nucl Med Mol Imaging* (2020) 47:1412–1426, published during the last reporting period).

- **What do you plan to do during the next reporting period to accomplish the goals?**

Planned activity: Perform blood and tissue pharmacokinetic studies with the initial candidate peptide probes in mice with orthotopic PDX GBM tumors. The objective is to determine the in vivo stability of the peptide and to identify optimal time points to perform in vivo NIRF or PET imaging analyses. Anticipated completion date: March 1, 2022.

Originally planned activity: Identification of additional candidate MMP-14 peptide probes at Stanford and shipment to UAB. This originally planned activity may not be pursued in the next reporting period, because the initial candidate peptides meet criteria as "lead" probes for the remaining studies. If further studies (e.g., pharmacology) do not support further development of the initial candidate peptides developed at the current stage of the project, additional candidate peptides will be generated and tested. Anticipated date to decide if this activity will or will not be further pursued: March 1, 2022.

Originally planned activity: NIRF and PET/CT pharmacokinetic and biodistribution studies with additional candidate substrate, binding, and substrate-binding peptide probes in mice with orthotopic PDX GBM tumors (one xenoline). This task will be performed to characterize the specificity and pharmacology of additional imaging candidates, if they are developed as indicated based on the above criteria. If this activity is pursued, the anticipated target date for completion will be: March 1, 2022.

Milestone Achieved: Lead substrate-peptide conjugate identified for further in vivo studies. The cumulative in vitro and in vivo data from the above studies will be assessed to determine the lead peptide probe for subsequent studies. The probe with the highest specificity for imaging tumor relative to normal brain within 6 h of dosing. Target completion from SOW: August 31, 2019. Anticipated completion date: March 1, 2022.

Planned activity: Explore 1 nmol and 10 nmol doses of the peptides at 3 time points in mice with orthotopic PDX GBM tumors (one xenoline); use peptide block and non-tumor groups as controls. These in vivo PET and NIRF imaging studies will be performed to assess the effects of various doses on signal accumulation and target specificity. Target completion from SOW: November 31, 2019. Anticipated completion date: March 1, 2022.

Planned activity: Histological and zymography analyses of MMP-14 in resected tumors and brain sections from dose optimization studies, according to established methods used in studies to date. This task is performed to correlate target MMP-14 expression and probe signal accumulation. Target completion from SOW: November 31, 2019. Anticipated completion date: March 1, 2022.

Projected Milestone: Identification of optimal dose and imaging time point for the lead peptide probe. Target completion from SOW: November 31, 2019. Anticipated completion date: March 1, 2022.

Planned activity: Fluorescence imaging with 5-ALA, and PET/CT imaging with ^{18}F[FDG] and ^{18}F[FET] in mice with orthotopic PDX GBM tumors (one xenoline). This task is performed to compare the lead candidate imaging performance with current gold standards

for fluorescence or PET imaging. Target completion from SOW: December 31, 2019. Anticipated completion date: March 1, 2022.

Projected Milestone: Sensitivity, specificity, PPV, NPV of lead peptide probe determined.
Target completion from SOW: December 31, 2019. Anticipated completion date: March 1, 2022.

Planned activity: Explore *in vivo* imaging of the lead peptide probe at optimal dose/time point in 4 additional PDX models (four xenolines). NIRF and PET imaging studies with the probe will be performed in groups of mice that have orthotopic PDX GBM tumors from xenolines with varying levels of MMP-14 expression and molecular characteristics. This task is performed to assess the broad application of the imaging agent among different GBM tumors. Target completion from SOW: June 30, 2020. Anticipated completion date: March 1, 2022.

Planned activity: Histological and zymography analyses of MMP-14 in resected tumors and brain sections from additional PDX model (one xenoline), according to established methods used in studies to date. This task is performed to correlate target MMP-14 expression and probe signal accumulation. Target completion from SOW: June 30, 2020. Anticipated completion date: March 1, 2022..

Projected Milestone: Global sensitivity, specificity, PPV, NPV of lead peptide probe determined across multiple PDX models. Target completion from SOW: June 30, 2020. Anticipated completion date: March 1, 2022.

Projected Milestone: Submit additional extramural research proposals (DOD, NIH) for subsequent stages of investigation (surgical resection in mice with PDX tumors). Target completion from SOW: August 31, 2020. Anticipated completion date: September 31, 2022.

4. **IMPACT:**

- **What was the impact on the development of the principal discipline(s) of the project?**

Projected impact (included in the prior reporting period): The project, if successful in the long-term, has the potential to significantly impact the prognosis for patients with malignant glioma. The proposed strategy is anticipated in the long-term to positively impact both neurosurgeons and patients by mediating rational, individualized, synergistic assessment of GBM for pre-surgical biopsy, marking tumor boundaries, and enhancing successful maximal safe resection in a timely and seamless manner. These factors would overcome significant limitations of currently approved imaging agents to distinguish GBM from normal brain tissue. The proposed project is anticipated to reveal novel cross-correlations between biological parameters (genomic, transcriptomic, kinomic, histologic) of the GBM xenografts and clinically relevant sensitivity, specificity, and predictive metrics that will be defined with the novel MMP-14 activatable PET/NIRF imaging probes. Synergistically employing these novel parameters and integrating them into imaging systems using alternative modalities (e.g., MRI) would foreseeably enable rational, personalized planning for surgical resection or alternative therapeutic interventions in future stages of research. If successful, these advancements are anticipated to improve the prognosis for individuals with GBM.

- **What was the impact on other disciplines?**

Projected impact (included in the prior reporting period): The project aims to validate a novel molecular imaging approach, where the same enzyme is responsible for both activation of the imaging signal and binding to the cancer cells. Other activatable probes in existing research target separate cellular or physiological pathways. As a result, it can be difficult to distinguish the primary mechanism of action that results in target enhancement. The proposed strategy aims to simplify the straightforward co-registration of NIRF and PET signals as a result of both components detecting a single molecular target. Many different types of cancer (e.g., breast cancer, melanoma) overexpress MMP-14 relative to normal tissues; therefore, the project has the potential to significantly impact management of clinical care across a variety of cancers.

- **What was the impact on technology transfer?**

  Nothing to report.

- **What was the impact on society beyond science and technology?**

Projected impact (included in the prior reporting period): The proposed project has the potential to impact the lives and well-being of individuals diagnosed with brain tumors, as well as their family members and friends. Currently, GBM is understood to be essentially non-curable and has a very short time frame for survival after diagnosis (less than 2 years). People who hear this news understandably face fear and anxiety. As the proposed strategy may significantly impact the prognosis and extend the survival of people with GBM, these negative emotional and psychological impacts could foreseeably be diminished. The result would positively contribute to society, as the individuals could perform normally in their daily lives and work activities.

5. **CHANGES/PROBLEMS:**

- **Changes in approach and reasons for change**

As noted above, the results with the initial candidate peptides are consistent with a "lead" candidate for further evaluation. Therefore, it is likely that the originally planned activities to develop "additional candidate" peptides for evaluation will not be necessary. Forthcoming results from planned experiments in the next several months will determine whether or not additional peptide constructs will be developed. This is not a significant change that would alter the course of the project.

No other significant changes have been made to the approach since the last reporting period.

- **Actual or anticipated problems or delays and actions or plans to resolve them**

The work indicated above was significantly delayed because the fluorescence dyes were on back-order from the company (LI-COR) at the time more peptides were being prepared for planned experiments, and because of mandatory shutdowns to research activities at our institutions (University of Alabama at Birmingham, and sub-contract site Stanford University). The mandatory closures, due to Covid19, caused delays during the closure period and also the months before and after laboratories were closed. The length of these closures surpassed the estimated time frame when we initially submitted the No-Cost Extension request in 2020. Additionally, we've had changes in non-essential laboratory personnel that were assisting with the project, and have now trained incoming personnel to continue working on the tasks indicated above.

- **Changes that had a significant impact on expenditures**

Due to the delays specified above, we filed an additional 6-month no-cost extension for the project. No other significant changes have been made to expenditures.

- **Significant changes in use or care of human subjects, vertebrate animals, biohazards, and/or select agents**

  Nothing to report.

- **Significant changes in use or care of human subjects**.

  Nothing to report.

- **Significant changes in use or care of vertebrate animals.**

  ACURO approval expired in 2020 during the mandatory closure due to Covid19; ACURO approval has been granted again as of August 19, 2021. No changes in the animal protocol were made prior to or subsequent to ACURO review.

- **Significant changes in use of biohazards and/or select agents.**

  Nothing to report.

6. **PRODUCTS:**

- **Publications, conference papers, and presentations**.

  - **Journal publications.**

Peer-reviewed article (new for this annual report): Tiara S Napier, Neha Udayakumar, Aditi H Jani, Yolanda E Hartman, Hailey A Houson, Lindsay Moore, Hope M Amm, Nynke S van den Berg, Anna G Sorace, Jason M Warram; "Comparison of Panitumumab-IRDye800CW and 5-Aminolevulinic Acid to Provide Optical Contrast in a Model of Glioblastoma Multiforme." *Molecular Cancer Therapeutics*; 19(9):1922-1929; Published; acknowledgment of federal support: Yes

Peer-reviewed article (from prior reporting period): Benjamin B. Kasten, Ke Jiang, Denzel Cole, Aditi Jani, Neha Udayakumar, G. Yancey Gillespie, Guolan Lu, Tingting Dai, Eben L. Rosenthal, James M. Markert, Jianghong Rao, Jason M. Warram; "Targeting MMP-14 for dual PET and fluorescence imaging of glioma in preclinical models;" *European Journal of Nuclear Medicine and Molecular Imaging;* 47(6), 2020; 1412-1426; Published; acknowledgment of federal support: Yes.

Published abstract (from prior reporting period): Hailey Houson, Benjamin Kasten, Ke Jiang, Jianghong Rao, Jason Warram; "MMP-14 as a noninvasive marker for PET and NIRF imaging of glioblastoma multiforme;" *Journal of Nuclear Medicine*; 60(no. supplement 1):2019;1033; published.

- **Books or other non-periodical, one-time publications.**

  Nothing to report.

- **Other publications, conference papers, and presentations.**

Presentation at international meeting (from prior reporting period): Hailey Houson, Benjamin Kasten, Ke Jiang, Jianghong Rao, Jason Warram; "MMP-14 as a noninvasive marker for PET and NIRF imaging of glioblastoma multiforme;" poster presentation; SNMMI 2019 Annual Meeting; 2019 Jun 22-25; Anaheim, CA.

- **Website(s) or other Internet site(s)**
  Nothing to report.

- **Technologies or techniques**
  Nothing to report.

- **Inventions, patent applications, and/or licenses**
  Nothing to report.

- **Other Products**

  Nothing to report.

7. PARTICIPANTS & OTHER COLLABORATING ORGANIZATIONS

- **What individuals have worked on the project?**

Name: Jason Warram
Project Role: Principal Investigator
ORCID ID: 000-0001-5230-0011
Nearest person month worked: 1
Contribution to Project: Dr. Warram has supervised and oversee lab personnel, conducted and analyzed data, reported results.
Funding Support: Partial salary support from the NIH as Co-Investigator on unrelated projects.

Name: Jianghong Rao
Project Role: Site PI
ORCID ID: 0000-0002-5143-9529
Nearest person month worked: 1
Contribution to Project: Dr. Jianghong oversees the subtask 1.1 and subtask 3.1 delivered to the UAB team.
Funding Support: Partial salary support from NIH on unrelated projects.

Name: Yolanda Hartman "no change from initial submission"
Project Role:
Nearest person month worked:
Contribution to Project
Funding Support:

Name: Benjamin Kasten
Project Role: Postdoctoral Scholar
Nearest person month worked: 7
Contribution to Project: Dr. Kasten contributed to the subtask 1.1, 1.2, and 4.3 including radiolabeling and peptide probe characterization, as well as data analysis of MMP-14 protein expression.
Funding Support: Partial salary support from NIH on unrelated projects

- **Has there been a change in the active other support of the PD/PI(s) or senior/key personnel since the last reporting period?**
  Dr. Jason Warram
  Newly Extended Projects:
  W81XWH1810160 Warram (PI) 09/01/2018 - 02/28/2022 1.2 Cal Mo
  DOD PRCRP (No Cost Extension)
  Dual PET/Fluorescence Imaging of Glioma with an MMP-14 Activatable Peptide Probe

- **What other organizations were involved as partners?**
  - *Nothing to report*

8. **SPECIAL REPORTING REQUIREMENTS**

   - **COLLABORATIVE AWARDS:** *not applicable*

   - **QUAD CHARTS:** *not applicable*

9. **APPENDICES:**
   - Accepted Publication "Comparison of Panitumumab-IRDye800CW and 5-Aminolevulinic Acid to Provide Optical Contrast in a Model of Glioblastoma Multiforme." accepted by *Molecular Cancer Therapeutics*
   - Supplementary Materials and Methods
   - Abstract "MMP-14 as a noninvasive marker for PET and NIRF imaging of glioblastoma multiforme" presented at the Society of Nuclear Medicine and Molecular Medicine, 2019 Meeting

Published OnlineFirst June 30, 2020; DOI: 10.1158/1535-7163.MCT-19-0819

Comparison of Panitumumab-IRDye800CW and 5-Aminolevulinic Acid to Provide Optical Contrast in a Model of Glioblastoma Multiforme

Tiara S. Napier[1], Neha Udayakumar[2], Aditi H. Jani[3], Yolanda E. Hartman[4], Hailey A. Houson[4], Lindsay Moore[4], Hope M. Amm[5], Nynke S. van den Berg[6], Anna G. Sorace[7,8], and Jason M. Warram[4,8]

ABSTRACT

Maximal safe resection of malignant tissue is associated with improved progression-free survival and better response to radiation and chemotherapy for patients with glioblastoma (GBM). 5-Aminolevulinic acid (5-ALA) is the current FDA-approved standard for intraoperative brain tumor visualization. Unfortunately, autofluorescence in diffuse areas and high fluorescence in dense tissues significantly limit discrimination at tumor margins. This study is the first to compare 5-ALA to an investigational new drug, panitumumab-IRDye800CW, in the same animal model. A patient-derived GBM xenograft model was established in 16 nude mice, which later received injections of 5-ALA, panitumumab-IRDye800CW, IRDye800CW, 5-ALA and IRDye800CW, or 5-ALA and panitumumab-IRDye800CW. Brains were prepared for multi-instrument fluorescence imaging, IHC, and quantitative analysis of tumor-to-background ratio (TBR) and tumor margin accuracy. Statistical analysis was compared with Wilcoxon rank-sum or paired *t* test. Panitumumab-IRDye800CW had a 30% higher comprehensive TBR compared with 5-ALA ($P = 0.0079$). SDs for core and margin regions of interest in 5-ALA–treated tissues were significantly higher than those found in panitumumab-IRDye800CW–treated tissues ($P = 0.0240$ and $P = 0.0284$, respectively). Panitumumab-IRDye800CW specificities for tumor core and margin were more than 10% higher than those of 5-ALA. Higher AUC for panitumumab-IRDye800CW indicated strong capability to discriminate between normal and malignant brain tissue when compared with 5-ALA. This work demonstrates that panitumumab-IRDye800CW shows potential as a targeting agent for fluorescence intraoperative detection of GBM. Improved margin definition and surgical resection using panitumumab-IRDye800 has the potential to improve surgical outcomes and survival in patients with GBM compared with 5-ALA.

Introduction

Glioblastoma (GBM) is the most lethal adult primary tumor of the central nervous system (1, 2), accounting for 52% of all primary brain tumors in the United States (2). The current standard of care for high-grade gliomas such as GBM is surgical resection followed by adjuvant chemotherapy and radiation (3). However, even for patients who undergo treatment, the 5-year survival rate is approximately 9.8%, and the median survival rate is only 14.6 months (1, 4, 5). Several studies have shown that the most important factor influencing patient survival is extent of tumor resection (6–8). Maximal safe resection of malignant tissue is associated with improved progression-free survival, greater overall survival, and better therapeutic response to radiation and chemotherapy (8–11).

To meet the challenge of accurately identifying tumor tissue during resection surgery, 5-aminolevulinic acid (5-ALA) has been approved for visualization of malignant brain neoplasms (12, 13). 5-ALA is a hemoglobin precursor that is able to penetrate the blood–brain barrier (BBB) and induce accumulation of proto-porphyrin IX (PPIX) within malignant brain tumor cells (12). It permits violet-red fluorescence after excitation with 405 nm wavelength blue light (12). Compared with white light surgical resections, in which more than 50% of patients with high-grade glioma do not undergo gross total resection, 5-ALA increases the likelihood of achieving a gross total resection by 28% (14). However, recent findings on 5-ALA fluorescence show that the agent is not without limitations (15–18).

One study evaluating the influence of fluorescence porphyrins in GBM found that solid red fluorescence correlated to highly perfused, tumor dense regions with associated neovascularity (15). Diffuse pink fluorescence, on the other hand, indicated the transition zone between tumor and normal brain parenchyma (15). Stummer and colleagues went on to show that this zone contained either infiltrating tumor cells of medium density or edematous brain tissue (15). Therefore, PPIX fluorescence in fluid-filled, nonmalignant tissue may be one source of false positives found with 5-ALA (12). In addition, intense fluorescence in dense tumor areas has been shown to significantly limit discrimination at tumor margins (17, 18). Furthermore, in diffuse tumors, high tissue autofluorescence is often detected (19, 20). Overall, 5-ALA's sensitivity and specificity for detection of malignant tissue in patients with high-grade glioma was reported at 85% and 82%, respectively (16).

A possible solution to address the limitations of current intraoperative imaging tools is the use of fluorescently labeled antibodies that emit at near-infrared wavelength (21, 22). In principle, these antibodies target cell membrane receptors that are overexpressed at the

[1]Graduate Biomedical Sciences, University of Alabama at Birmingham, Birmingham, Alabama. [2]School of Medicine, University of Alabama at Birmingham, Birmingham, Alabama. [3]Department of Medicine, University of Alabama at Birmingham, Birmingham, Alabama. [4]Department of Otolaryngology, University of Alabama at Birmingham, Birmingham, Alabama. [5]Department of Oral and Maxillofacial Surgery, University of Alabama at Birmingham, Birmingham, Alabama. [6]Department of Otolaryngology, Stanford University Medical School, Stanford, California. [7]Department of Radiology, University of Alabama at Birmingham, Birmingham, Alabama [8]O'Neal Comprehensive Cancer Center, University of Alabama at Birmingham, Birmingham, Alabama.

Corresponding Author: Jason M. Warram, University of Alabama at Birmingham, Volker Hall G082 1670 University Blvd., Birmingham, AL 35294. Phone: 205-976-5009; Fax: 205-934-3993; E-mail: mojack@uab.edu

Mol Cancer Ther 2020;19:1922–9

doi: 10.1158/1535-7163.MCT-19-0819

Published OnlineFirst June 30, 2020; DOI: 10.1158/1535-7163.MCT-19-0819

protein level in malignant tissue (21–23). One such antibody is panitumumab, a fully human IgG_2 mAb developed to specifically bind EGFR (K_d ~0.05 nmol/L; refs. 24, 25). Because EGFR is often amplified in GBM tumors (26, 27), it is hypothesized that panitumumab conjugated to a fluorescent dye can be used for tumor margin detection during GBM resection surgery. To date, no studies have directly compared the performance of fluorophore-labeled panitumumab to the current intraoperative imaging standard, 5-ALA, for GBMs. Therefore, this work evaluates tumor-to-background ratio (TBR), tumor margin accuracy, and target efficacy of panitumumab-IRDye800 versus 5-ALA in a patient-derived xenograft (PDX) GBM model.

Table 1. Imaging agent given to five groups of PDX animal models and time of each agent *in vivo*.

Imaging agent	Mouse no.	*n*	Time of each agent *in vivo* (hours)
5-ALA alone	M1-3	3	4
IRDye800 alone	M4-6	3	24
Panitumumab-IRDye800CW alone	M7-9	3	72
5-ALA + IRDye800	M10-12	3	28
5-ALA + panitumumab-IRDye800CW	M13-16	4	76

Materials and Methods

Reagents

5-ALA hydrochloride (Abcam, catalog no. ab142998) was diluted to 12.5 mg/mL in sterile PBS. Mice receiving 5-ALA were injected via tail vein with 200 μL of the solution for a final dose of 0.1 mg/g body weight. Panitumumab (Vectibix; Amgen) is a recombinant, fully humanized monoclonal anti-EGFR antibody. IRDye800CW-*N*-hydroxysuccinimide ester (IRDye800CW-NHS-ester; LI-COR Biosciences, Inc., catalog no. 929-70020) is a near-infrared dye used frequently in fluorescence-guided surgery (FGS) studies. Panitumumab was conjugated to IRDye800CW-NHS-ester according to the manufacturer's protocol by diluting panitumumab to 1 mg/mL in sterile PBS and incubating the diluted antibody in the dark at room temperature for 2 hours. The conjugate (hereafter referred to as panitumumab-IRDye800CW) was subsequently purified using spin columns and stored in the dark at 4°C. Mice receiving panitumumab-IRDye800CW were injected via tail vein with 200 μg of the conjugate. No aggregation was observed. Mice in the control group received 200 μg IRDye800CW Carboxylate (IRDye800CW; LI-COR Biosciences, Inc., catalog no. 929-08972) via tail vein.

PDX animal models

Female nude mice (Charles River Laboratories) were orthotopically injected, as described previously (28, 29), with 5×10^5 patient-derived GBM cells (GBM6) generously provided by Dr. Jann Sarkaria (Mayo Clinic, Rochester, MN). Two weeks after implantation, animals were administered 5-ALA ($n = 3$), IRDye800CW ($n = 3$), panitumumab-IRDye800CW ($n = 3$), 5-ALA in combination with IRDye800CW ($n = 3$), and 5-ALA in combination with panitumumab-IRDye800CW ($n = 4$) via tail vein injections. Animals were sacrificed at 4, 24, 72, 28 (24 hours with IRDye800CW + 4 hours with 5-ALA), or 76 hours (72 hours with panitumumab-IRDye800CW + 4 hours with 5-ALA), respectively (**Table 1**). Time courses for duration of animal incubation with 5-ALA and panitumumab-IRDye800CW were determined on the basis of previously published literature, as well as clinical relevance (22, 30–34). Mouse brains were harvested, formalin-fixed, and sectioned for fluorescence imaging (1 mm) for tissue staining (5 μm).

Fluorescence imaging and contrast power comparison

Imaging for 5-ALA–treated tissues was performed using a custom Leica, MZFLIII Stereo Microscope (Leica). A liquid-crystal tunable wavelength filter in the Leica Spectral Camera was set for collection of emission images from 600 to 720 nm in 5-nm increments. Composite images (unmixed composites) were generated for each image cube by separating the spectral signature of the PPIX molecule from those of background autofluorescence using a spectral library that was compiled from numerous spectral profiles collected from control tissue under the same conditions. For PPIX imaging using the Odyssey CLx (LI-COR Biosciences), an external ultraviolet source (405 nm) was used for excitation of PPIX and fluorescence emission was collected in the 700 nm channel. Imaging for tissues treated with panitumumab-IRDye800CW and IRDye800CW was performed using the Pearl Trilogy Imaging System (LI-COR Biosciences). The Odyssey CLx (LI-COR Biosciences) was used for high-resolution fluorescence scans.

Tissue staining

Paraffin-embedded tissue sections were prepared for IHC and stained for hematoxylin and eosin (H&E). Antigen retrieval and blocking were performed as described previously (35). Rabbit anti-protoporphyrinogen oxidase (PPOX; Abcam, catalog no. ab170884; 1:50) and rabbit anti-EGFR (Thermo Fisher Scientific, catalog no. RM-2111-R7) were used to assay for protein distribution overnight at 4°C. Anti-rabbit secondary antibody (Pierce Protein Biology, catalog no. 32260; 1:100) was applied to tissues for 2 hours. Tissues were incubated with 3,3′-diaminobenzidine (Dako, catalog no. K3468) substrate and dehydrated with xylene baths.

Tumor margin accuracy analysis

Imaging data were randomized and regions of interest (ROI) were drawn in a blinded fashion. ROIs were drawn around core tumor area and tumor margins for tissue slices in Image Studio v. 3.1 (LI-COR Biosciences) according to H&E validation of tumor location (**Fig. 1**). To compare average SD of mean fluorescence intensity (MFI) for each agent, large ROIs were drawn (**Fig. 1B**). To compare average TBRs for **Fig. 4**, smaller ROIs ($n = 3$ for each variable in Eqns. A–C) were drawn (**Fig. 1B**). To compare between groups, shown in **Fig. 5**, ROIs shown in **Fig. 1A** were drawn.

$$\text{Core TBR} = \frac{\textit{Mean Core Fluorescence}}{\left[\frac{(\textit{Proximal Background Fluorescence} + \textit{Distal Background Fluorescence})}{2}\right]} \quad \text{(A)}$$

$$\text{Margin TBR} = \frac{\textit{Mean Margin Fluorescence}}{\left[\frac{(\textit{Proximal Background Fluorescence} + \textit{Distal Background Fluorescence})}{2}\right]} \quad \text{(B)}$$

$$\text{Comprehensive TBR} = \frac{(\textit{Mean Core Fluorescence} + \textit{Mean Margin Fluorescence})}{(\textit{Proximal Background Fluorescence} + \textit{Distal Background Fluorescence})} \quad \text{(C)}$$

Proximal background fluorescence measurements were taken close to the tumor margin. Distal background fluorescence measurements were taken at the edge of the brain as far away from the tumor as

Published OnlineFirst June 30, 2020; DOI: 10.1158/1535-7163.MCT-19-0819

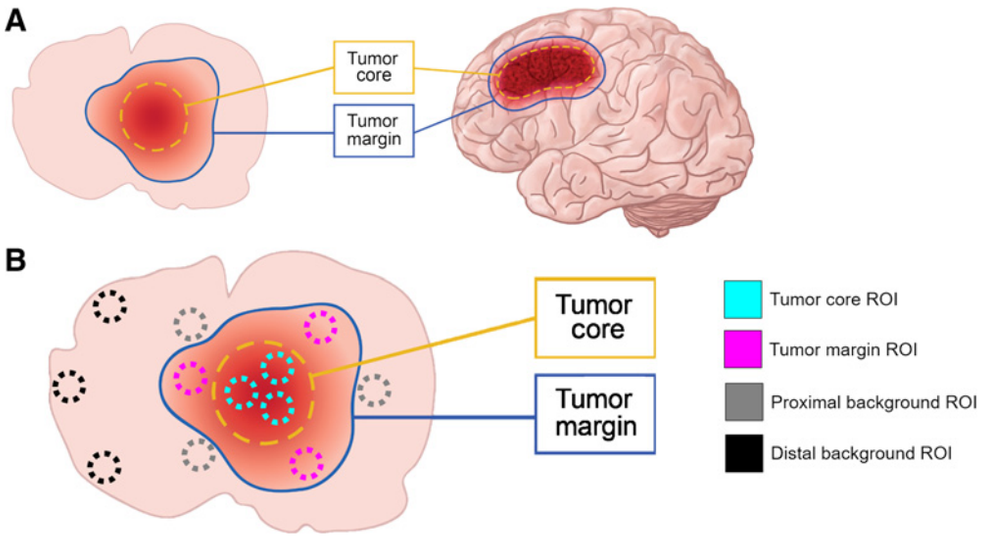

Figure 1.
Core and tumor margin ROIs. **A,** Core tumor ROI is outlined by a dashed yellow line. Tumor margin ROI is outlined by a solid blue line. **B,** Smaller ROIs for tumor core, tumor margin, proximal background, and distal background were drawn as indicated.

possible. All fluorescence signals are reported in arbitrary units. H&E stains were used to determine true tumor.

Statistical analysis

Statistical analysis was performed using GraphPad Prism (GraphPad Software). For TBR comparison, a Wilcoxon rank-sum test was used. For mice receiving both 5-ALA and panitumumab-IRDye800CW, multiple samples of each ROI were taken ($n = 3$) and t tests were performed between samples. For comparison of average SD in MFI, a paired t test was used. For ROC curve analysis, pixel intensities from H&E images were compared with pixel intensities from panitumumab-IRDye800 images and with 5-ALA images. Prism was used to calculate sensitivity and specificity. Using the formula below, Youden statistics were calculated for each 95% confidence interval and the maximum Youden index (J), which denotes the classification threshold, was determined (36).

$$J = max_c(sensitivity_c + specificity_c - 1)$$

The Hanley method was used to evaluate whether the ROC curves were statistically significant (37). A $P < 0.05$ was considered significant (*).

Results

5-ALA metabolism and fluorescence show nonspecific binding

PPOX catalyzes oxidation of proto-porphyrinogen-IX to form PPIX and is essential for conversion of 5-ALA to heme (38). For mice receiving 5-ALA alone, IHC revealed diffuse fluorescence in the mouse brain overall and no accumulation of PPOX in the tumor area (**Fig. 2**). The first column in **Fig. 2** shows anti-PPOX (brown)-stained tissues that were counterstained with hematoxylin (purple). Although, H&E reveals tumor staining in the right hemisphere, fluorescence images of that brain slice do not show an accumulation of fluorophore in mice treated with 5-ALA alone (**Fig. 2**, top row). Mice receiving 5-ALA with IRDye800CW or 5-ALA with panitumumab-IRDye800CW demonstrate PPIX localization in the tumor area (**Fig. 2**, second and third row).

Panitumumab-IRDye800CW specifically binds patient-derived GBM tumors

Brain slices from mice receiving panitumumab-IRDye800CW alone show tumor-specific accumulation of the compound in the brain (**Fig. 3A**). A digital scan of the tissue slice was taken using 800-nm channel. Subsequently, thinner slices (5 μm) were paraffin-embedded and scanned with a fluorescence slide scanner (**Fig. 3B**). Accurate visualization of the tumor site was validated histologically (**Fig. 3C**) and compared with anti-EGFR staining (**Fig. 3D**).

Panitumumab-IRDye800CW has higher TBRs than 5-ALA

Fluorescence images of mice receiving both 5-ALA and panitumumab-IRDye800CW ($n = 4$) were compared with H&E (**Fig. 4**). In Image Studio, ROIs were drawn around core tumor areas and margin areas were defined by less intense fluorescence indicating the transition area between tumor and normal tissue (three measurements per mouse for **Figs. 4** and **6**). Background ROIs both proximal and distal to the tumor site were also drawn. MFIs for all areas on each tissue slice were obtained. MFIs of core, margin, and comprehensive tumor were divided by average MFIs of the background to obtain TBR (**Figs. 4** and **5**). Specifically, M13 had a core, margin, and comprehensive TBR of 0.022 ± 0.02, 8.18 ± 2.90, and 8.64 ± 3.08 with 5-ALA (**Fig. 4**). M13 had a core, margin, and comprehensive TBR of 14.20 ± 2.34, 5.53 ± 0.40, and 9.86 ± 1.23 with panitumumab-IRDye800CW. M14 had a core, margin, and comprehensive TBR of 0.004 ± 0.004, 8.74 ± 3.33, and 9.99 ± 3.66 with 5-ALA (**Fig. 4**). M14 had a core, margin, and comprehensive TBR of 32.41 ± 11.47, 17.62 ± 9.33, and 25.01 ± 10.40 with panitumumab-IRDye800CW. M15 had a core, margin, and comprehensive TBR of 0.04 ± 0.03, 29.37 ± 24.46, and 31.17 ±26.29 with 5-ALA (**Fig. 4**). M15 had a core, margin, and comprehensive TBR of 46.83 ± 23.92, 35.95 ± 14.54, and 41.39 ± 19.23 with panitumumab-IRDye800CW. M16 had a core, margin, and comprehensive TBR of 0.11 ± 0.08, 7.36 ± 0.86, and 12.18 ± 1.32 with 5-ALA (**Fig. 4**). M16 had a core, margin, and comprehensive TBR of

Published OnlineFirst June 30, 2020; DOI: 10.1158/1535-7163.MCT-19-0819

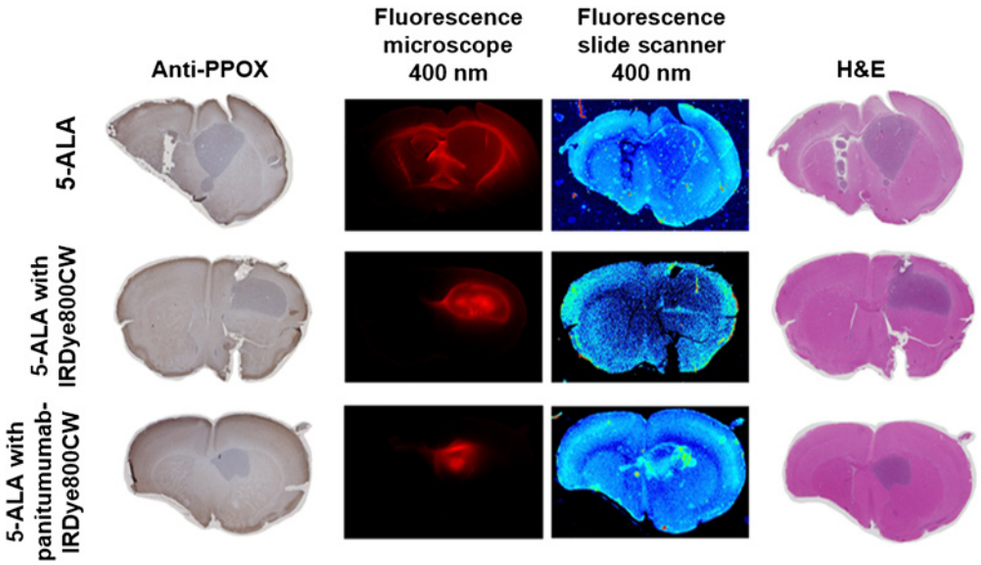

Figure 2.

5-ALA target efficacy. IHC with anti-PPOX staining (shown in brown, column one), fluorescence microscopy (column two, 1-mm section), and digital fluorescence scans (column three, 5-μm section) compared with H&E (column four) of mouse brain slices from mice that received 5-ALA. Row 1 received 5-ALA alone. Row 2 received 5-ALA and IRDye800CW. Row 3 received both 5-ALA and panitumumab-IRDye800CW. Images in the second and third columns were taken while exciting the tissues with 405 nm light source. 5-ALA induces localization of fluorescence molecules to the tumor area in two of the three cases shown here.

43.57 ± 19.76, 33.40 ± 9.81, and 38.48 ± 14.77 with panitumumab-IRDye800CW.

In addition, ROIs drawn according to **Fig. 1A** were used to obtain TBRs for 5-ALA and panitumumab-IRDye800CW. Specifically, average core, margin, and comprehensive TBRs for 5-ALA were 6.13 ± 1.48, 5.22 ± 0.99, and 5.67 ± 1.17 (**Fig. 5A**). Average core, margin, and comprehensive TBRs for panitumumab-IRDye800CW were 41.87 ± 12.53, 21.71 ± 12.84, and 28.91 ± 17.62 (**Fig. 5B**). In mice that received both agents, average core, margin, and comprehensive TBRs for 5-ALA were 8.11 ± 1.489, 7.32 ± 1.66, and 7.71 ± 1.57, respectively (**Fig. 5C**). In these mice, average core, margin, and comprehensive TBRs for panitumumab-IRDye800CW were 51. 46 ± 25.30, 32.77 ± 19.79, and 42.12 ± 22.48, respectively (**Fig. 5C**). For each mouse receiving both 5-ALA and panitumumab-IRDye800CW, panitumumab-IRDye800CW showed a significantly higher core TBR than 5-ALA and showed statistically higher margin and comprehensive TBRs ($P = 0.0102$ and 0.0373, respectively; **Fig. 5C**).

Panitumumab-IRDye800CW showed less SD for both the core and marginally defined ROIs than 5-ALA (**Fig. 6A**). SDs for core and margin ROIs in 5-ALA–treated tissues were significantly higher than those outlined in tissues treated with panitumumab-IRDye800CW ($P = 0.0240$ and $P = 0.0284$, respectively; *, $P < 0.05$). ROIs of the tumor core revealed that the mean SD of MFI for 5-ALA and panitumumab-IRDye800CW were 602 ± 322 0.0708 ± 0.0426, respectively (**Fig. 6A**). ROIs of the tumor margin revealed that the mean SDs of MFI for 5-ALA and panitumumab-IRDye800CW were 845 ± 527 and 0.1,040 ± 0.0604, respectively (**Fig. 6A**). This analysis highlights the heterogeneity of tumor-specific signal when using 5-ALA compared with panitumumab-IRDye800CW, which is relatively homogenous throughout the tumor.

The AUC ROC estimate of core response was 0.9375 for panitumumab-IRDye800CW and 0.9000 for 5-ALA (**Fig. 6B**). While both agents yielded a small P value ($P = 0.0011$ for panitumumab-IRDye800CW and $P = 0.0007$ for 5-ALA), the higher AUC for panitumumab-IRDye800CW indicates that it is better able to discriminate between normal brain tissue and core tumor. The AUC estimate for margin response was 0.9375 for panitumumab-IRDye800CW and 0.8813 for 5-ALA (**Fig. 6C**). Again, both agents

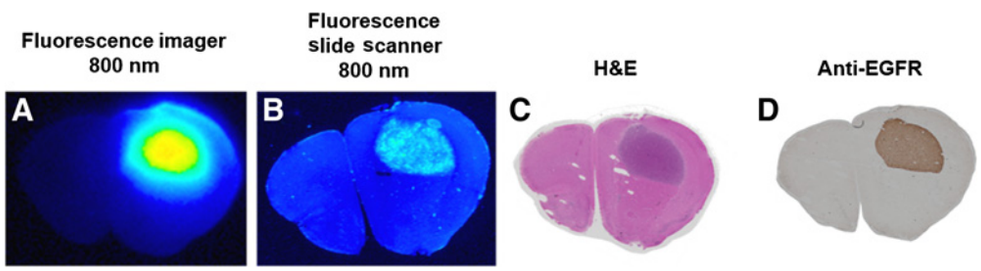

Figure 3.

Panitumumab-IRDye800CW target efficacy. **A,** Fluorescence imaging of 1–2 mm tissue slice performed with a fluorescence scanner using the 800 nm channel. **B,** Fluorescence imaging of 5-μm tissue slices performed with high-sensitivity slide scanner using the 800 nm channel. **C,** H&E staining of true tumor in mouse brain slice taken from mouse that received panitumumab-IRDye800CW alone. **D,** Anti-EGFR staining. Panitumumab-IRDye800CW localizes to the tumor area.

Published OnlineFirst June 30, 2020; DOI: 10.1158/1535-7163.MCT-19-0819

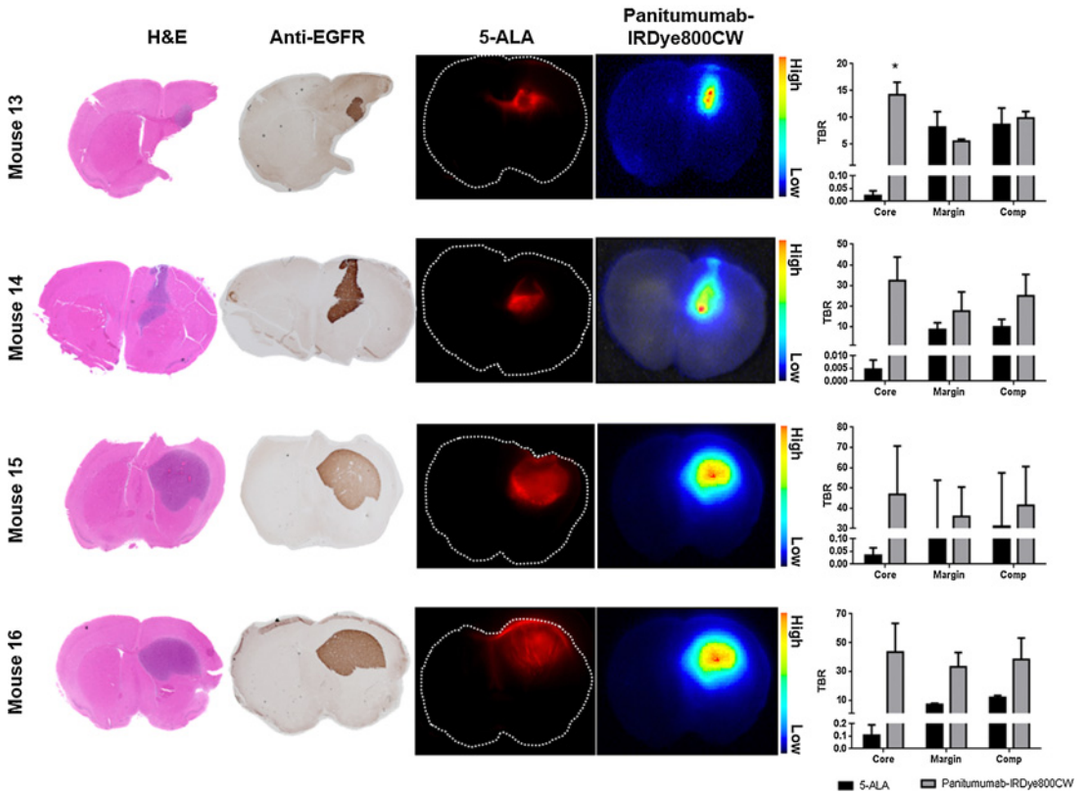

Figure 4.

Comparison of 5-ALA and panitumumab-IRDye800CW in mice receiving both agents. Each row in the figure represents a mouse that received both 5-ALA and panitumumab-IRDye800CW. The first column shows H&E stains, the second column shows EGFR staining, the third column shows 5-ALA–induced fluorescence, the fourth column shows panitumumab-IRDye800CW fluorescence, and the last column shows mean TBRs for both fluorescence images. Bar graphs show TBR (mean ± SD, $n = 3$). Statistically higher core TBRs were found with panitumumab-IRDye800CW in all four mice ($P = 0.0005$, 0.0081, 0.0276, and 0.0189, respectively). The last mouse showed statistically higher margin and comprehensive (comp) TBRs as well ($P = 0.0102$ and 0.0373, respectively). * in the top graph indicates $P < 0.05$, specifically $P = 0.0079$.

yielded a small P value ($P = 0.0011$ for panitumumab-IRDye800CW and $P = 0.0013$ for 5-ALA). The higher AUC for panitumumab-IRDye800CW indicates it is better able to discriminate between normal brain tissue and tumor margin.

The Youden Index was used to determine sensitivity and specificity cutoffs for panitumumab-IRDye800CW and 5-ALA (**Table 2**; ref. 36). Panitumumab-IRDye800CW and 5-ALA showed 100% sensitivity for margin as well as core tumor area. However, panitumumab-IRDye800CW showed higher specificity than 5-ALA for these tumor ROIs. 5-ALA showed a higher specificity for margin tumor area than for core tumor.

Discussion

Several studies report prolonged progression-free survival in patients with GBM who have undergone complete resection as confirmed by MRI contrast uptake (39–41). However, the invasive and heterogeneous nature of GBM tumors makes complete surgical resection challenging (42). While some studies show that 5-ALA–guided surgery increases diagnostic accuracy and extent of resection, other reports highlight the nonspecific nature of 5-ALA tumor localization (43, 44). In addition, broad variation of PPIX concentration within viable grade IV tumor tissue has been shown (45, 46). Many limitations with 5-ALA originate from a lack of complete understanding on mechanisms of tumor-specific PPIX uptake (47). Still, FGS demonstrates great potential as it removes the concern of brain shift during surgery and has many other advantages, including low cost and real-time capabilities (47, 48).

As an alternative to the use of a heme precursor for FGS, the high specificity and low toxicity of mAbs makes them ideal for targeted imaging approaches (22, 34, 49, 50). Low tissue autofluorescence at the 800 nm wavelength makes IRDye800CW well-suited for tumor visualization (51). Therapeutic antibodies that have been conjugated to IRDye800CW include bevacizumab, cetuximab, and panitumumab (21, 52). All three conjugated imaging agents have demonstrated preclinical success and safe administration in humans (21, 52). This avenue of research has great translational relevance because real-time fluorescence imaging with antibodies has the potential to reduce morbidity and operative time during ablative procedures such as tumor resection (49). These benefits, coupled with the need for a high extent of complete resection in GBM cases, underline the importance of FGS advancements.

This study is the first to compare an FDA-approved agent to an investigational new drug that is a clinically studied agent for GBM tumor visualization. First, we confirmed the target efficacy of each imaging agent via IHC staining (**Figs. 2–4**). The significantly higher

Published OnlineFirst June 30, 2020; DOI: 10.1158/1535-7163.MCT-19-0819

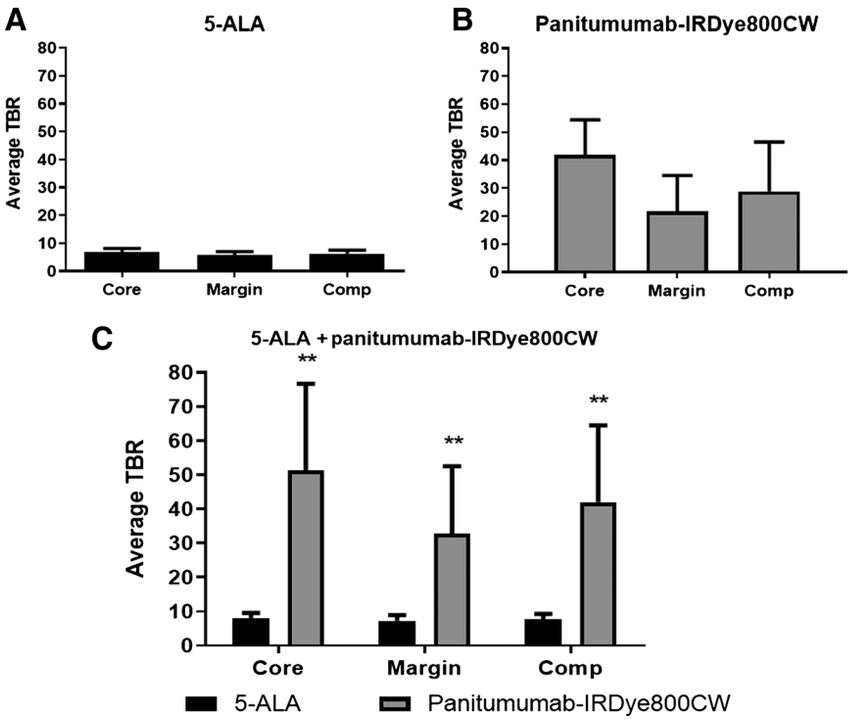

Figure 5.

Average TBRs. **A,** In the mice receiving 5-ALA ($n = 3$), core, margin, and comprehensive (comp) TBR averages were less than 10. **B,** In the group receiving panitumumab conjugated with IRDye800CW ($n = 3$), core, margin, and comprehensive TBR averages were 42, 22, and 29, respectively. **C,** In the group receiving both 5-ALA and panitumumab-IRDye800CW ($n = 4$), average TBRs for 5-ALA were less than 10, while both core and margin TBR averages for panitumumab-IRDye800CW were statistically higher (Wilcoxon rank-sum test, $P = 0.0079$; **, $P < 0.01$).

TBR found when panitumumab-IRDye800CW was used compared with when 5-ALA was used indicates that it is superior in discriminating between tumor and normal tissue (**Figs. 4** and **5**). This result is important because strong tumor signal is crucial for minimizing false positives and performing maximal safe resection (53).

An analysis was performed comparing the SDs in MFI at the tumor core and margin areas, which indicate variability in the fluorescence signal within the tumor. 5-ALA showed significantly higher SDs in both the core and margin compared with panitumumab-IRDye800CW (**Fig. 6A**). This result reveals variability of 5-ALA fluorescence in the tumor area that was not seen with fluorescence provided by panitumumab-IRDye800CW. Finally, sensitivity and specificity of both agents were measured (**Table 2**) and plotted on ROC curves (**Fig. 6B** and **C**).

Panitumumab-IRDye800CW had a greater AUC than 5-ALA (**Fig. 6B** and **C**). AUC combines both sensitivity and specificity to

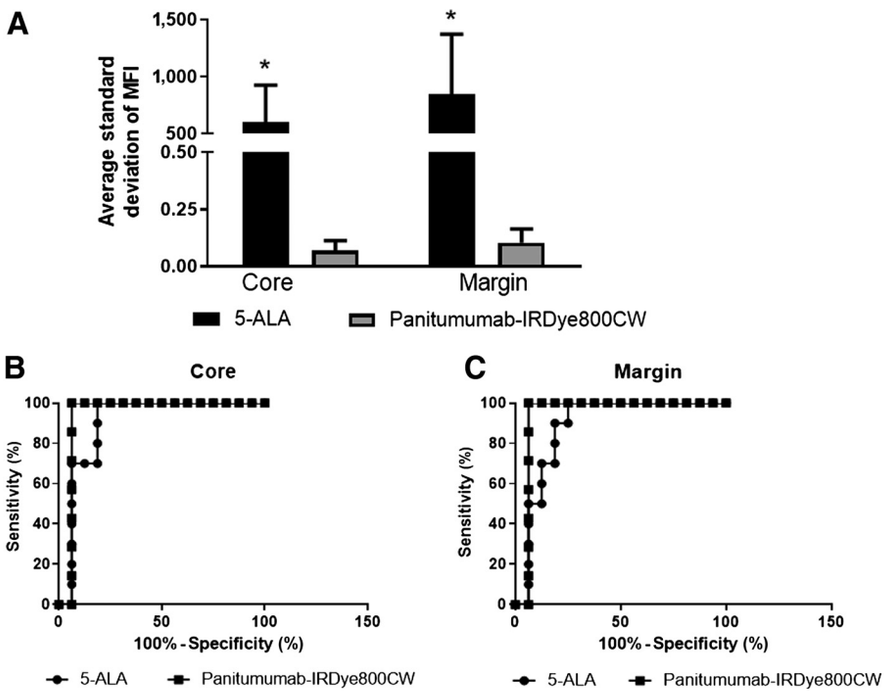

Figure 6.

SD comparison and ROC curves. **A,** MFIs were confirmed using Image Studio software. **B,** ROC curve analysis of panitumumab-IRDye800CW and 5-ALA core pixel areas revealed an AUC of 0.9375 and 0.9000, respectively. H&E was used as the standard from which sensitivity and specificity were derived. **C,** ROC curve analysis of panitumumab-IRDye800CW and 5-ALA revealed an AUC of 0.9375 and 0.8813, respectively. H&E was used as the standard from which sensitivity and specificity were derived. * indicates $P < 0.05$; specifically, * over the first bar indicates $P = 0.0240$ and over the second bar indicates $P = 0.0284$.

Published OnlineFirst June 30, 2020; DOI: 10.1158/1535-7163.MCT-19-0819

Table 2. Sensitivity and specificity of panitumumab-IRDye800CW compared with 5-ALA.

	Panitumumab-IRDye800CW		5-ALA	
	Core	Margin	Core	Margin
Sensitivity (%)	100.00	100.00	100.00	100.00
Specificity (%)	93.75	93.75	75.00	81.25

measure overall performance of a diagnostic agent (54). Higher AUC indicates greater ability to distinguish between normal and diseased tissue (27), an important function for a tumor visualization agent. In addition, panitumumab-IRDye800CW specificities for tumor core and margin were over 10% higher than those of 5-ALA (**Table 2**).

Primary limitations of this study include low sample size and incompatible imaging devices. Having equipment built to measure a wide range of fluorescence would remove any potentially confounding variables. In addition, a comparison of 5-ALA and panitumumab-IRDye800CW fluorescence in lower grade gliomas was not performed in this study. Lower grade gliomas represent an interesting avenue for future studies due to the differences in their BBBs, as well as differences in their brain adjacent to the tumor when compared with higher grade gliomas (55). Finally, prospective comparisons of panitumumab-IRDye800CW with 5-ALA should take into account heterogeneous BBB permeability, as well as BBB priming and promising methods of BBB modulation (56, 57). Future studies should also examine blood vessel penetration into the tumor, which could explain variability in 5-ALA fluorescence (47).

Conclusions

This work is the first to compare a fluorescently labeled antibody to the current gold standard for FGS, 5-ALA. It successfully demonstrates the efficacy of molecularly targeted imaging using fluorescently labeled antibodies compared with 5-ALA. Our results show that both the target efficacy and TBR of panitumumab-IRDye800CW exceeds that of 5-ALA. Our findings are in-line with other studies that demonstrate the clinical utility of panitumumab-IRDye800CW in detection and removal of malignant tumors (22, 34). Overall, the data suggests that a clinical study comparing standard of care to new research should be performed. It also suggests panitumumab-IRDye800CW may be a suitable targeting agent for fluorescence intraoperative detection of GBM.

Disclosure of Potential Conflicts of Interest

No potential conflicts of interest were disclosed.

Authors' Contributions

T.S. Napier: Data curation, formal analysis, writing-original draft, writing-review and editing, project administration. **N. Udayakumar:** Conceptualization, methodology, data curation, writing-original draft, writing-review and editing. **A.H. Jani:** Conceptualization, methodology, data curation. **Y.E. Hartman:** Conceptualization, data curation. **H.A. Houston:** Data curation, formal analysis. **L. Moore:** Data curation, formal analysis, writing-original draft, writing-review and editing. **H.M. Amm:** Data curation, writing-original draft, writing-review and editing. **N.S. van den Berg:** Conceptualization, writing-original draft, writing-review and editing. **A.G. Sorace:** Conceptualization, methodology, formal analysis, writing-original draft, writing-review and editing, study supervision. **J.M. Warram:** Conceptualization, methodology, data curation, formal analysis, writing-original draft, writing-review and editing, project administration.

Acknowledgments

This work was financially supported by the United States Army Department of Defense (PRCRPCA170769), the UAB O'Neal Comprehensive Cancer Center Preclinical Imaging Shared Facility Grant (P30CA013148), and the Robert Jack Armstrong Fund (to J.M. Warram). The Biostatistics, Epidemiology and Research Design core of the Center for Clinical and Translational Science, particularly Dr. Kimberly Martin, is thanked for statistical analysis assistance.

The costs of publication of this article were defrayed in part by the payment of page charges. This article must therefore be hereby marked *advertisement* in accordance with 18 U.S.C. Section 1734 solely to indicate this fact.

Received August 23, 2019; revised January 16, 2020; accepted June 15, 2020; published first June 30, 2020.

References

1. Zhang J, Stevens MF, Bradshaw TD. Temozolomide: mechanisms of action, repair and resistance. Curr Mol Pharmacol 2012;5:102–14.
2. de Robles P, Fiest K, Frolkis A, Pringsheim T, Atta C, Germain-Smith CS, et al. The worldwide incidence and prevalence of primary brain tumors: a systematic review and meta-analysis. Neuro Oncol 2015;17:776–83.
3. Lacroix M, Toms SA. Maximum safe resection of glioblastoma multiforme. J Clin Oncol 2014;32:727–8.
4. Lara-Velazquez M, Al-Kharboosh R, Jeanneret S, Vazquez-Ramos C, Mahato D, Tavanaiepour D, et al. Advances in brain tumor surgery for glioblastoma in adults. Brain Sci 2017;7:166.
5. von Neubeck C, Seidlitz A, Kitzler HH, Beuthien-Baumann B, Krause M. Glioblastoma multiforme: emerging treatments and stratification markers beyond new drugs. Br J Radiol 2015;88:20150354.
6. Sanai N, Polley MY, McDermott MW, Parsa AT, Berger MS. An extent of resection threshold for newly diagnosed glioblastomas. J Neurosurg 2011;115:3–8.
7. Chaichana KL, Jusue-Torres I, Lemos AM, Gokaslan A, Cabrera-Aldana EE, Ashary A, et al. The butterfly effect on glioblastoma: is volumetric extent of resection more effective than biopsy for these tumors? J Neurooncol 2014;120:625–34.
8. Senft C, Bink A, Franz K, Vatter H, Gasser T, Seifert V. Intraoperative MRI guidance and extent of resection in glioma surgery: a randomised, controlled trial. Lancet Oncol 2011;12:997–1003.
9. Kiesel B, Mischkulnig M, Woehrer A, Martinez-Moreno M, Millesi M, Mallouhi A, et al. Systematic histopathological analysis of different 5-aminolevulinic acid-induced fluorescence levels in newly diagnosed glioblastomas. J Neurosurg 2018;129:341–53.
10. Young RM, Jamshidi A, Davis G, Sherman JH. Current trends in the surgical management and treatment of adult glioblastoma. Ann Transl Med 2015;3:121.
11. Della Puppa A, De Pellegrin S, d'Avella E, Gioffrè G, Rossetto M, Gerardi A, et al. 5-aminolevulinic acid (5-ALA) fluorescence guided surgery of high-grade gliomas in eloquent areas assisted by functional mapping. Our experience and review of the literature. Acta Neurochir 2013;155:965–72.
12. Hadjipanayis CG, Widhalm G, Stummer W. What is the surgical benefit of utilizing 5-aminolevulinic acid for fluorescence-guided surgery of malignant gliomas? Neurosurgery 2015;77:663–73.
13. Day KE, Sweeny L, Kulbersh B, Zinn KR, Rosenthal EL. Preclinical comparison of near-infrared-labeled cetuximab and panitumumab for optical imaging of head and neck squamous cell carcinoma. Mol Imaging Biol 2013;15:722–9.
14. Stummer W, Pichlmeier U, Meinel T, Wiestler OD, Zanella F, Reulen HJ. Fluorescence-guided surgery with 5-aminolevulinic acid for resection of malignant glioma: a randomised controlled multicentre phase III trial. Lancet Oncol 2006;7:392–401.
15. Stummer W, Novotny A, Stepp H, Goetz C, Bise K, Reulen HJ. Fluorescence-guided resection of glioblastoma multiforme utilizing 5-ALA-induced porphyrins: a prospective study in 52 consecutive patients. J Neurosurg 2000;93:1003–13.

16. Ferraro N, Barbarite E, Albert TR, Berchmans E, Shah AH, Bregy A, et al. The role of 5-aminolevulinic acid in brain tumor surgery: a systematic review. Neurosurg Rev 2016;39:545–55.
17. Stummer W, Tonn JC, Goetz C, Ullrich W, Stepp H, Bink A, et al. 5-Aminolevulinic acid-derived tumor fluorescence: the diagnostic accuracy of visible fluorescence qualities as corroborated by spectrometry and histology and postoperative imaging. Neurosurgery 2014;74:310–9.
18. Kanick SC, Davis SC, Zhao Y, Hasan T, Maytin EV, Pogue BW, et al. Dual-channel red/blue fluorescence dosimetry with broadband reflectance spectroscopic correction measures protoporphyrin IX production during photodynamic therapy of actinic keratosis. J Biomed Opt 2014;19:75002.
19. Motekallemi A, Jeltema HR, Metzemaekers JDM, van Dam GM, Crane LMA, Groen RJM. The current status of 5-ALA fluorescence-guided resection of intracranial meningiomas—a critical review. Neurosurg Rev 2015;38:619–28.
20. Masubuchi T, Kajimoto Y, Kawabata S, Nonoguchi N, Fujishiro T, Miyatake S, et al. Experimental study to understand nonspecific protoporphyrin IX fluorescence in brain tissues near tumors after 5-aminolevulinic acid administration. Photomed Laser Surg 2013;31:428–33.
21. Gao RW, Teraphongphom N, de Boer E, van den Berg NS, Divi V, Kaplan MJ, et al. Safety of panitumumab-IRDye800CW and cetuximab-IRDye800CW for fluorescence-guided surgical navigation in head and neck cancers. Theranostics 2018;8:2488–95.
22. Heath CH, Deep NL, Sweeny L, Zinn KR, Rosenthal EL. Use of panitumumab-IRDye800 to image microscopic head and neck cancer in an orthotopic surgical model. Ann Surg Oncol 2012;19:3879–87.
23. Bernhard W, El-Sayed A, Barreto K, Gonzalez C, Hill W, Parada AC, et al. Near infrared fluorescence imaging of EGFR expression in vivo using IRDye800CW-nimotuzumab. Oncotarget 2017;9:6213–27.
24. Giusti RM, Shastri KA, Cohen MH, Keegan P, Pazdur R. FDA drug approval summary: panitumumab (Vectibix). Oncologist 2007;12:577–83.
25. Jakobovits A, Amado RG, Yang X, Roskos L, Schwab G. From XenoMouse technology to panitumumab, the first fully human antibody product from transgenic mice. Nat Biotechnol 2007;25:1134.
26. Padfield E, Ellis HP, Kurian KM. Current therapeutic advances targeting EGFR and EGFRvIII in glioblastoma. Front Oncol 2015;5:5.
27. Brennan Cameron W, Verhaak Roel GW, McKenna A, Campos B, Noushmehr H, Salama Sofie R, et al. The somatic genomic landscape of glioblastoma. Cell 2013;155:462–77.
28. Warram JM, de Boer E, Korb M, Hartman Y, Kovar J, Markert JM, et al. Fluorescence-guided resection of experimental malignant glioma using cetuximab-IRDye 800CW. Br J Neurosurg 2015;29:850–8.
29. Han X, Zhang W, Yang X, Wheeler CG, Langford CP, Wu L, et al. The role of Src family kinases in growth and migration of glioma stem cells. Int J Oncol 2014;45:302–10.
30. Asher SA, Peters GE, Pehler SF, Zinn K, Newman JR, Rosenthal EL. Fluorescent detection of rat parathyroid glands via 5-aminolevulinic acid. Laryngoscope 2008;118:1014–8.
31. Golub D, Hyde J, Dogra S, Nicholson J, Kirkwood KA, Gohel P, et al. Intraoperative MRI versus 5-ALA in high-grade glioma resection: a network meta-analysis. J Neurosurg 2020;1–15. doi: 10.3171/2019.12.JNS191203.
32. Bettag C, Hussein A, Behme D, Maragkou T, Rohde V, Mielke D. Endoscopic fluorescence-guided resection increases radicality in glioblastoma surgery. Oper Neurosurg 2020;18:41–6.
33. Schipmann S, Muther M, Stogbauer L, Zimmer S, Brokinkel B, Holling M, et al. Combination of ALA-induced fluorescence-guided resection and intraoperative open photodynamic therapy for recurrent glioblastoma: case series on a promising dual strategy for local tumor control. J Neurosurg 2020:1–11. doi: 10.3171/2019.11.JNS192443.
34. Bhattacharyya S, Patel N, Wei L, Riffle LA, Kalen JD, Hill GC, et al. Synthesis and biological evaluation of panitumumab-IRDye800 conjugate as a fluorescence imaging probe for EGFR-expressing cancers. MedChemComm 2014;5:1337–46.
35. de Boer E, Warram JM, Tucker MD, Hartman YE, Moore LS, de Jong JS, et al. In vivo fluorescence immunohistochemistry: localization of fluorescently labeled cetuximab in squamous cell carcinomas. Sci Rep 2015;5:10169.
36. Ruopp MD, Perkins NJ, Whitcomb BW, Schisterman EF. Youden Index and optimal cut-point estimated from observations affected by a lower limit of detection. Biom J 2008;50:419–30.
37. Hanley JA, McNeil BJ. A method of comparing the areas under receiver operating characteristic curves derived from the same cases. Radiology 1983;148:839–43.
38. Taketani S, Inazawa J, Abe T, Furukawa T, Kohno H, Tokunaga R, et al. The human protoporphyrinogen oxidase gene (PPOX): organization and location to chromosome 1. Genomics 1995;29:698–703.
39. Kreth FW, Thon N, Simon M, Westphal M, Schackert G, Nikkhah G, et al. Gross total but not incomplete resection of glioblastoma prolongs survival in the era of radiochemotherapy. Ann Oncol 2013;24:3117–23.
40. Stummer W, Reulen HJ, Meinel T, Pichlmeier U, Schumacher W, Tonn JC, et al. Extent of resection and survival in glioblastoma multiforme: identification of and adjustment for bias. Neurosurgery 2008;62:564–76.
41. Schucht P, Beck J, Abu-Isa J, Andereggen L, Murek M, Seidel K, et al. Gross total resection rates in contemporary glioblastoma surgery: results of an institutional protocol combining 5-aminolevulinic acid intraoperative fluorescence imaging and brain mapping. Neurosurgery 2012;71:927–35.
42. Davis ME. Glioblastoma: overview of disease and treatment. Clin J Oncol Nurs 2016;20:S2–S8.
43. Zhao S, Wu J, Wang C, Liu H, Dong X, Shi C, et al. Intraoperative fluorescence-guided resection of high-grade malignant gliomas using 5-aminolevulinic acid-induced porphyrins: a systematic review and meta-analysis of prospective studies. PLoS One 2013;8:e63682.
44. Barone DG, Lawrie TA, Hart MG. Image guided surgery for the resection of brain tumours. Cochrane Database Syst Rev 2014;2014:CD009685.
45. Johansson A, Palte G, Schnell O, Tonn J-C, Herms J, Stepp H. 5-Aminolevulinic acid-induced protoporphyrin IX levels in tissue of human malignant brain tumors. Photochem Photobiol 2010;86:1373–8.
46. Eleouet S, Rousset N, Carre J, Vonarx V, Vilatte C, Louet C, et al. Heterogeneity of delta-aminolevulinic acid-induced protoporphyrin IX fluorescence in human glioma cells and leukemic lymphocytes. Neurol Res 2000;22:361–8.
47. Stepp H, Stummer W. 5-ALA in the management of malignant glioma. Lasers Surg Med 2018;50:399–419.
48. Nagaya T, Nakamura YA, Choyke PL, Kobayashi H. Fluorescence-guided surgery. Front Oncol 2017;7:314.
49. Rosenthal EL, Warram JM, de Boer E, Chung TK, Korb ML, Brandwein-Gensler M, et al. Safety and tumor specificity of cetuximab-IRDye800 for surgical navigation in head and neck cancer. Clin Cancer Res 2015;21:3658–66.
50. Zinn KR, Korb M, Samuel S, Warram JM, Dion D, Killingsworth C, et al. IND-directed safety and biodistribution study of intravenously injected cetuximab-IRDye800 in cynomolgus macaques. Mol Imaging Biol 2015;17:49–57.
51. Peng X, Draney DR, Volcheck WM, Bashford GR, Lamb DT, Grone DL, et al. Phthalocyanine dye as an extremely photostable and highly fluorescent near-infrared labeling reagent. In: Proceedings of SPIE BiOS, 2006 Feb 14; San Jose, CA.
52. DeLong JC, Lwin TM, Kiyuna T, Murakami T, van Dam GM, Yazaki PJ, et al. Bevacizumab-IRDye800 is an effective alternative to anti-carcinoembryonic antigen (CEA) for labeling low CEA-expressing colorectal tumors. J Am Coll Surg 2017;225:S38.
53. Keereweer S, Sterenborg HJ, Kerrebijn JD, Van Driel PB, Baatenburg de Jong RJ, Lowik CW. Image-guided surgery in head and neck cancer: current practice and future directions of optical imaging. Head Neck 2012;34:120–6.
54. Park SH, Goo JM, Jo C-H. Receiver operating characteristic (ROC) curve: practical review for radiologists. Korean J Radiol 2004;5:11–8.
55. Hirschberg H, Uzal FA, Chighvinadze D, Zhang MJ, Peng Q, Madsen SJ. Disruption of the blood-brain barrier following ALA-mediated photodynamic therapy. Lasers Surg Med 2008;40:535–42.
56. Zhou Q, Wilson C, Vogel H, Teraphongphom N, Ertsey R, Chu P, et al. Reversible blood-brain barrier modulation enhances in vivo delivery of panitumumab-IRDye800 to high-grade glioma in cranial window model (conference presentation). In: Proceedings of SPIE BiOS, 2019 March 4; San Francisco, CA.
57. Lampson LA. Monoclonal antibodies in neuro-oncology: getting past the blood-brain barrier. MAbs 2011;3:153–60.

Published OnlineFirst June 30, 2020; DOI: 10.1158/1535-7163.MCT-19-0819

Molecular Cancer Therapeutics

Comparison of Panitumumab-IRDye800CW and 5-Aminolevulinic Acid to Provide Optical Contrast in a Model of Glioblastoma Multiforme

Tiara S. Napier, Neha Udayakumar, Aditi H. Jani, et al.

Mol Cancer Ther 2020;19:1922-1929. Published OnlineFirst June 30, 2020.

SUPPLEMENTARY MATERIAL

Supplementary Materials and Methods

Cell lines and cell culture

Human GBM cell lines and animal models were maintained and generated by the UAB Brain Tumor Animal Models Core Facility. D-54MG (D54 cells) and U-251MG (U251 cells) were gifts from Darell D. Bigner (Duke University, Durham NC), and U-87MG (U87 cells) was obtained from the American Tissue Type Collection (Manassas, VA). Cell lines were genetically modified with a luciferase-expressing construct (Addgene, Cambridge, MA). Cells were cultured as adherent monolayers in Dulbecco's Modified Eagle's Medium supplemented with 10% fetal bovine serum and prophylactic plasmocin. Experiments with cell lines were performed within 10-12 months of thawing frozen stocks. Cell line authentication analyses were not performed during the time of these studies. For *in vitro* NIRF activation studies, cells were seeded in 96-well plates at 5,000-40,000 cells/well 1-2 days before the experiment. For immunocytochemistry, Western blot, and gel zymography analyses, cells were seeded near confluency in 12-well or 6-well plates the day before the experiment.

Western blot

Adherent monolayers of glioma cells were rinsed 2x with ice-cold PBS and lysed with RIPA buffer containing protease inhibitors on ice for 5 min. The supernatants were clarified by centrifugation at 4 °C, analyzed for protein concentration, aliquoted, and frozen at -20 °C until use. Cell lysates (20-25 μg) were separated by SDS-PAGE and transferred to a PVDF membrane. Membranes were blocked with 3% BSA in TBST, probed with primary antibodies overnight at 4 °C (1/2000 dilution for anti-MMP-14 mAb, Abcam ab51074; 1/1000 dilution for anti-MMP-2 antibody, Abcam ab37150; 1/2000 dilution for anti-β-actin antibody, Santa Cruz Biotechnology sc-47778), rinsed, probed with HRP-conjugated secondary antibody (Santa Cruz Biotechnology sc-2004, 1/1000 dilution), rinsed, and visualized by enzymatic chemical luminescence substrate (ECL) through exposure to X-ray film. Relative band intensities on the developed film were quantified by ImageJ. The experiment was performed in triplicate.

Animal subjects and husbandry, and *in vivo* tumor xenografts

Animal studies were approved by the University of Alabama at Birmingham Institutional Animal Care and Use Committee (20366) and performed in compliance with guidelines from the Public Health Service Policy and Animal Welfare Act of the United States. 5-8 week old female athymic nude mice from Envigo (Indianapolis, IN) or from Charles River (Wilmington, MA) were used for all *in vivo* studies. Standard show and water was available *ad libitum.* All *i.v.* injections were performed *via* the lateral tail vein. For NIRF imaging of flank GBM xenografts, anesthetized mice were implanted *s.c.* in the right hind flank with 2 million D54 or U87 cells (n=5 mice per tumor type). NIRF imaging experiments with the MMP-14 peptide probes were performed 3-4 weeks later, when tumors were 5-8 mm in diameter. Orthotopic PDX GBM xenografts were generated as previously described [1]. Briefly, PDX JX12 tumors passaged in the flanks of athymic nude mice were harvested and dissociated into single cell suspensions. Anesthetized mice were implanted intracranially with 500,000 dissociated PDX tumor cells (5 μL methylcellulose suspension) 2 mm anterior and 1 mm lateral to the bregma at a depth of 2 mm over 2 min. Mice were monitored until fully recovered from anesthesia. Imaging and biodistribution studies were performed 13-17 days after PDX tumor cell implantation. Mice were anesthetized with isoflurane during all live imaging procedures.

General chemistry methods

All chemicals were purchased from commercial sources (such as Aldrich, Synpeptide). Commercially available reagents were used without further purification, unless noted otherwise. All chemicals were reagent grade or better. The rink amide MBHA resin (100-200 mesh) was purchased from Millipore Sigma. The peptides were synthesized according to standard solid-phase peptide synthesis (SPPS); The NHS ester or maleimide coupling reactions were according to thermos fisher scientific coupling protocols. MALDI-MS spectrometric analyses were performed at the Mass Spectrometry Facility of Stanford University. HPLC was performed on a Dionex HPLC System (Dionex Corporation) equipped with a GP50 gradient pump and an in-line diode array UV-Vis detector. A reversed-phase (RP) C18 (Phenomenax, 5 μm, 4.6x250 mm, 5 μm, 10x250 mm or 21.2x250 mm) column was used for analysis and semi-preparative purification. UV absorbance of the probe was recorded on an Agilent 8453 UV spectrophotometer. Fluorescence was recorded on a Fluoromax-3 spectrafluorometer (Jobin Yvon). Unless noted, the compounds were analyzed by RP-HPLC (1 mL/min flow rate) or purified by semi-preparative RP-HPLC (3 mL/min flow rate), using water containing 0.1% trifluoroacetic acid (TFA) (solvent A) and acetonitrile containing 0.1% TFA (solvent B) as the eluates, or using 50 mM pH 5.5 triethylammonium acetate buffer (solvent C) and acetonitrile (solvent D) as the eluates, according to the following gradient: 0-21 min linear gradient from 0% B (or D) to 50% B (or D), 21-25 min linear gradient to 100% B (or D), 25-27 min hold 100% B (or D), 27-31 min linear gradient to 0% B (or D) and equilibrate in 0% B (or D).

Synthesis of substrate peptide: The peptide 1 (Figure S2) was synthesized using rink amide MBHA resin (100-200 mesh) according to standard SPPS methods. Peptide X (1.27 mg, 1 μmol, 1 eq), IRDye800CW-maleimide (1.19 mg, 1 μmol, 1 eq) and 0.5 mL of pH 7.4 PBS buffer were combined in a 1 mL vial and stirred at room temperature for 2 h. Then the quencher QC-1-NHS ester (1.24 mg, 1 μmol, 1 eq) was added to solution and stirred overnight. The reaction was purified directly by semi-preparative RP-HPLC using solvents C and D as eluates to afford light blue substrate-peptide 2 (1.1 mg, 32%). >99% purity was achieved after purification. MS: calcd. for $C_{160}H_{205}ClN_{23}O_{43}S_9$ $[(M+H)^+]$: 3459.17; found Maldi-Tof MS: m/z 3460.32 (Figure S5).

Synthesis of binding peptide: The peptide 2 (Figure S3) was synthesized using rink amide MBHA resin (100-200 mesh) according to standard SPPS methods. Peptide Y (1.9 mg, 1 μmol, 1 eq), NOTA-maleimide (0.85 mg, 2 μmol, 2 eq) and 0.5 mL of pH 7.4 PBS buffer were combined in a 1 mL vial and stirred at room temperature for 2 h. The reaction was purified directly by semi-preparative RP-HPLC using solvents A and B as eluates to afford white binding peptide 1 (1.65 mg, 71%). >99% purity was achieved after purification. MS: calcd. for $C_{105}H_{157}N_{34}O_{26}S$ [$(M+H)^+$]: 2342.16; found Maldi-Tof MS: m/z 2342.30 (Figure S6).

Synthesis of substrate-binding peptide: To a 1 mL glass vial was added 0.34 mg of substrate peptide (~0.1 μmol), 150 μL of pH 7.4 PBS buffer, 100 μL of *N,N*-dimethylformamide, 0.46 mg of binding peptide (~0.2 μmol), a premixed solution of 25 μL of 20 mM $CuSO_4$ and 50 μL of 50 mM THPTA (tris(3-hydroxypropyltriazolylmethyl)amine), 100 μL of 500 mM sodium ascorbate, and 100 μL of 500 mM aminoguanidine hydrochloride. The vial was capped tightly and stirred at room temperature for 1 h. Excess EDTA was added to the stirred solution and then the mixture was purified directly by preparative RP-HPLC using solvents C and D as eluates to afford the substrate-binding peptide (0.31 mg, 54%). >99% purity was achieved after purification. MS: calcd. for $C_{265}H_{361}ClN_{57}O_{69}S_{10}$ [$(M+H)^+$]: 5800.33; found Maldi-Tof MS: m/z 5803.03 (Figure S7).

Radiolabeling and radio HPLC analyses

Radioactive RP-HPLC analyses were performed on an Agilent 200 liquid chromatography system outfitted with an Agilent Zorbax SB-C18 RP-HPLC column (3x250 mm, 5 μm particle size) and a matching guard cartridge (3x7 mm). Gradient elutions at a flow rate of 0.5 mL/min were performed with solvent A and solvent D according to the following method: 0-15 min linear gradient from 90% A/10% B to 60% A/40% B, 15-17 min linear gradient to 5% A/95% B, 17-20 min hold at 5% A/95% B, 20 min return to 90% A/10% B and equilibrate. UV-Vis was monitored at 254 and 775 nm. An attached radiodetector (model 105-S, Carroll & Ramsey Associates) was used to monitor elution of radioactive compounds.

^{68}Ga-binding peptide: 135 MBq ^{68}Ga eluate (0.18 mL) in a screw-cap vial was adjusted to pH ~4.5 with 2 M NaOH and 1 M sodium acetate. To this solution (0.2 mL) was added 7.5 nmol binding peptide and the solution was heated at 90 °C for 20 min, after which it was cooled on ice and an aliquot was analyzed by radio RP-HPLC (Supplementary Figure S5). Aliquots of the crude radiolabeling reaction were diluted with PBS, or with PBS containing 50 nmol unlabeled binding peptide (block dose), to give 0.2 mL (2.2-4.5 MBq) per mouse dose. Molar activity at the time of dosing was approximately 6.1 GBq/μmol (non-blocked group).

^{64}Cu-substrate-binding peptide: 198 MBq ^{64}Cu (7 μL), 0.5 M pH 6.0 sodium acetate buffer containing 1% gentisic acid (50 μL), acetonitrile (25 μL), and 5 nmol substrate-binding peptide were combined in a plastic microcentrifuge tube. After sitting at room temperature for 20 min, and aliquot was analyzed by radio RP-HPLC (Supplementary Figure S9). Nitrogen gas was blown into the reaction tube for 20 min to evaporate residual acetonitrile, and aliquots of the residual crude solution were diluted with PBS containing 4.3% EtOH, or with PBS containing 4.3% EtOH and 22 nmol unlabeled binding peptide (block dose), to give 0.2 mL (6.3-6.5 MBq) per mouse dose. Molar activity at time of dosing was approximately 46.6 GBq/μmol (non-blocked group).

Supplementary Figures

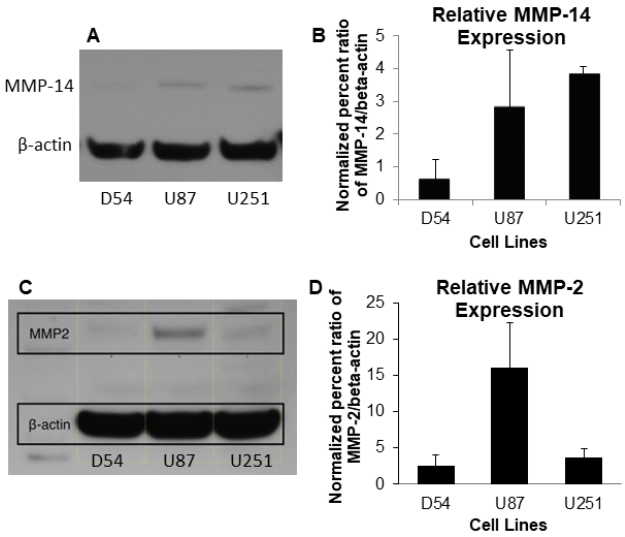

Figure S1. Western blots of MMP-14 (A) or MMP-2 (C) with quantification of respective blot intensities (B,D) from lysates of adherent GBM cells grown *in vitro* (average±SD, n=3/group).

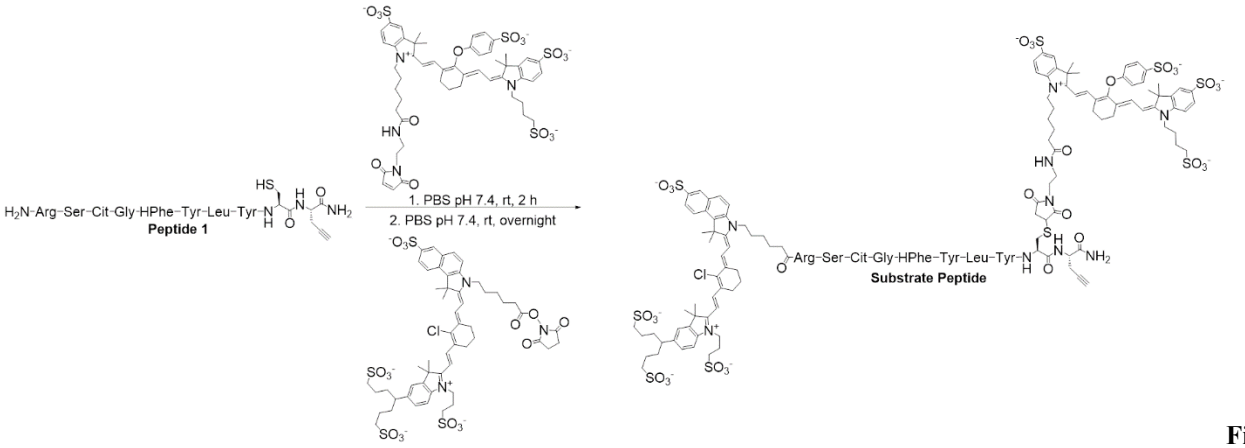

Figure S2. Synthetic scheme and structure of MMP-14 substrate peptide.

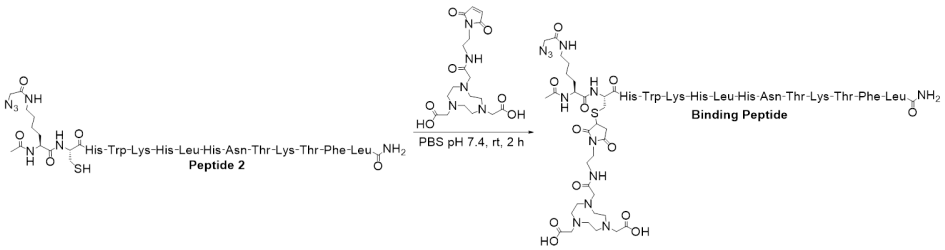

Figure S3. Synthetic scheme and structure of MMP-14 binding peptide.

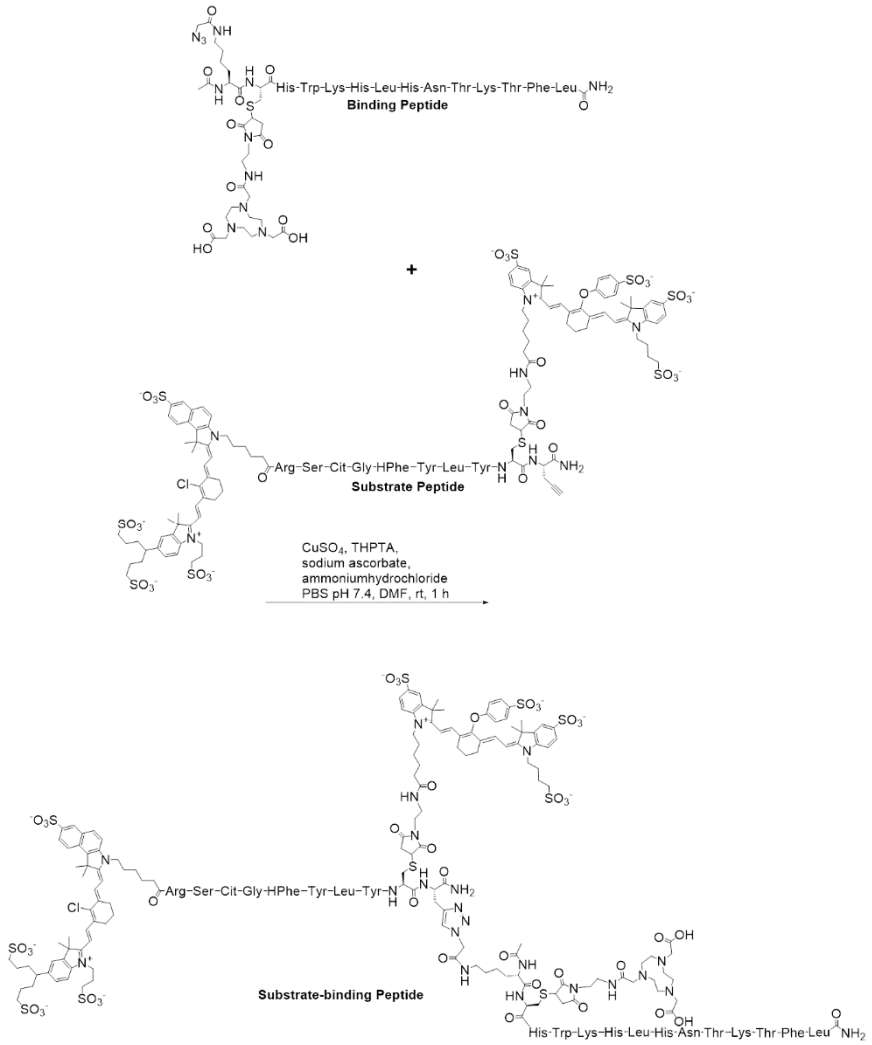

Figure S4. Synthetic scheme and structure of MMP-14 substrate-binding peptide.

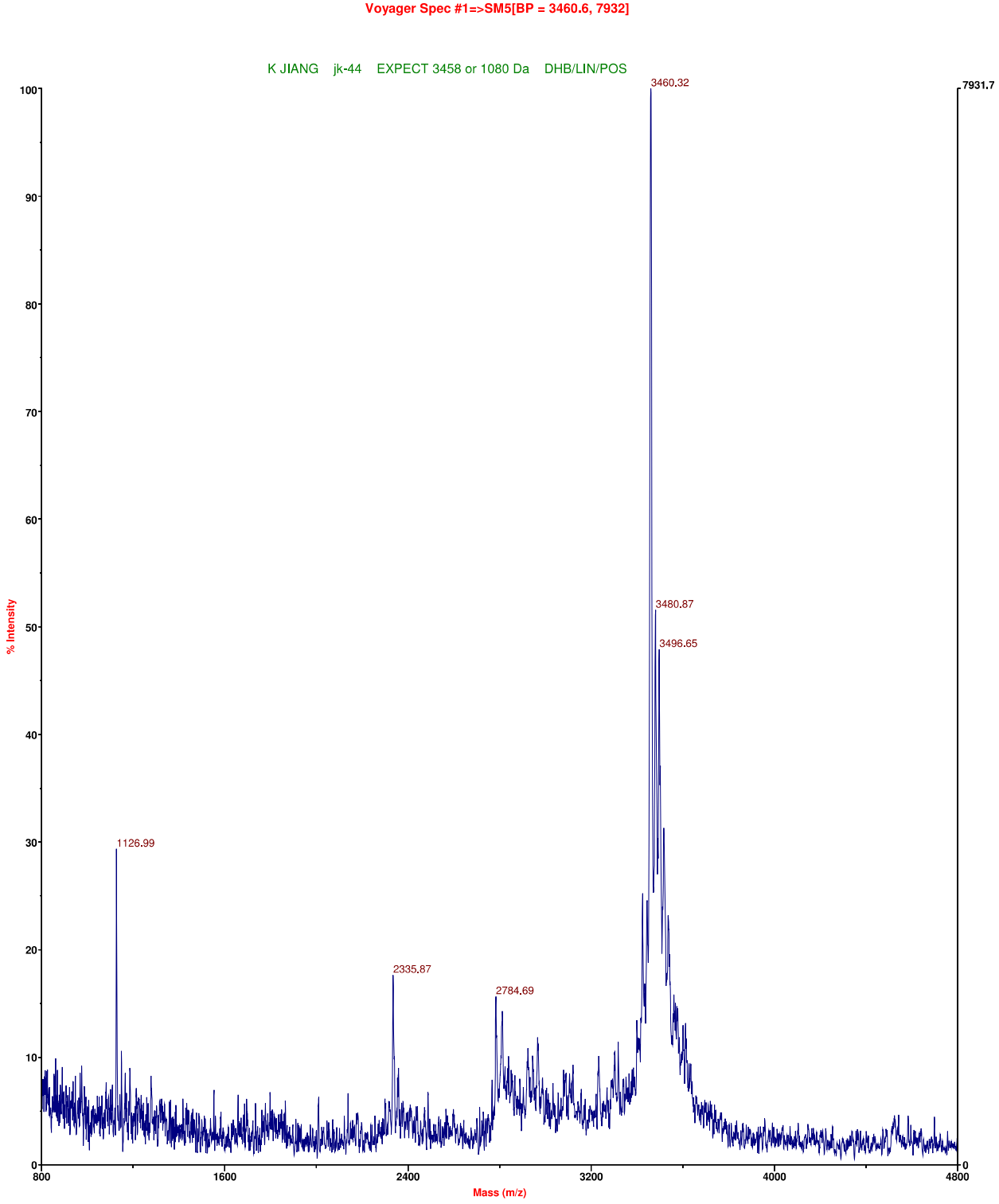

K JIANG jk-44 EXPECT 3458 or 1080 Da DHB/LIN/POS
C:\...\jk-44_0002.dat
Acquired: 14:57:00, February 13, 2018

Figure S5. Maldi-Tof MS spectrum of substrate peptide.

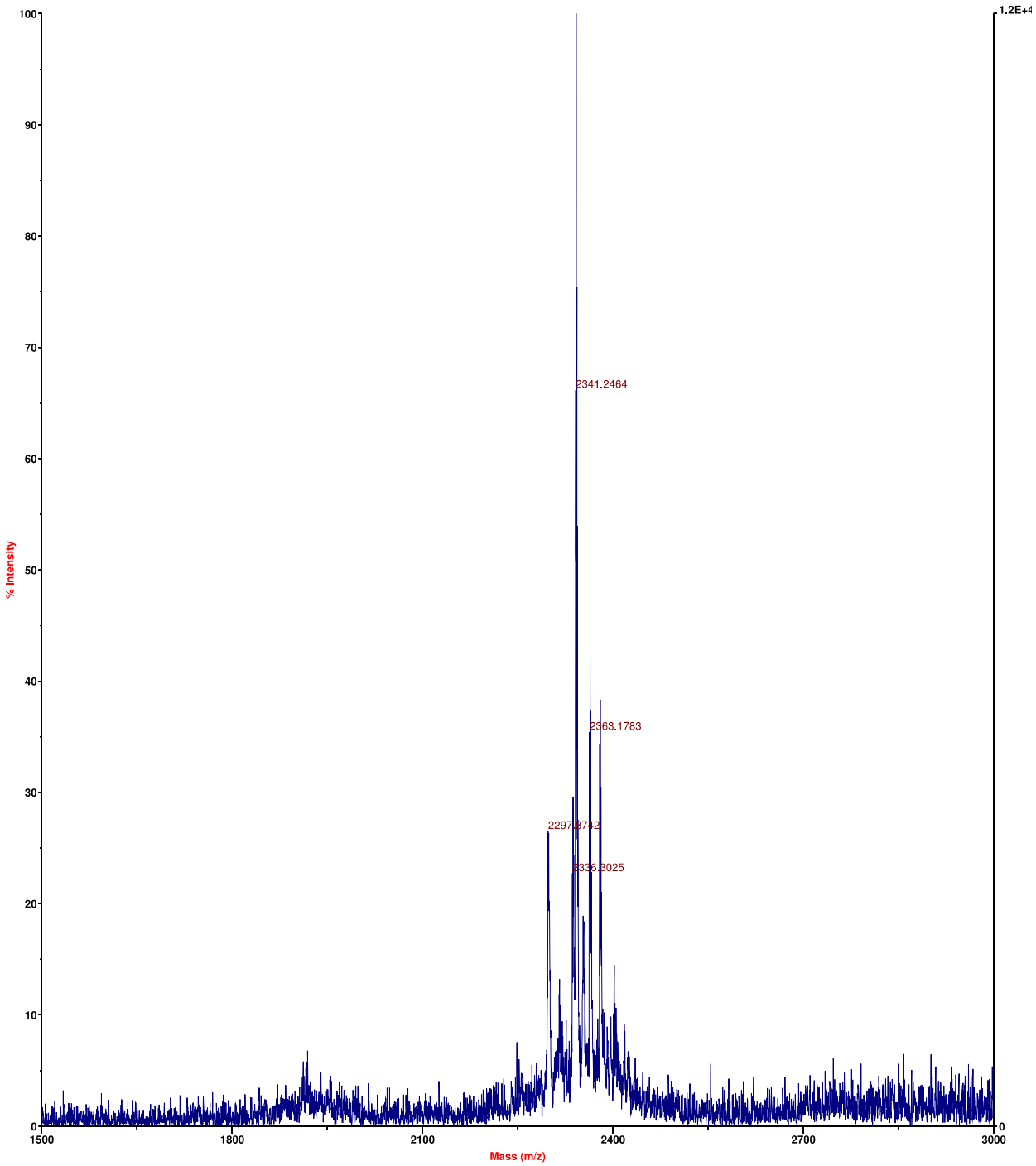

J Kiang jk-27 Expect 2341 Da DHB/ref/pos
C:\...\jk-27_0002.dat
Acquired: 12:57:00, July 14, 2016

Figure S6. Maldi-Tof MS spectrum of binding peptide.

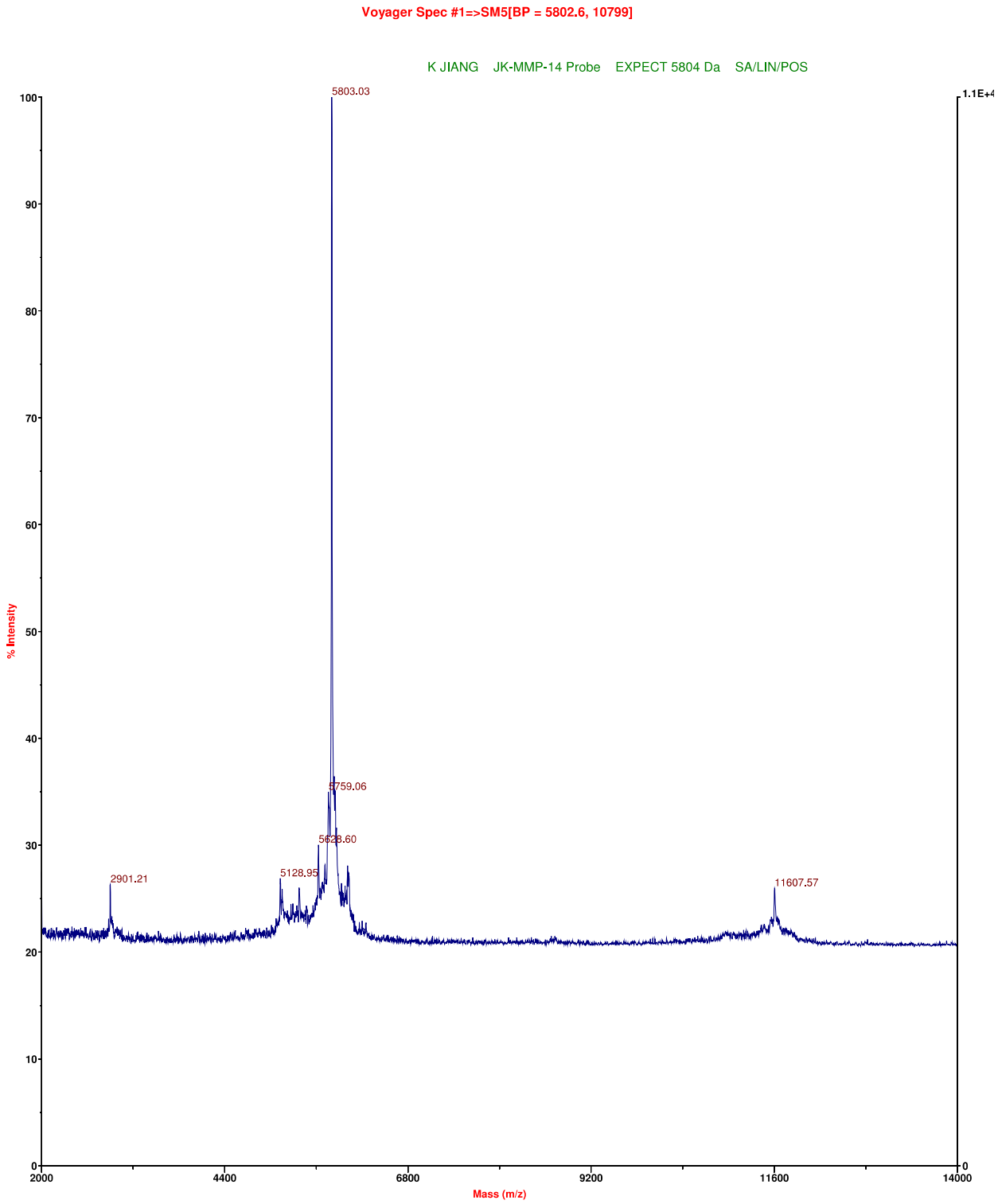

K JIANG JK-MMP-14 Probe EXPECT 5804 Da SA/LIN/POS
C:\...\JK-MMP-14 Probe_0002.dat
Acquired: 13:54:00, March 06, 2018

Figure S7. Maldi-Tof MS spectrum of substrate-binding peptide.

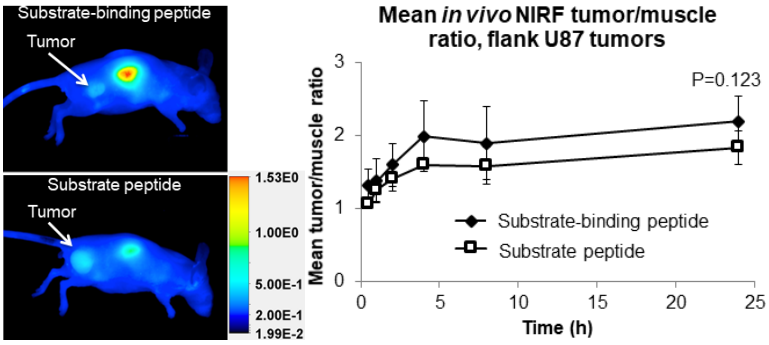

Figure S8. Mice bearing *s.c.*U87 xenografts were injected *i.v.* with 10 nmol of the substrate peptide or the substrate-binding peptide (n=5 mice/group) and imaged from 0-24 h on a Pearl imaging system (LI-COR). Left, representative *in vivo* NIRF images of mice at the 24 h time point after injection of the substrate-binding peptide (top) or the substrate peptide (bottom). Tumors are indicated by arrows. Right, mean *in vivo* NIRF tumor/muscle ratios at various time points (0.5-24 h) after injection of the substrate-binding peptide. No significant difference in NIRF tumor/muscle ratios between groups of mice was observed (p=0.123 at 24 h p.i.).

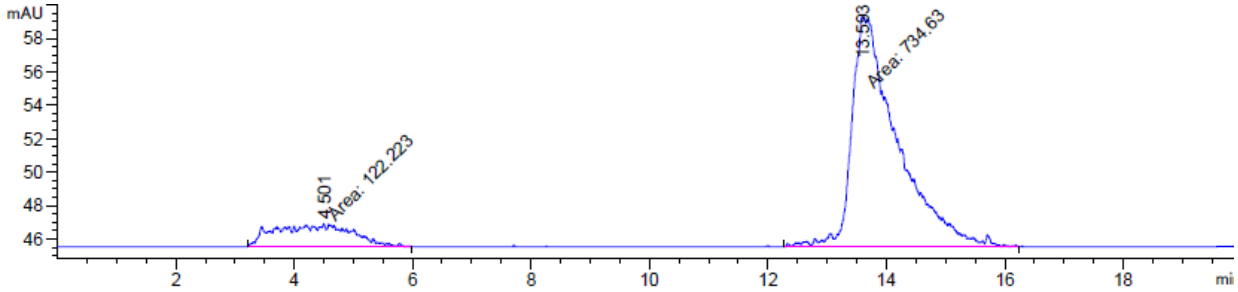

Figure S9. Radio RP-HPLC analysis of ^{68}Ga-binding peptide reaction. Product retention time: 13.6 min. Retention time of the non-labeled binding peptide: 13.4 min.

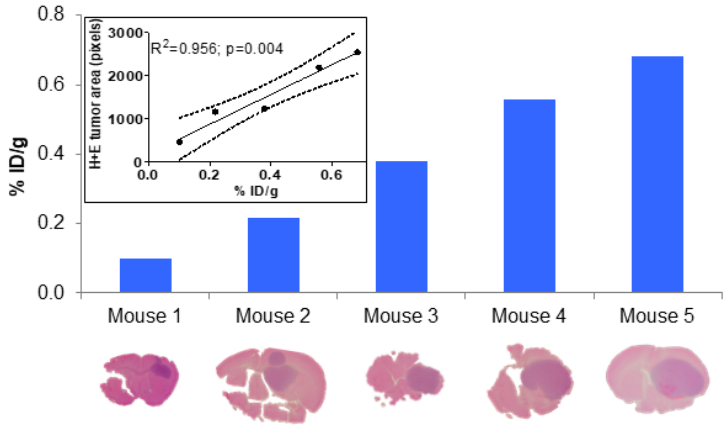

Figure S10. Correlation between the activity of ^{68}Ga-binding peptide in brains of mice bearing orthotopic PDX JX12 GBM tumors and tumor size. Athymic nude mice (n=5) with orthotopic PDX JX12 GBM tumors were injected *i.v.* with the ^{68}Ga-labeled binding peptide (4.4-9.6 MBq, 5.8 nmol peptide), imaged by PET/CT at 1 h, and euthanized for biodistribution analyses at 1.5 h *p.i.* The graph shows the % injected dose per gram (%ID/g) of radioactivity in individual mouse brains after resection. Inset, correlation between %ID/g in resected brains and quantification of tumor area in H+E stained sections (5 µm) containing the widest tumor diameter (as shown in lower panels). Tumor area was quantified in ImageJ by calculating the pixel area from pictures of H+E stained sections.

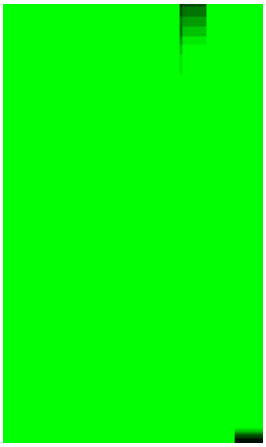

Figure S11. Representative maximum intensity projection PET/CT image of a mouse bearing an orthotopic PDX JX12 GBM tumor at 2 h after *i.v.* injection of ^{68}Ga-binding peptide. (PET SUV scale 0.1 to 3.0)

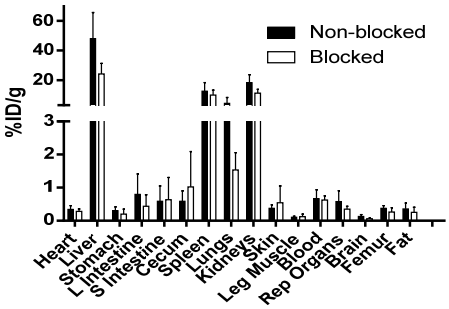

Figure S12. Biodistribution results (average±SD) of ^{68}Ga-binding peptide from resected tissues of mice bearing orthotopic PDX JX12 GBM tumors. Mice (n=5 mice for non-blocked group, n=4 mice for blocked group) were euthanized at 3.5 h *p.i.* of ^{64}Cu-substrate-binding peptide.

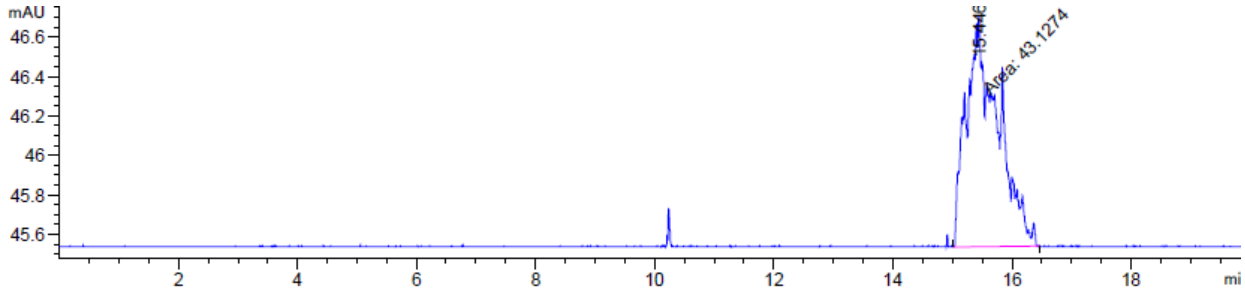

Figure S13. Radio RP-HPLC analysis of ^{64}Cu-substrate-binding peptide reaction. Product retention time: 15.4 min. Retention time of the non-labeled substrate-binding peptide: 15.3 min.

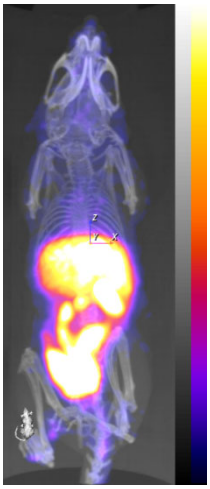

Figure S14. Representative maximum intensity projection PET/CT image of a mouse bearing an orthotopic PDX JX12 GBM tumor at 2 h after *i.v.* injection of ^{64}Cu-substrate-binding peptide. (PET SUV scale 0.25 to 3.15)

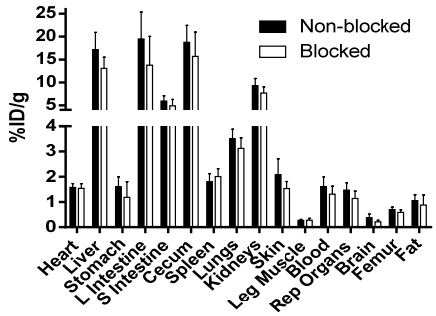

Figure S15. Biodistribution results (average±SD) of ^{64}Cu-substrate-binding peptide from resected tissues of mice bearing orthotopic PDX JX12 GBM tumors. Mice (n=8 mice for non-blocked group, n=7 mice for blocked group) were euthanized at 5.5 h *p.i.* of ^{64}Cu-substrate-binding peptide.

Table S1. *Ex vivo* NIRF signal (measured by the Odyssey scanner) metrics of positive predictive value, negative predictive value, sensitivity, and specificity from the substrate peptide or the substrate-binding peptide, relative to histologic verification of tumor (by H+E), measured in 5 μm sections of paraffin-embedded brain slices from mice bearing orthotopic PDX glioma tumors.

	Positive predictive value	**Negative predictive value**	**Sensitivity**	**Specificity**
Substrate peptide, 4 h	67.9%	100.0%	100.0%	58.3%
Substrate peptide, 24 h	50.0%	91.7%	83.3%	73.3%
Substrate-binding peptide, 4 h	85.7%	50.0%	85.7%	100.0%
Substrate-binding peptide, 24 h	83.3%	100.0%	100.0%	60.0%

Supplementary References

1. Warram, J. M.; de Boer, E.; Korb, M. L.; Hartman, Y. E.; Kovar, J.; Markert, J. M.; Gillespie, G. Y.; Rosenthal, E. L., Fluorescence-guided resection of experimental malignant glioma using cetuximab-IRDye 800CW. *British Journal of Neurosurgery* **2015,** *29* (6), 850-858.

MMP-14 as a noninvasive marker for PET and NIRF imaging of glioblastoma multiforme

Hailey Houson, Benjamin Kasten, Ke Jiang, Jianghong Rao, Jason Warram

Background: Glioblastoma multiforme (GBM) is a rapidly proliferating and invasive cancer originating from the glial cells of the brain. GBMs are diffuse, with indistinct tumor margins leading to incomplete surgical resection and subsequent recurrence. Matrix metalloproteinase 14 (MMP-14) is an enzyme that degrades the extracellular matrix. MMP-14 is highly expressed in GBM, and is involved in the invasion of the cancerous cells into the surrounding tissue. The primary treatment for GBM is surgery, with an increasing percentage of the tumor removed correlating to improved survival of the patient. However, current imaging of GBM pre-surgery is difficult to translate during surgery due to shift in the tissue. Combinatorial imaging of MMP-14 pre-surgery with PET and intra-operatively with near infrared fluorescence (NIRF) would allow for improved surgical resection of the tumor.
We have developed peptides to bind MMP-14, which are suitable for both PET and NIRF imaging.
Methods: Several peptide constructs were developed and used for imaging in mice bearing intracranial implants of patient derived xenograft GBMs. Construct 1 exhibited binding affinity to MMP-14, construct 2 was a substrate for MMP-14, and construct 3 was a combination of 1 and 2. Constructs 1 and 3 were labeled with ^{68}Ga or ^{64}Cu and used for PET imaging. Constructs 2 and 3 were fluorescent and were used for NIRF imaging.
Results: Immunohistochemistry showed the presence of MMP-14 in the tumor areas, which was co-localized with fluorescence signal from probes 2 and 3. Radiolabeled probes 1 and 3 showed accumulation in the tumor, which could be significantly reduced with the addition of non-labeled blocking peptides ($p<0.01$ and $p<0.05$ respectively). Additionally, in vivo PET and ex vivo NIRF was well correlated as shown using construct 3 ($R^2 = 0.80$).
Conclusions: All 3 constructs showed accumulation in the tumor area. Results warrant further investigation of probes in additional preclinical GBM models. Development of probes to image MMP-14 could improve noninvasive detection of the tumor area before surgery, guided tumor resection, and surveillance for recurrence.

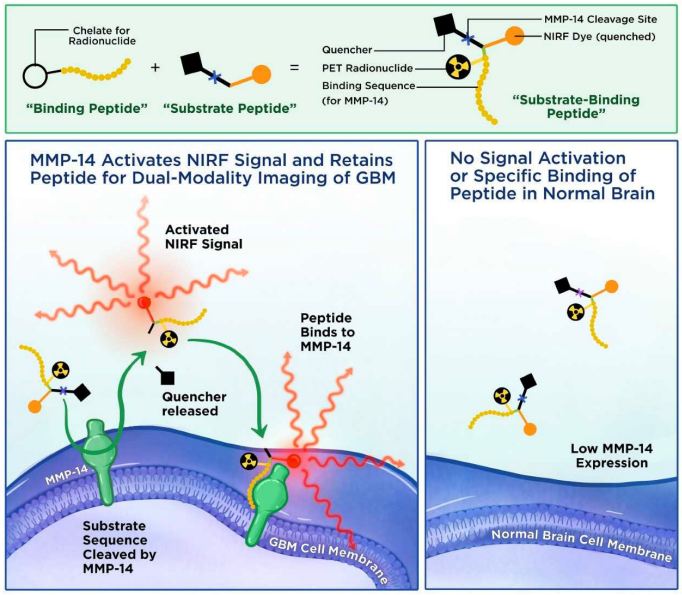

European Journal of Nuclear Medicine and Molecular Imaging (2020) 47:1412–1426
https://doi.org/10.1007/s00259-019-04607-x

ORIGINAL ARTICLE

Targeting MMP-14 for dual PET and fluorescence imaging of glioma in preclinical models

Benjamin B. Kasten[1] · Ke Jiang[2] · Denzel Cole[3] · Aditi Jani[4] · Neha Udayakumar[4] · G. Yancey Gillespie[1] · Guolan Lu[5] · Tingting Dai[2] · Eben L. Rosenthal[5] · James M. Markert[1] · Jianghong Rao[2] · Jason M. Warram[3]

Received: 14 August 2019 / Accepted: 7 November 2019 / Published online: 26 November 2019

Abstract

Purpose There is a clinical need for agents that target glioma cells for non-invasive and intraoperative imaging to guide therapeutic intervention and improve the prognosis of glioma. Matrix metalloproteinase (MMP)-14 is overexpressed in glioma with negligible expression in normal brain, presenting MMP-14 as an attractive biomarker for imaging glioma. In this study, we designed a peptide probe containing a near-infrared fluorescence (NIRF) dye/quencher pair, a positron emission tomography (PET) radionuclide, and a moiety with high affinity to MMP-14. This novel substrate-binding peptide allows dual modality imaging of glioma only after cleavage by MMP-14 to activate the quenched NIRF signal, enhancing probe specificity and imaging contrast.

Methods MMP-14 expression and activity in human glioma tissues and cells were measured in vitro by immunofluorescence and gel zymography. Cleavage of the novel substrate and substrate-binding peptides by glioma cells in vitro and glioma xenograft tumors in vivo was determined by NIRF imaging. Biodistribution of the radiolabeled MMP-14-binding peptide or substrate-binding peptide was determined in mice bearing orthotopic patient-derived xenograft (PDX) glioma tumors by PET imaging.

Results Glioma cells with MMP-14 activity showed activation and retention of NIRF signal from the cleaved peptides. Resected mouse brains with PDX glioma tumors showed tumor-to-background NIRF ratios of 7.6–11.1 at 4 h after *i.v.* injection of the peptides. PET/CT images showed localization of activity in orthotopic PDX tumors after *i.v.* injection of ^{68}Ga-binding peptide or ^{64}Cu-substrate-binding peptide; uptake of the radiolabeled peptides in tumors was significantly reduced ($p < 0.05$) by blocking with the non-labeled-binding peptide. PET and NIRF signals correlated linearly in the orthotopic PDX tumors. Immunohistochemistry showed co-localization of MMP-14 expression and NIRF signal in the resected tumors.

Conclusions The novel MMP-14 substrate-binding peptide enabled PET/NIRF imaging of glioma models in mice, warranting future image-guided resection studies with the probe in preclinical glioma models.

Keywords MMP-14 · Glioma · NIRF · PET · Molecular imaging · Dual modality

Benjamin B. Kasten and Ke Jiang contributed equally to this work.

This article is part of the Topical Collection on Preclinical Imaging

Electronic supplementary material The online version of this article (https://doi.org/10.1007/s00259-019-04607-x) contains supplementary material, which is available to authorized users.

✉ Jianghong Rao
jrao@stanford.edu

✉ Jason M. Warram
mojack@uab.edu

[1] Department of Neurosurgery, University of Alabama at Birmingham, Birmingham, AL 35294, USA

[2] Departments of Radiology and Chemistry, Molecular Imaging Program at Stanford, Stanford University School of Medicine, Stanford, CA 94305, USA

[3] Department of Otolaryngology, University of Alabama at Birmingham, Birmingham, AL 35294, USA

[4] School of Medicine, University of Alabama at Birmingham, Birmingham, AL 35294, USA

[5] Department of Otolaryngology – Head and Neck Surgery, Stanford University, Stanford, CA 94305, USA

Introduction

Malignant glioma is the most common and deadly primary brain malignancy in adults. The current standard of care, comprised of maximal safe surgical resection followed by radiochemotherapy, is associated with a median survival of less than 18 months [1]. Clinical trials are testing novel therapeutic strategies in attempts to improve the current prognosis of patients with glioma. Studies have shown that the extent of surgical resection correlates with patient outcomes [2, 3]. Unfortunately, malignant tissues are frequently difficult to differentiate from normal brain parenchyma, making complete surgical resection of all glioma while sparing vital healthy brain a significant clinical challenge. Developing agents that specifically target aggressive glioma cells for both non-invasive and intraoperative imaging is an attractive strategy to guide effective therapeutic intervention. Glioma is known for its invasive and diffuse growth pattern, which is indicative of matrix metalloproteinase (MMP) activity [4–7]. Activated MMP-14, also called MT1-MMP, is overexpressed in glioma while it is not expressed at significant levels in normal brain (cerebral) tissue. MMP-14 expression is known to increase with the grade of glioma and correlates with poor patient outcome [8–11]. Preclinical studies have demonstrated that MMP-14 can be exploited as a biomarker for molecular imaging of glioma with various non-invasive or intraoperative reporting modalities [12–14].

Non-invasive imaging of glioma patients through positron emission tomography (PET) with radiolabeled amino acid analogs has enabled preoperative planning for biopsy or surgery, mapping for radiotherapy, and assessing therapeutic response [15–22]. However, clinical PET suffers from low spatial resolution (> 3 mm) and does not permit real-time surgical guidance. Problems with brain shift further hamper co-registration of PET and anatomical images. While clinical PET complements the information from MRI [23], these modalities remain insufficient to guide real-time surgical resection of occult glioma. The US Food and Drug Administration (FDA) recently approved 5-aminolevulinic acid (5-ALA), which is converted into the fluorescent metabolite protoporphyrin IX (PpIX) in rapidly proliferating tumor cells (e.g., glioma), for fluorescence-guided surgical resection of glioma. Phase III trials have shown 5-ALA fluorescence-guided resection in glioma patients was well tolerated and mediated greater rates of complete resection compared to MRI alone [24, 25]. Nonetheless, the optical properties of PpIX are not ideal for in vivo imaging. Significant tissue autofluorescence and photon attenuation at the wavelengths of excitation (~ 405 nm) and emission (635 nm) reduce spatial resolution and tumor-to-background ratios (TBRs) associated with 5-ALA imaging of glioma [26–28]. Molecular imaging strategies that use near-infrared fluorescence (NIRF) reporters are attractive for in vivo imaging and fluorescence-guided resection due to the minimal tissue autofluorescence and significantly less photon attenuation in the NIR window (700–900 nm) [29–31]. Several molecular targeted compounds with NIRF reporters are currently being evaluated for resecting glioma in preclinical and clinical studies [14, 29, 30, 32–34].

The purpose of the present work was to design a novel, MMP-14-activatable dual PET/NIRF peptide probe for imaging and guiding resection of glioma (Fig. 1). The peptide probe combined (1) a NIRF reporter and quencher pair separated by a peptide sequence (MMP-14 "substrate peptide") that is cleaved specifically by activated MMP-14 to release the quencher and allow visualization of the NIRF dye and (2) a chelate for radionuclides attached to a peptide sequence that binds to MMP-14 (MMP-14 "binding peptide") and enables PET imaging. The following in vitro and in vivo studies tested the ability of these MMP-14-targeted imaging probes to detect preclinical models of human glioma. Glioma cells in vitro and orthotopic xenograft tumors in mice in vivo cleaved the substrate and the substrate-binding peptides to activate the NIRF signal of the initially quenched peptide probes, yielding favorable imaging contrast in tumors relative to the normal brain. In vivo PET/CT imaging showed notable activity in orthotopic glioma tumors relative to normal brain after *i.v.* injection of the radiolabeled-binding or substrate-binding peptides. PET and NIRF signals from the substrate-binding peptide correlated linearly in the orthotopic PDX tumors and co-localized with MMP-14 expression in the resected tumors. The results from these initial studies indicate the success of the proposed dual-modality imaging strategy to detect MMP-14 in glioma models with the first-generation substrate-binding peptide probe.

Results

Human glioma tumor tissues and cell lines express varying levels of MMP-14

Immunofluorescence staining of a human glioma tissue microarray was performed to determine the relative protein expression of MMP-14 in glioma and normal brain specimens. Consistent with previous reports [8–11], the immunofluorescence results showed significant overexpression of MMP-14 in all grades of glioma relative to normal cerebral tissue (1.6 ± 0.6, 2.2 ± 0.7, 2.5 ± 0.8, 3.0 ± 1.2 glioma/normal brain ratios for grade 1, grade 2, grade 3, and grade 4, respectively; $p < 0.05$), with highest expression in grade 4 glioma (Fig. 2A). Western blot, immunofluorescence, and gel zymography studies were then performed to characterize the in vitro expression and activity of MMP-14 and MMP-2 in immortalized human glioma cell lines. Absolute expression of MMP-14 does not necessarily correlate to MMP-14 activity, as the latter is regulated partly through tissue inhibitors of metalloproteinases (TIMPs). For instance, TIMP-2 binds to the catalytic domain

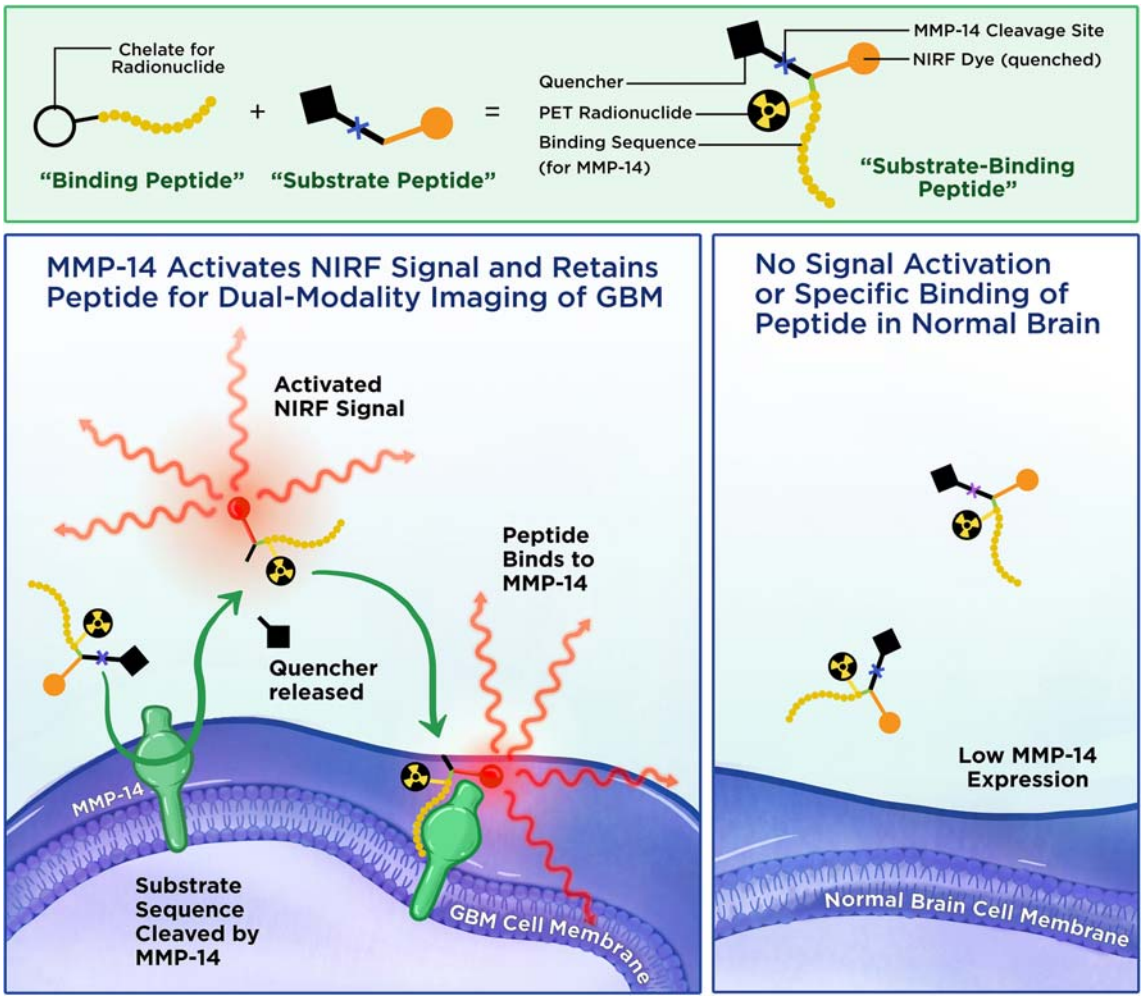

Fig. 1 Diagram showing general scheme for dual-modality PET/NIRF imaging of glioma (GBM) with an MMP-14 activatable peptide

of MMP-14, thus blocking enzymatic activity. TIMP-2 is also required in a ternary complex with MMP-14 and proMMP-2 prior to enzymatic cleavage by a second MMP-14 enzyme to activate MMP-2 [7]. U251 cells in our studies displayed the highest expression of MMP-14 by immunofluorescence (Fig. 2B) and Western blot analyses (Fig. S1A,B), while U87 cells displayed the highest level of MMP-14 activity as indirectly determined through gel zymography analyses of MMP-2 activity (Fig. 2C), which is catalyzed by MMP-14 as described [5, 35]. U87 cells showed the highest MMP-2 expression by Western blot (Fig. S1C,D). Although TIMP expression was not determined in our studies, the zymography assay confirmed MMP-14 activity in the glioma cells. These results indicate the cell lines would be suitable in assays that employ peptide probes as enzymatic substrates for MMP-14.

Description of the novel MMP-14 activatable peptide probes

We and others have used an MMP-14 substrate peptide sequence (RSCitG-HPhe-YLY) to generate peptide probes for imaging and therapy studies in human xenograft tumors that over-express MMP-14 [36–38]. For the present studies, this sequence was used between the NIRF IRDye800 and quencher IR QC-1 pair [39, 40] to generate the MMP-14 activatable NIRF substrate peptide (Supplementary Fig. S2). This strategy allows the initially quenched signal from IRDye800, which is suitable for NIRF imaging in vivo, to become activated upon cleavage of the peptide by MMP-14. For the second peptide component, an MMP-14-binding peptide sequence (HWKHLHNTKTFL) was selected that has previously been described with an apparent k_d of 47.4 nM for MMP-14 [41]. This binding peptide sequence has been joined to various reporting moieties and used in a rat orthotopic glioma model [12] as well as human xenograft tumors that overexpress MMP-14 [41–43]. For the present studies, a derivative of the NOTA (1,4,7-triazacyclononane-1,4,7-triacetic acid) chelate for coordination with ^{64}Cu(II) or ^{68}Ga(III) was attached to the peptide sequence to generate the MMP-14-binding peptide (Supplementary Fig. S3) for in vivo PET imaging of MMP-14 expression. The two peptide precursors were synthesized separately by standard solid phase synthesis, NHS, and

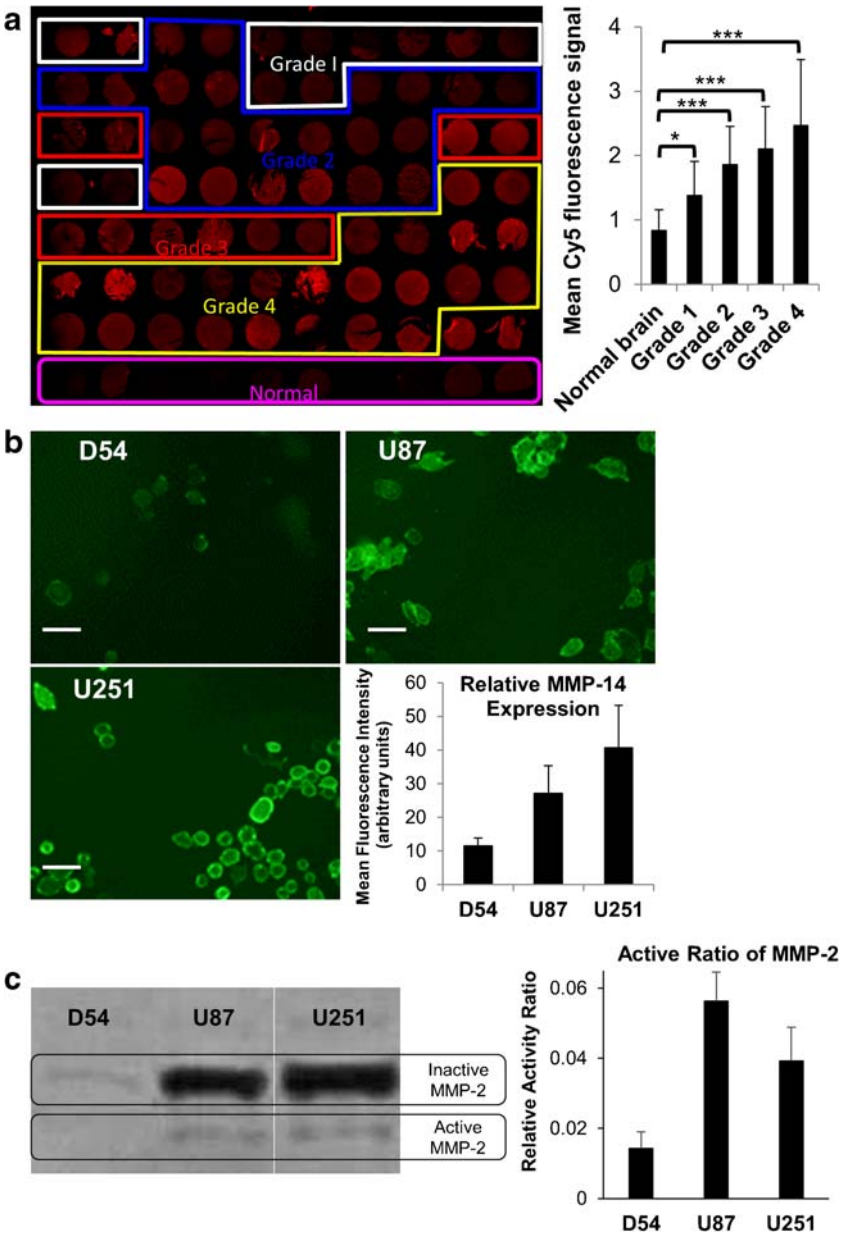

Fig. 2 Human glioma patient specimens and cell lines grown in vitro express different levels of MMP-14. **A** MMP-14 immunofluorescence (left) and quantification of fluorescence signal (right) in a human tissue microarray (mean ± SD, n = 10–24 tissue sections/group); **B** MMP-14 immunofluorescence of adherent GBM cells grown in vitro and quantification of fluorescence signal (bottom right; mean ± SD, n = 25–30/group); **C** MMP-2 gel zymography (left) and quantification of relative active/latent MMP-2 band intensity (right) from supernatants of adherent GBM cells grown in vitro (mean ± SD, n = 3/group); scale bar in B, 20 μm; *$p < 0.05$; ***$p < 0.001$

maleimide coupling reactions and then joined via a cycloaddition reaction between the azide and alkyne moieties present on the corresponding precursor peptides to generate the combined MMP-14 substrate-binding peptide (Supplementary Fig. S4). Mass spectroscopic analyses were consistent with the anticipated peptide structures (Supplementary Figs. S5, S6, S7).

MMP-14 and human glioma cells activate the NIRF signals of the MMP-14 peptide probes in vitro

With the novel MMP-14-targeted peptides in hand, in vitro NIRF activation studies with the catalytic domain of MMP-14 were performed. Previous studies have shown that appending fluorescence dyes or other moieties to the N- and C-termini of the core substrate peptide sequence does not abrogate cleavage of the peptide by MMP-14 [37, 44]. However, studies to date have not determined if incorporation of an MMP-14-binding ligand into the same scaffold as an MMP-14 substrate sequence affects cleavage of the substrate peptide by the enzyme.

As presented in Fig. 3A, both the substrate and the substrate-binding peptides showed NIRF activation over time relative to the quenched starting moieties during incubation with MMP-14. The relative NIRF activation of the substrate peptide appeared to stabilize within the first 10 min, while NIRF activation of the substrate-binding peptide continued to increase beyond 1 h. The fold of increase in the

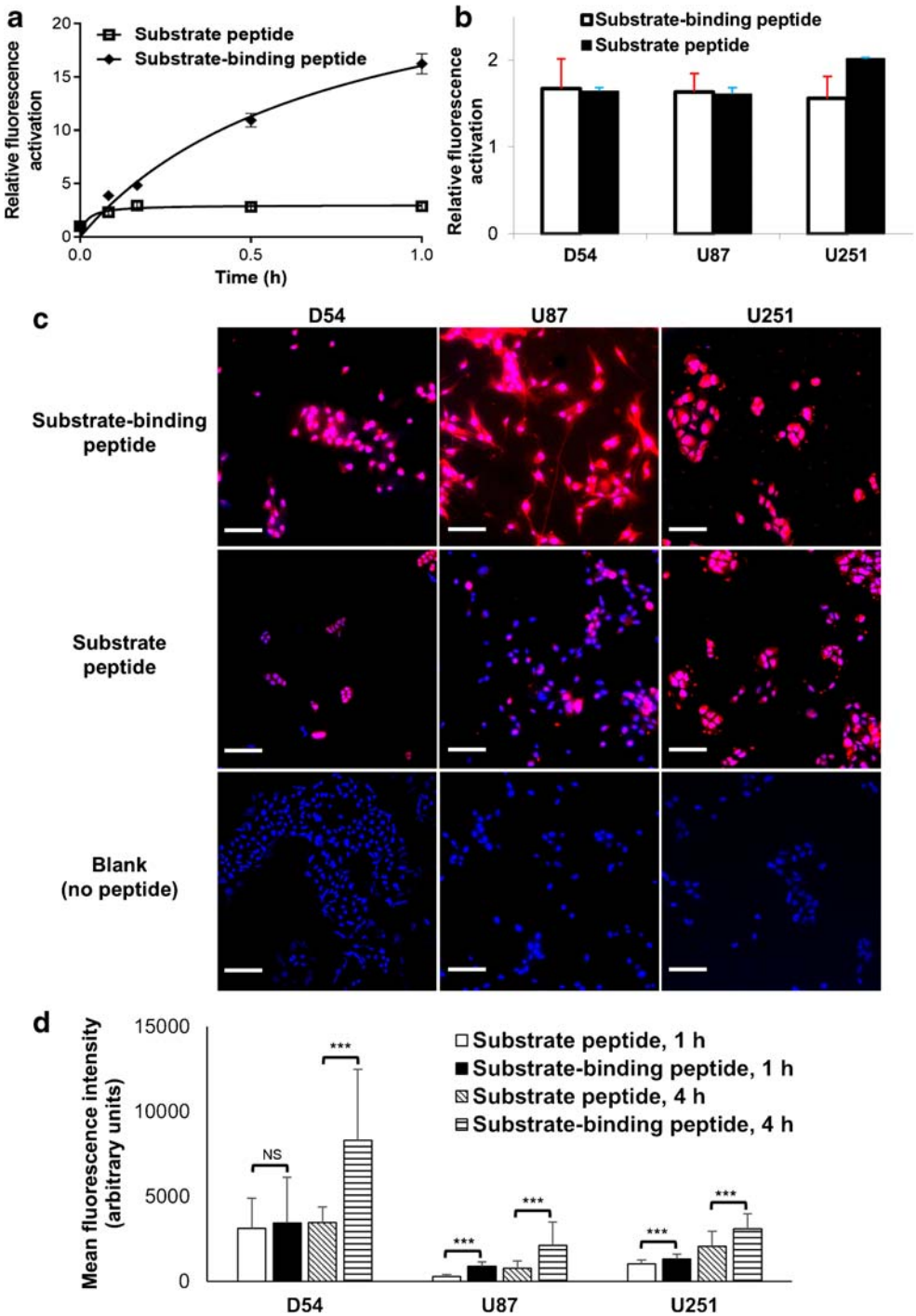

Fig. 3 Human MMP-14 enzyme and glioma cells activate the NIRF signals of the MMP-14 peptides in vitro. **A**, relative increase in NIRF activation at various time points (0–1 h) after incubating the substrate-binding peptide or the substrate peptide (0.5 μM) with the recombinant catalytic domain of MMP-14 at 37 °C. **B**, relative increase in NIRF activation released into the supernatant after incubating the substrate-binding peptide or the substrate peptide (0.5 μM) with human glioma cell lines (D54, U87, U251) at 37 °C for 2 h (mean ± SD, n = 2–4/group). **C**, NIRF microscopy showing the cell-associated NIRF signal (red) in glioma cells (D54, U87, U251) 1 h after incubation with the substrate-binding peptide (top), substrate peptide (middle), or buffer control without peptide (bottom); cell nuclei were counter-stained with DAPI (blue); scale bar: 50 μm. **D**, quantification of cell-associated NIRF signal at 1 or 4 h after incubating glioma cells in vitro with the substrate or substrate-binding peptide (mean ± SD, n = 30/group). ***$p < 0.001$; NS, not significant

fluorescence with the substrate-binding peptide was much higher than that with the substrate peptide. Based on these initial results, it is possible that the binding sequence may influence the kinetics of the substrate-binding peptide cleavage reaction by MMP-14.

NIRF signal activation of the substrate and substrate-binding peptides was apparent in supernatant solutions (Fig. 3B) and associated with the cells (Fig. 3C) during in vitro incubation with the glioma cell lines. Similar increases in NIRF intensities released into the supernatant were observed during incubation of the peptides with all three glioma cell lines (Fig. 3B) regardless of their relative expression of active MMP-14 (Fig. 2C). NIRF microscopy showed that U87 and U251 cells had significantly higher cell-associated mean NIRF signal at both 1 and 4 h after incubation with the substrate-binding peptide relative to the substrate peptide ($p < 0.001$) at the respective time points (Fig. 3D). In D54 cells, which had lower MMP-14 expression and activity relative to

the other cells (Fig. 2B,C), the cell-associated NIRF signal was significantly higher for the substrate-binding peptide compared to the substrate peptide at 4 h ($p < 0.001$) but not at 1 h ($p > 0.05$; Fig. 3D). These results are consistent with the anticipated mechanism of the substrate-binding peptide, where the MMP-14 binding moiety mediates cellular retention of the residual fluorophore-containing product following cleavage of the substrate sequence by MMP-14. The observed NIRF signal associated with cells incubated with the substrate peptide, which lacks the MMP-14-binding component, likely indicates nonspecific cell uptake of the substrate peptide or the fluorophore-containing product following cleavage by MMP-14. Collectively, these results indicate that glioma cells, including those with relatively low MMP-14 activity, are capable of cleaving the novel peptide substrates in vitro.

NIRF signals of the MMP-14 activatable peptide probes localize in human glioma xenografts in nude mice in vivo

Having confirmed that glioma cells activate the NIRF signal of the peptides in vitro, NIRF imaging studies were performed to determine if the peptide probes showed uptake in glioma xenograft tumors in vivo. At 24 h after *i.v.* injection of the substrate-binding peptide, in vivo NIRF imaging showed a low TBR (1.3 ± 0.2 relative to muscle) in subcutaneous (*s.c.*) D54 tumors and significantly higher TBR in *s.c.* U87 tumors (2.2 ± 0.4; $p < 0.001$) (Fig. 4A, B). Low NIRF signal was observed in all normal tissues except the kidneys (Fig. 4A), indicating predominantly renal clearance of the peptide. *S.c.* U87 tumors from groups of mice injected *i.v.* with either the substrate peptide or the substrate-binding peptide showed no significant difference in TBR or mean NIRF intensity at the 24 h time point (Supplementary Fig. S8). These initial studies demonstrated that glioma tumors show uptake of NIRF signal after administering the quenched peptide substrates. The moderate NIRF TBRs observed for the flank tumors could be due to endogenous expression of MMP-14 in the tissues surrounding the tumors (e.g., muscle, skin) [45].

NIRF imaging studies with the substrate or substrate-binding peptides were subsequently performed in mice bearing orthotopic patient-derived xenograft (PDX) glioma tumors. Relative to flank xenografts of immortalized cell lines, these orthotopic PDX tumors more accurately retain characteristics of clinical glioma [46, 47]. Furthermore, orthotopic tumors were anticipated to better demonstrate the signal contrast from the peptide probes in glioma tumors relative to the endogenous surrounding tissue (e.g., normal brain). The low expression of MMP-14 in normal brain was anticipated to result in a low background NIRF signal, resulting in a higher and more appropriate TBR in the orthotopic glioma tumor model than was observed in

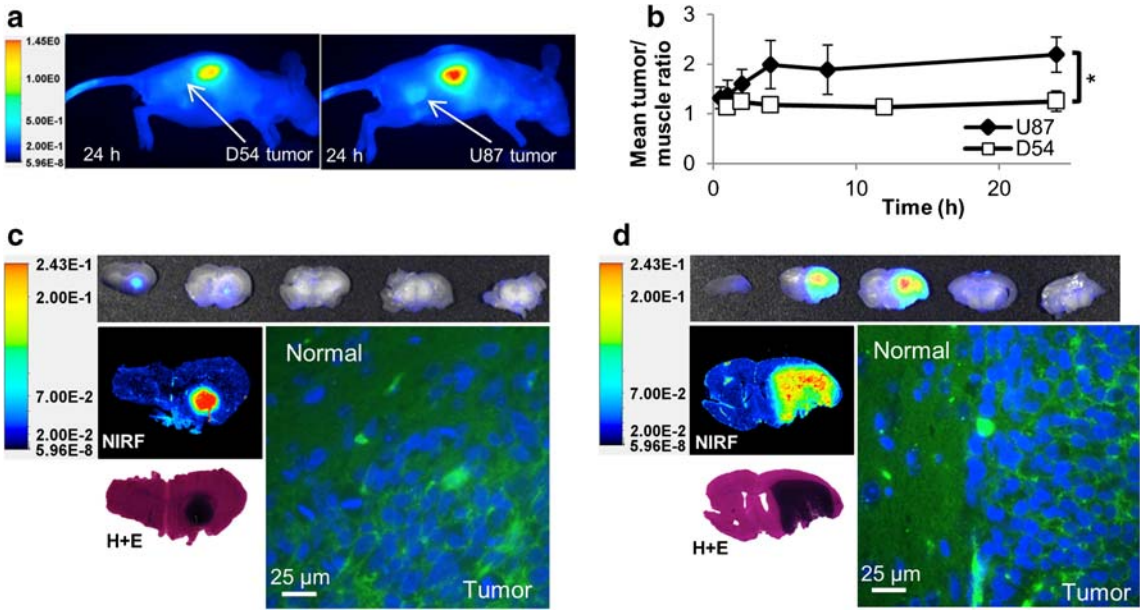

Fig. 4 NIRF signals from the MMP-14 peptide probes localize in human glioma xenograft tumors in mice in vivo. **A**, in vivo NIRF images of live mice bearing flank D54 or U87 glioma tumors at 24 h after *i.v.* injection of the substrate-binding peptide. **B**, mean in vivo tumor/muscle NIRF ratios at various time points (0.25–24 h) after injection of the substrate-binding peptide in mice bearing flank D54 or U87 glioma tumors (mean ± SD, n = 5 mice/group). **C**,**D**, mice bearing orthotopic PDX JX12 glioma tumors were injected *i.v.* either with the substrate peptide (C) or with the substrate-binding peptide (D). Mice were euthanized 1 h later, when the brains were resected, fixed in formalin overnight and serially sectioned (2 mm). Gross tissue NIRF imaging (Pearl system) showed localization of NIRF signals in the serial tumor-bearing sections (2 mm sections, top panels), as confirmed by higher resolution NIRF imaging (Odyssey system) of 5 μm tissue sections and H + E stained 5 μm tissue sections. NIRF microscopy of DAPI-stained tissue sections (5 μm, right panels, 630× magnification) showed NIRF signal accumulation (yellow channel) in the leading tumor edge but not adjacent normal brain (blue channel, DAPI). *$p < 0.05$

the flank tumor studies. High contrast of the NIRF signal in PDX JX12 tumors relative to adjacent normal brain was apparent in gross slices of resected brains at 1, 4, and 24 h after *i.v.* injection of either the substrate peptide (Fig. 4C) or the substrate-binding peptide (Fig. 4D). NIRF analyses of gross brain slices from the 4 and 24 h time points (Table 1) showed significantly higher ($p < 0.001$) mean NIRF signal in the tumor relative to adjacent normal brain from mice given the substrate-binding peptide. This result is consistent with retention of the cleaved peptide moiety containing the fluorophore within the tumor and low accumulation of the cleaved peptide in normal brain, which has negligible expression of MMP-14. The NIRF signal in the tumor was significantly higher than in normal brain of mice at 4 h ($p < 0.001$), but not at 24 h ($p = 0.074$), after injection of the substrate peptide. The group of mice analyzed at 24 h after injecting the substrate peptide had fewer evaluable tumors compared to the other groups, which could have impacted the statistical outcome of the NIRF signal comparison in these mice. While the NIRF mean tumor signals and TBRs were higher in mice given the substrate-binding peptide relative to the substrate peptide (Table 1), the TBRs were not significantly different at the time points examined ($p > 0.05$, ANOVA). NIRF microscopy showed dispersion of the activated NIRF signal from the peptides throughout the tumors, including near the leading edge of tumor progression (Figs. 4C, D). Both peptides also yielded positive NIRF signals in regions of diffuse glioma cell growth beyond the bulk tumor (data not shown). Comparing histological tissue sections with confirmed glioma growth by H + E to NIRF signals measured in tissue sections yielded sensitivities above 83% for the substrate peptide and above 85% for the substrate-binding peptide (Supplementary Table S1) at the 4 h and 24 h time points. These results confirmed that the novel MMP-14 peptides could be used for NIRF imaging of orthotopic models of human glioma. These findings support future studies that utilize the peptides for intraoperative resection of preclinical glioma tumors in vivo.

PET signals of the radiolabeled MMP-14 peptide probes localize in human glioma orthotopic xenografts in nude mice in vivo

The second goal of this work was to determine if the peptides could be used for in vivo PET imaging of orthotopic models of human glioma tumors in mice. A preliminary study was performed using the binding peptide labeled with ^{68}Ga (^{68}Ga-binding peptide) in mice with orthotopic PDX JX12 tumors. The radiolabeled peptide was obtained in 87–91% radiochemical conversion after heating with ^{68}Ga at 90 °C for 20 min; further heating did not improve the yield of the product ^{68}Ga-binding peptide (Supplementary Fig. S9). Tumor-bearing mice were dosed *i.v.* with 0.4–0.8 nmol ^{68}Ga-binding peptide from the diluted reaction solution (molar activity approximately 6.1 GBq/μmol at time of dosing). At 2 h after dosing, the tumors were visible during PET/CT imaging, while normal brain showed low uptake of activity (Fig. 5A). Ex vivo biodistribution analyses indicated significantly more uptake of radioactivity in brains of mice injected with ^{68}Ga-binding peptide (0.16 ± 0.02 %ID/g) compared to brains of mice injected with ^{68}Ga-binding peptide and 60-fold excess non-labeled-binding peptide as a blocking agent (0.07 ± 0.02 %ID/g, $p < 0.01$) (Fig. 5B), thus supporting the specific retention of the radiolabeled peptide in the PDX tumors. The amount of ^{68}Ga in resected brains correlated with qualitative tumor burden determined by H + E tissue analyses (Supplementary Fig. S10). PET images and ex vivo biodistribution analyses showed high accumulation of activity in the liver, spleen, and kidneys (Supplementary Figs. S11, S12), which was likely due to the relative hydrophobicity of the peptide at physiological pH.

A separate cohort of mice bearing orthotopic PDX JX12 tumors were used for PET imaging and biodistribution analyses with ^{64}Cu-labeled substrate-binding peptide (^{64}Cu-substrate-binding peptide). ^{64}Cu (12.7 h half-life) was used as the radionuclide with the substrate-binding peptide to allow PET imaging analyses at later time points (e.g., 4 h) that were used in the NIRF imaging studies. The relatively short half-

Table 1 Ex vivo NIRF signal intensities and TBRs from the substrate peptide or the substrate-binding peptide measured in 2 mm gross brain slices from mice bearing orthotopic PDX glioma tumors

	Mean NIRF signal in tumor	Mean NIRF signal in normal brain	*p* value (tumor vs. normal brain NIRF signal)	Mean ± SD TBR (range)
Substrate peptide, 4 h	0.012 ± 0.007	0.002 ± 0.001	< 0.001	7.6 ± 2.9 (2.7–10.9)
Substrate peptide, 24 h	0.011 ± 0.010	0.001 ± 0.00	0.074	8.7 ± 6.3 (2.9–17.1)
Substrate-binding peptide, 4 h	0.024 ± 0.011	0.002 ± 0.001	< 0.001	11.1 ± 4.5 (7.8–18.9)
Substrate-binding peptide, 24 h	0.021 ± 0.010	0.002 ± 0.001	< 0.001	13.3 ± 3.7 (6.0–17.6)

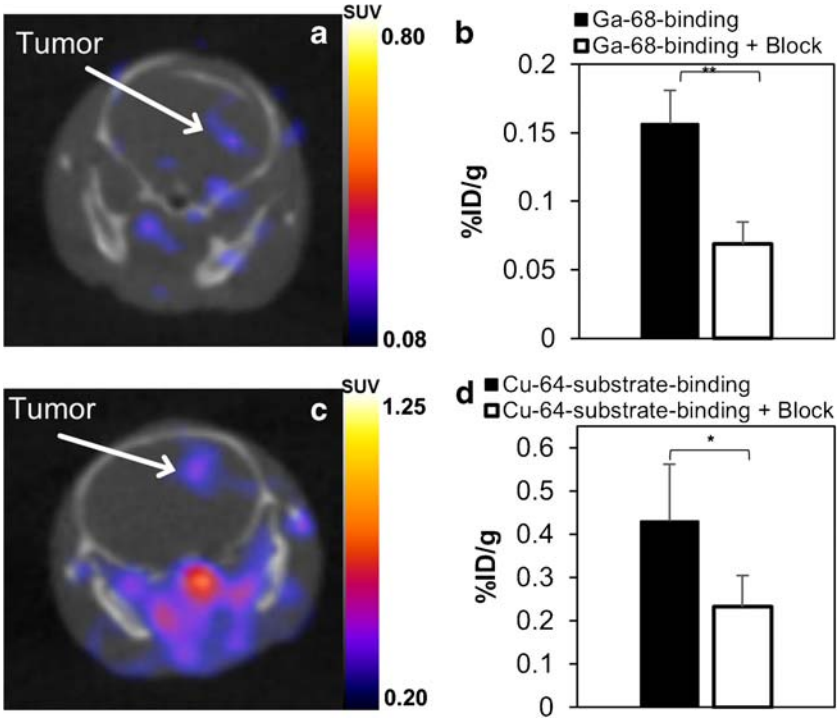

Fig. 5 PET imaging and biodistribution show specific localization of radiolabeled peptide probes in orthotopic PDX glioma tumors in vivo. **A**, representative transverse PET/CT image at 2 h after *i.v.* injection of ^{68}Ga-binding peptide in athymic nude mice bearing orthotopic PDX JX12 glioma tumors, showing localization of activity in the tumor. **B**, ex vivo biodistribution showing whole-brain activity at 3.5 h after *i.v.* injection of ^{68}Ga-binding peptide or of ^{68}Ga-binding peptide + block (non-labeled-binding peptide) in athymic nude mice bearing orthotopic PDX JX12 glioma tumors. Full biodistribution analyses are available in the Supplementary Data. **C**, representative transverse PET/CT image at 4 h after *i.v.* injection of ^{64}Cu-substrate-binding peptide in athymic nude mice bearing orthotopic PDX JX12 glioma tumors, showing localization of activity in the tumor. Activity in soft tissues of the neck (e.g., blood vessels, muscle, lymph nodes) was apparent at the scaling intensity shown in the PET image. **D**, ex vivo biodistribution showing whole-brain activity at 5.5 h after *i.v.* injection of ^{64}Cu-substrate-binding peptide or ^{64}Cu-substrate-binding peptide + block (non-labeled-binding peptide) in athymic nude mice bearing orthotopic PDX JX12 glioma tumors. Full biodistribution analyses are available in the Supplementary Data. *p < 0.05; **p < 0.01; SUV, standardized uptake value

life of ^{68}Ga (67.7 min) precludes PET imaging analyses beyond 3 h. The ^{64}Cu-substrate-binding peptide was generated quantitatively after labeling with ^{64}Cu at room temperature for 20 min (Supplementary Fig. S13). Tumor-bearing mice were dosed *i.v.* with 0.13 nmol ^{64}Cu-substrate-binding peptide from the diluted reaction solution (molar activity approximately 46.6 GBq/μmol at time of dosing). At 4 h after dosing, PET/CT imaging showed significant contrast in the tumor relative to normal brain (Fig. 5C), yielding a standardized uptake value ratio (SUVR: ratio of tumor SUV_{mean} to normal brain SUV_{mean}) of 3.9 ± 0.5. The SUVR was lower in a group of tumor-bearing mice (2.5 ± 1.3) that had been co-injected with 80-fold excess of the non-labeled binding peptide as a blocking agent, although the difference between the two groups of mice was not significant (p = 0.056). The activity present in whole resected brains from mice in the ^{64}Cu-substrate-binding peptide group (0.43 ± 0.13 %ID/g) was significantly higher than that in the blocked group (0.23 ± 0.07 %ID/g; p < 0.05) (Fig. 5D). This result suggests that the binding peptide is able to partially block binding of the substrate-binding peptide to PDX glioma tumors in vivo. Biodistribution analyses of resected tissues were consistent with the PET images, indicating predominantly hepatobiliary accumulation of activity (Supplementary Figs. S14, S15).

NIRF signals from the ^{64}Cu-substrate-binding peptide correlate with PET signals and co-localize with MMP-14 expression in human glioma orthotopic xenografts

The resected brains from mice injected with the ^{64}Cu-substrate-binding peptide in the above studies were sectioned and used for NIRF analyses. Gross imaging showed high contrast between the NIRF signal in PDX tumor regions compared to contralateral normal brain, yielding a TBR of 7.2 ± 1.3 (p < 0.001). The summed NIRF signal from tumor regions in these tissue sections correlated linearly (R^2 = 0.84, p < 0.0001) with the in vivo PET %ID/cm^3 signal present in the tumor-bearing brain regions (Fig. 6A). Microscopic imaging of hematoxylin and eosin (H + E) stained tissue sections confirmed that the NIRF signal co-localized in the PDX glioma tumors, which showed high expression of MMP-14 relative to normal brain (Fig. 6B-G). These results support the hypothesis that the NIRF signal from the cleavable peptide was

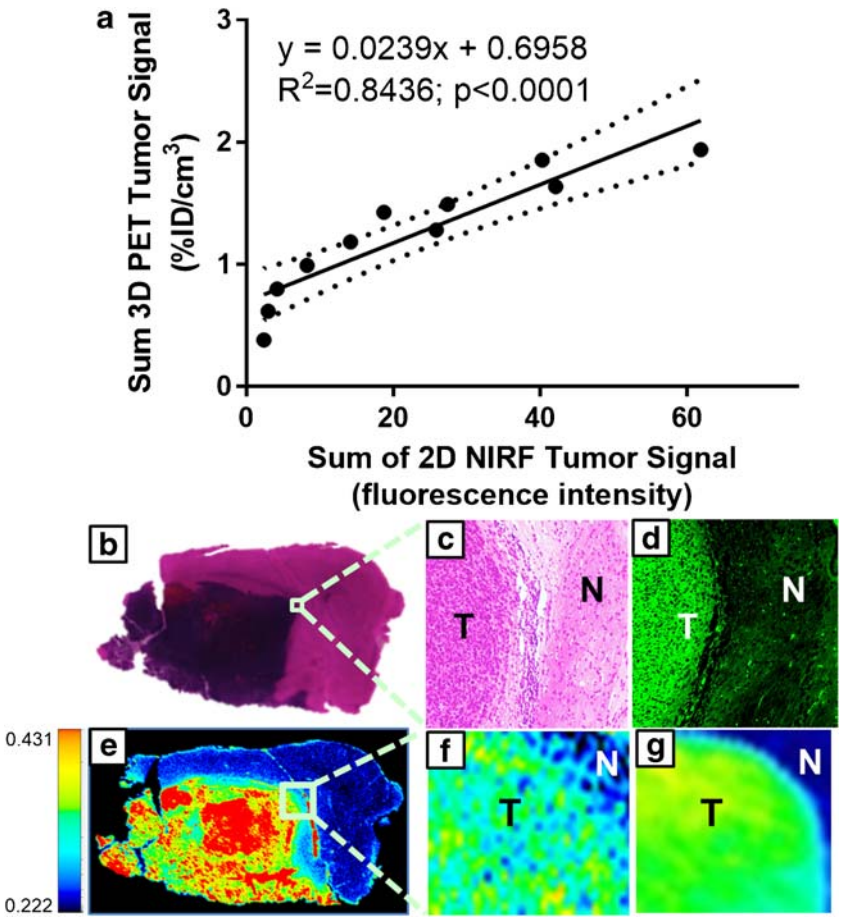

Fig. 6 NIRF signals from the radiolabeled substrate-binding peptide show high concordance with PET signal, orthotopic PDX glioma localization, and MMP-14 expression. **A**, linear correlation between in vivo PET (%ID/cm^3) and ex vivo NIRF signals from brains from mice bearing orthotopic PDX JX12 glioma tumors after *i.v.* injection of the ^{64}Cu-substrate-binding peptide (0.13 nmol); dotted lines show the 95% confidence interval of the correlation. Co-localization of H + E stained tumor (**B**, **C**), IRDye800 fluorescence on Odyssey scanner (**E**, **F**), and MMP-14 expression (**D**, **G**) in brain sections from mice bearing orthotopic PDX JX12 glioma tumors after *i.v.* injection of the ^{64}Cu-substrate-binding peptide. Separate sections were probed using an anti-MMP-14 antibody conjugated to either dye Alexa Fluor 488 for microscopy (**D**) or dye Cy5 for Odyssey scanner (**G**, 21 μm resolution). Microscopic images (**C**, **D**) are 100x. T, tumor; N, normal brain

specifically retained in the PDX glioma tumors due to the expression of MMP-14 in the tumors. The absolute NIRF signal from brains of mice injected with the ^{64}Cu-substrate-binding peptide was lower than that from mice in the study with the non-labeled substrate-binding peptide. This result was anticipated due to the different mass dose of the peptides used for the two studies. These studies support the feasibility of dual-modality PET and NIRF imaging with the radiolabeled peptide probe in a PDX glioma model. A goal of future work will be to determine the effect of the labeled and non-labeled peptide doses on the TBR for the PET and NIRF signals separately.

Discussion

The membrane-bound collagenase MMP-14 is a key enzyme in initiating and propagating the invasive phenotype associated with malignant glioma progression. MMP-14 processes other MMPs (e.g., proMMP-2) to their active state and cleaves adhesion proteins (e.g., CD44, integrins, etc.) in addition to extracellular collagen [5, 35, 48–50]. MMP-14 is also expressed on tumor-associated glial cells and macrophages, which can comprise up to 30% of the tumor bulk and have been implicated in promoting glioma cell invasion, expansion, and pathogenesis [51–53]. These combined factors formed the rationale for exploiting MMP-14 as a biomarker for imaging glioma. The peptide probes developed here may also be relevant for imaging other malignancies (e.g., breast cancer, melanoma) that overexpress MMP-14 [54–57].

Our imaging approach is unique in that the substrate-binding peptide probe exploits MMP-14 for both enzymatic NIRF signal activation and specific localization of the PET and activated NIRF signals. Most existing PET and activatable fluorescence dual-imaging probes utilize different molecular targets for fluorescence signal activation and binding to the tumor cells. The proposed approach exploits enzymatic amplification of the NIRF signal to enable high-contrast intraoperative imaging of tumors that express activated MMP-14. Exploiting a single biological target for both PET and NIRF reporters can potentially enable straightforward co-registration of the imaging signals for intraoperative fluorescence imaging with high spatial resolution [58–62], which is otherwise challenging when employing separate probes that have differing pharmacokinetic and localization patterns [63]. It remains to be determined if the substrate-binding peptide

first binds to MMP-14, thus preventing the substrate from being activated by the same MMP-14. Mechanistic studies to determine factors affecting peptide cleavage were beyond the scope of our proof-of-concept experiments discussed above. Future experiments will more fully characterize peptide cleavage kinetics and potential mechanisms of inhibition caused by the peptides on MMP-14 enzymatic activity. Since MMP-14 is located on the cell surface, the kinetics in vivo may not be the same as that determined in solution. As endogenous substrates of MMP-14 are large tertiary protein complexes (e.g., proMMP-2, TIMP-2, MMP-14), it is likely a second MMP-14 on the cell surface could process the substrate sequence in the peptide-MMP-14 complex to produce fluorescence activation. Other MMP-14 activatable fluorescence imaging probes do not include a targeted binding moiety, resulting in diffusion of the activated probe away from the target cells [64, 65]. Incorporating the binding peptide into the substrate-binding probe in our studies was anticipated to cause specific retention of the PET and activated NIRF signals on glioma cells, which would enhance signal contrast of the tumor cells relative to adjacent healthy brain. Glioma cell lines showed up to 2.8-fold higher cell-associated NIRF signal at 4 h after in vitro incubation with the substrate-binding peptide relative to the substrate peptide (Fig. 3D; $p < 0.001$), thus supporting the hypothesis that the binding peptide component enhances cell retention of the activated NIRF signal. In addition to ligand-protein interactions that result in signal retention on target cells, factors such as probe extravasation and clearance from tumors also influence TBRs in vivo. The above NIRF imaging results of PDX glioma tumors in resected brain tissues showed comparable TBRs for the substrate-binding peptide and substrate peptide at 4 and 24 h p.i. (Table 1). At the 24 h time point, however, the substrate peptide resulted in the lowest NIRF signal among the groups examined, which is consistent with lower specific retention of the cleaved substrate peptide due to its lack of a binding component.

The results from this work are in agreement with prior studies that have targeted MMP-14 as a biomarker for imaging glioma in preclinical animal models. Favorable PET SUVR (3.9) and NIRF TBR (13.3) signals from the substrate-binding peptide probe were observed in the present studies with an orthotopic PDX glioma model. Previous studies in glioma models or in humans with glioma have used dual-modality imaging probes targeted to other proteins that are overexpressed in glioma relative to normal brain tissue. For instance, preclinical studies using a dual PET/NIRF peptide that binds to EphB4 (Cy5.5-TNYL-RAWK-^{64}Cu-DOTA) in rodents with orthotopic human glioma xenografts indicated TBRs of 9 for PET imaging and 6–7 for fluorescence imaging [58]. A clinical trial using a dual PET/NIRF probe that targets the gastrin releasing peptide receptor (^{68}Ga-BBN-IRDye800) in glioma patients showed a PET SUVR of 13.4 and a NIRF TBR of 4.9 [66].

A primary goal of future studies is to assess if the activatable NIRF probes are suitable for optical-guided resection of glioma models in vivo. The TBRs and specific localization of the NIRF signals in the resected PDX glioma tumors from the present studies suggest the probes would be worthwhile candidates for NIRF-guided resection of glioma. Several preclinical studies in rodents with orthotopic brain tumors have shown TBRs ranging from 3 to 16 for various established (e.g., 5-ALA) or experimental fluorescence imaging agents [14, 32, 33, 63, 67]. Clinical therapy trials in patients with glioma are in progress to evaluate fluorescence-guided resection using imaging agents that include 5-ALA (NCT02119338, NCT01502280, NCT02632370, NCT00752323, NCT02191488, NCT01811121, NCT02379572), ABY-029 (NCT02901925), BLZ-100 (recently completed NCT02234297), panitumumab-IRDye800 (NCT03510208), ^{68}Ga-BBN-IRDye800 (NCT03407781), and fluorescein (NCT03291977, NCT02691923, [68]). These studies highlight the continued thrust to incorporate fluorescence-guided resection to improve outcomes for patients with glioma. Conceptually, it would be ideal to perform fluorescence-guided resection using an imaging probe with minimal photon attenuation in human tissue. While the spectral properties of NIRF fluorophores result in less photon attenuation relative to that of fluorescein or 5-ALA when imaging in human tissues, safe resection is the most critical factor during intraoperative brain tumor surgery. Maintaining the patient's quality of life governs the extent of surgical resection in critical brain tissues, even if those regions contain detectable tumor infiltration, regardless of the sensitivity or specificity of the imaging probe employed during fluorescence-guided resection.

In our pilot studies above, we observed relatively low PET signal in the orthotopic glioma tumors. This result may be due to moderate expression of MMP-14 relative to alternative biomarkers, restricted extravasation of the peptide into tumor parenchyma, moderate molar activity of the radiolabeled probes, sub-optimal mass doses of the probes, or other pharmacokinetic factors. Many small molecule PET probes show moderate accumulation and contrast (TBR 2-5 [69–73]) in glioma, partly due to rapid blood clearance kinetics and short PET radionuclide half-life, while macromolecule-based PET probes often show high accumulation due to significantly longer circulation times that allow the tracer to access tumors through disrupted blood-brain barrier (BBB) regions [13, 74]. The results from the in vivo blocking experiment support the conclusion that the radiolabeled peptide probes showed specific binding in the tumor. It was beyond the scope of these proof-of-concept studies to quantify nonspecific pooling of the probes in glioma tumors due to a disrupted BBB. In human patients, glioma often contains significant portions of tumor cell infiltration in non-contrast-enhancing regions of the brain. Therefore, it would be worthwhile in future experiments to investigate the

accumulation of the novel probes in spontaneous glioma models with tumor invasion in intact BBB regions. The PET studies presented here did not contain an additional method to confirm the size or location of the orthotopic PDX glioma tumors in vivo, although the observed probe uptake in brains during PET imaging was consistent with the histologically confirmed tumor regions identified by H + E and MMP-14 staining of resected brain tissue sections. Due to this limitation, it is possible that the tissue regions selected for in vivo PET measurements could have over- or underestimated the tumor volume and impacted the corresponding SUV results. Having an independent modality, such as MRI, to assess the in vivo tumor volume would increase the rigor of the PET analyses in the orthotopic xenografts. While MMP-14 is expressed in systemic tissues, the presence of tissue inhibitor of MMP-14 (TIMPs) may help minimize its activity in the circulation. Future studies to determine the specificity of glioma-mediated NIRF activation would benefit from comparing NIRF imaging with the probes above to control peptides that either lack the quencher molecule or that have a non-cleavable sequence separating the dye and quencher pair. It would also be useful to determine if different tumor infiltrating cells (e.g., tumor associated glial cells, macrophages) besides glioma cells contribute to the NIRF signal localization from the MMP-14 peptides within the tumor microenvironment [49, 51, 53].

Conclusion

The novel MMP-14 targeted and activatable peptide probes enabled dual PET and NIRF imaging of glioma in preclinical studies. High NIRF signal TBRs were observed in the resected brain sections of mice bearing PDX glioma tumors. Correlations between in vivo PET and ex vivo NIRF signals support the concept for dual-modality imaging of glioma with a single, MMP-14-targeted probe scaffold. The co-localization of NIRF signals and MMP-14 expression in the tumors observed by tissue staining confirmed the specific localization of the peptide probes. These results support future preclinical studies designed to test the efficacy of surgical resection of glioma with the MMP-14-targeted probes.

Materials and methods

General reagents

All general reagents were from commercial suppliers (Thermo Fisher, Waltham, MA, USA; Sigma, St. Louis, MO, USA) unless specified otherwise. Primary antibodies for MMP-14 (rabbit anti-MMP-14 monoclonal antibody (mAb), clone EP1264Y), MMP-2 (rabbit anti-MMP-2 polyclonal, ab37150), or isotype control (rabbit mAb, clone EPR25A) were from Abcam (Cambridge, MA). Fluorophore-conjugated goat anti-rabbit polyclonal secondary antibodies were from Invitrogen (Thermo Fisher). HRP-conjugated secondary antibodies were from Santa Cruz Biotechnology, Inc. (Dallas, TX). The recombinant catalytic enzyme domain of MMP-14 was from Invitrogen. ^{64}Cu was obtained in 0.1 M HCl from the *Mallinckrodt Institute of Radiology PET Nuclear Pharmacy and Cyclotron Facility of the Washington University Medical Center* or from the University of Alabama at Birmingham (UAB) Cyclotron Facility. ^{68}Ga, eluted in 0.1 M HCl from a ^{68}Ge/^{68}Ga generator, was obtained from the UAB Cyclotron Facility.

Gel zymography

Gel zymography was performed as previously described [75]. Briefly, adherent monolayers of glioma cells were rinsed with PBS and incubated in serum-free medium for 24 h. Supernatants were collected, analyzed for protein content, and loaded on zymogram gels (10% gelatin, Novex® Zymogram Gels, Thermo Fisher) according to the manufacturer's recommendations. Relative band intensities were quantified by ImageJ.

Immunofluorescence

Immunocytochemistry: Glioma cells were seeded at 100,000 cells/well in a 12-well plate and allowed to attach overnight. Adherent cells were rinsed in PBS, blocked with 1% BSA in PBS at room temperature for 45 min, incubated with the anti-MMP-14 mAb (Abcam ab51074) or isotype control mAb (Abcam ab172730) at 1 μg/mL in 0.1% BSA in PBS at room temperature for 30 min, rinsed 4 times with 0.1% BSA in PBS, incubated with Ready Probes Alexa Fluor 488-goat anti-rabbit antibody solution (R37116, Molecular Probes, Thermo Fisher) at room temperature for 30 min, rinsed 3 times with 0.1% BSA in PBS, and imaged on an inverted fluorescence microscope at 200× magnification. Mean fluorescence intensity per cell was quantified using ImageJ by randomly selecting 20–25 cells over four fields of view and measuring the mean fluorescence intensity.

Immunohistochemistry: A slide with a formalin-fixed paraffin-embedded (FFPE) human glioma tissue microarray (BS17016b, US Biomax, Inc, Derwood, MD) was deparaffinized and antigen was retrieved by heating for 10 min at 90 °C in citrate buffer pH 6 with 1 mM EDTA. Tissues were blocked in 5% BSA/TBST at room temperature, incubated overnight at 4 °C with anti-MMP-14 mAb at 1 μg/mL in 5% BSA/TBST, washed in TBST, incubated for 2 h at room temperature with Cy5-secondary antibody (A10523, Invitrogen, Thermo Fisher) at 1/1000 dilution in 5% BSA/TBST, rinsed in TBST, and mounted in DAPI-Fluoromount-

G (Southern Biotech, Birmingham, AL). Microarray tissues were imaged on an Odyssey scanner (LI-COR Biosciences, Lincoln, NE) using the 700 nm channel. Integrated instrument software (Image Studio, LI-COR) was used to determine mean fluorescence intensity as total counts/region of interest (ROI) pixel area. 5–6 μm FFPE sections from resected brains of mice bearing orthotopic PDX JX12 glioma tumors were processed using the same protocol, except Alexa Fluor 488-conjugated secondary antibody (A11008, Invitrogen, Thermo Fisher) was used (1/2000 dilution).

Production of peptide probes

The MMP-14 binding, substrate, and substrate-binding peptide probes were synthesized by solid phase techniques using protected amino acids and commercially available IRDye800CW-maleimide and quencher QC-1-NHS ester (LI-COR). The synthesized peptides were purified by semi-preparative reverse-phase high-performance liquid chromatography (RP-HPLC) and characterized by mass spectrometry. Additional details are provided in the Supplementary Materials.

In vitro NIRF activation and NIRF microscopy studies

The catalytic enzyme domain of MMP-14 (5 nM, 5 ng/well) or adherent glioma cells in 96-well plates (Corning Costar, Corning, NY) were incubated with 0.5 μM solutions of the substrate or substrate-binding peptide in 50 μL MMP-14 assay buffer (PBS with 1 mM $CaCl_2$, 0.5 mM $MgCl_2$, 10 μM $ZnCl_2$) at 37 °C, 5% CO_2 for 0–24 h. At designated time points, aliquots (1.5 μL) were removed and spotted on Whatman 1 chromatography paper. After drying at room temperature, NIRF signal of the blots was quantified by the Pearl imaging system (LI-COR). Alternatively, for quantification of the NIRF signal from the substrate peptide, the NIRF signal in the 96-well plates containing glioma cells was directly imaged on the Pearl system. As controls to determine relative fluorescence signal activation at each time point, solutions were used that contained the respective peptide solution without MMP-14 or glioma cells. Cell studies were performed in duplicate wells. For NIRF microscopy studies, glioma cell lines were seeded in 8-chamber slides (10^4 cells/chamber) 2 days before the experiment. On the day of the experiment, cells were rinsed with PBS and incubated at 37 °C, 5% CO_2 with the substrate or substrate-binding peptides (1 μM) in cell medium containing 1% FBS. Chambers were placed on ice at designated time points and medium was aspirated; chambers on ice were washed with ice-cold buffer (PBS, 1% BSA), fixed in formaldehyde at room temperature for 15 min, washed to remove formaldehyde, and mounted in Fluoromount-G prior to NIRF microscopy imaging at 100× magnification. Mean fluorescence intensity per cell was quantified using ImageJ by randomly selecting 30 cells over three fields of view and measuring the mean fluorescence intensity.

In vivo NIRF imaging studies

Mice bearing flank D54 or U87 xenografts (n = 5/group) were injected *i.v.* with 10 nmol substrate peptide or substrate-binding peptide (0.2 mL in PBS). Live, anesthetized mice were imaged on the Pearl system (LI-COR) from 0–24 h *p.i.* Mice bearing orthotopic PDX JX12 xenografts were injected *i.v.* with 0.8–0.9 nmol substrate peptide or substrate-binding peptide (0.2 mL in PBS) and euthanized at 1 h (n = 1 mouse/group), 4 h (n = 4–6 mice/group), or 24 h (n = 3–5 mice/group) *p.i.* Immediately after euthanizing anesthetized mice by cervical dislocation, the skin over the skull was removed, and NIRF signal was determined by the Pearl system. The whole brains were resected, fixed in 10% formalin overnight, and imaged by the Pearl system. Brains were then serially sectioned (1 or 2 mm coronal slices), and all slices were imaged by the Pearl system. Three or four slices containing tumor and adjacent normal brain without tumor were then dehydrated in 70% EtOH and processed for embedding in paraffin and further sectioning (5–6 μm). Unstained sections were imaged on an Odyssey system (LI-COR) or stained for H + E or immunofluorescence (anti-MMP-14 mAb or isotype control) as described above. NIRF signals from the Odyssey scans were defined as positive if they were above the following threshold: three-times the standard deviation above the pooled mean NIRF signal in negative regions (no tumor cells present by H + E histology). Odyssey images and H + E images at the same resolution were compared by ImageJ to define true positive, true negative, false positive, or false negative NIRF signal regions.

In vivo PET/CT imaging studies and biodistribution studies.

Mice bearing orthotopic PDX JX12 xenografts were used for PET/CT imaging and subsequent biodistribution studies with the radiolabeled peptide probes. Mice injected *i.v.* with ^{68}Ga-binding peptide (0.7–1.0 nmol, 2.2–4.5 MBq) with or without unlabeled binding peptide (50 nmol) (n = 3–4 mice/group) were imaged at 1 and 2 h time points *p.i.* Mice injected *i.v.* with ^{64}Cu-substrate-binding peptide (0.3 nmol, 6.3–6.5 MBq) with or without unlabeled binding peptide (22 nmol) (n = 5–6 mice/group) were imaged at 1 and 4 h time points *p.i.* PET (energy window 350–650 KeV; 15 min acquisition for ^{64}Cu studies, 20 min acquisition for ^{68}Ga studies) and CT (voltage 80 kVp, current 150 μA, 720 projections) images were acquired on a GNEXT PET/CT small animal scanner (Sofie Biosciences, Culver City, CA). The PET images were reconstructed using a 3D ordered-subset expectation maximization algorithm (24 subsets and 3 iterations), with random,

attenuation, and decay correction. The CT images were reconstructed using a modified Feldkamp algorithm. Reconstructed images were analyzed using VivoQuant software (version 3.5patch 2, Invicro, LLC, Boston, MA). Following the last imaging time point, anesthetized mice were euthanized by cervical dislocation. Whole brains and other selected tissues were resected, weighed, and counted on a gamma counter (1480 Wizard^2, Perkin Elmer, Shelton, CT). Percent uptake of the injected dose per gram (% ID/g) was calculated by comparing the tissue activity to solutions with known activity of the radionuclide of interest. Resected brains were then fixed in 10% formalin overnight, serially sectioned (1 or 2 mm coronal slices), and processed for further NIRF imaging, paraffin embedding, and tissue sectioning for H + E or immunofluorescence analyses as described above.

Statistical analyses

Data were analyzed using Microsoft Excel or GraphPad Prism (Version 6.1, GraphPad Software, La Jolla, CA, USA). Student's *t*-test was used when comparing two groups. When comparing multiple groups, one-way ANOVA tests, followed by Bonferroni corrections for multiple comparisons, were performed. All *p*-values correspond to two-tailed tests; significance was considered to be at $p < 0.05$.

Acknowledgments Yolanda Hartman, Catherine Langford, Savannah Ferch, Kurt Zinn, Andrew Prince, Marilyn Shackelford, Sally Jordan, Lauren Radford, Charlotte Jeffers, Jennifer Burkemper, Tolulope Aweda, Adriana Massicano, Kiranya Tipirneni, Jonathan McConathy, Suzanne Lapi, Jinda Fan, Jennifer Coleman, Norio Yasui, Dattatray Devalankar, Sharon Samuel, Sheila Bright, Erika McMillian, Himani Modi, Hailey Houson and Morgan Richardson are gratefully acknowledged for their contributions. LI-COR Biosciences is gratefully acknowledged for supplying IRDye800CW-maleimide and QC-1-NHS ester to prepare the peptide probes.

Funding information Funding was provided by the NIH/NINDS T32 UAB Training Program in Brain Tumor Biology (T32 NS048039), the UAB Brain Tumor Core Facility (USPHS NCI P20CA151129), the National Center for Advancing Translational Research of the National Institutes of Health (UL1TR001417), the Department of Defense Congressionally Directed Medical Research Program (CA170769), and the Comprehensive Cancer Center at UAB (NIH P30CA013148).

Compliance with ethical standards

Conflict of interest The authors declare that they have no conflicts of interest.

Ethical approval All applicable international, national, and institutional guidelines for the care and use of animals were followed. Animal studies were approved by the University of Alabama at Birmingham Institutional Animal Care and Use Committee (20366) and performed in compliance with guidelines from the Public Health Service Policy and Animal Welfare Act of the United States. This article does not contain any studies with human participants performed by any of the authors.

Abbreviations *5-ALA*, 5-aminolevulinic acid; *ANOVA*, analysis of variance; BBB, blood-brain barrier; BSA, bovine serum albumin; *CT*, computed tomography; *FDA*, Food and Drug Administration; *FFPE*, formalin-fixed paraffin-embedded; *GBM*, glioblastoma multiforme; *%ID/g*, percent injected dose per g; *i.v.*, intravenous; *mAb*, monoclonal antibody; *MMP*, matrix metalloproteinase; *NIR*, near-infrared; *NIRF*, near-infrared fluorescence; *NOTA*, 1,4,7-triazacyclononane-1,4,7-triacetic acid; *PDX*, patient-derived xenograft; *PET*, positron emission tomography; *p.i.*, post-injection; *PpIX*, protoporphyrin IX; *RIPA*, radioimmunoprecipitation assay; *s.c.*, subcutaneous; *SUVR*, standardized uptake value ratio; *TBR*, tumor-to-background ratio; *UAB*, University of Alabama at Birmingham

References

1. Delgado-López PD, Corrales-García EM. Survival in glioblastoma: a review on the impact of treatment modalities. *Clin Transl Oncol*. **2016**;*18*(11):1062–71.
2. Orringer D, Lau D, Khatri S, Grettel J. Zamora-Berridi; Kathy Zhang; Chris Wu; Neeraj Chaudhary; Oren Sagher, Extent of resection in patients with glioblastoma: limiting factors, perception of resectability, and effect on survival. *J Neurosurg*. **2012**;*117*(5):851–9.
3. Li YM, Suki D, Hess K, Sawaya R. The influence of maximum safe resection of glioblastoma on survival in 1229 patients: can we do better than gross-total resection? *J Neurosurg*. **2016**;*124*(4):977–88.
4. Shiomi T, Okada Y. MT1-MMP and MMP-7 in invasion and metastasis of human cancers. *Cancer Metastasis Rev*. **2003**;*22*(2):145–52.
5. Kessenbrock K, Plaks V, Werb Z. Matrix metalloproteinases: regulators of the tumor microenvironment. *Cell*. **2010**;*141*(1):52–67.
6. Beliën ATJ, Paganetti PA, Schwab ME. Membrane-type 1 matrix metalloprotease (MT1-MMP) enables invasive migration of glioma cells in central nervous system white matter. *J Cell Biol*. **1999**;*144*(2):373–84.
7. Fillmore HL, VanMeter TE, Broaddus WC. Membrane-type matrix metalloproteinases (MT-MMP)s: expression and function during glioma invasion. *J Neuro-Oncol*. **2001**;*53*(2):187–202.
8. Nakada M, Nakamura H, Ikeda E, Fujimoto N, Yamashita J, Sato H, et al. Expression and tissue localization of membrane-type 1, 2, and 3 matrix metalloproteinases in human astrocytic tumors. *Am J Pathol*. **1999**;*154*(2):417–28.
9. Wang L, Yuan J, Tu Y, Mao X, He S, Fu G, et al. Co-expression of MMP-14 and MMP-19 predicts poor survival in human glioma. *Clin Transl Oncol*. **2013**;*15*(2):139–45.
10. Forsyth PA, Wong H, Laing TD, Rewcastle NB, Morris DG, Muzik H, et al. Gelatinase-A (MMP-2), gelatinase-B (MMP-9) and membrane type matrix metalloproteinase-1 (MT1-MMP) are involved in different aspects of the pathophysiology of malignant gliomas. *Br J Cancer*. **1999**;*79*(11-12):1828–35.
11. Yamamoto M, Mohanam S, Sawaya R, Fuller GN, Seiki M, Sato H, et al. Differential expression of membrane-type matrix metalloproteinase and its correlation with gelatinase A activation in human malignant brain tumors *in vivo* and *in vitro*. *Cancer Res*. **1996**;*56*(2):384–92.
12. Gu G, Gao X, Hu Q, Kang T, Liu Z, Jiang M, et al. The influence of the penetrating peptide iRGD on the effect of paclitaxel-loaded MT1-AF7p-conjugated nanoparticles on glioma cells. *Biomaterials*. **2013**;*34*(21):5138–48.
13. de Lucas AG, Schuhmacher AJ, Oteo M, Romero E, Cámara JA, de Martino A, et al. Targeting MT1-MMP as an ImmunoPET-based strategy for imaging gliomas. *PLoS One*. **2016**;*11*(7):e0158634.
14. Shimizu Y, Temma T, Hara I, Makino A, Kondo N, Ozeki E, et al. In vivo imaging of membrane type-1 matrix metalloproteinase with

a novel activatable near-infrared fluorescence probe. *Cancer Sci*. **2014**;*105*(8):1056–62.
15. Albert NL, Weller M, Suchorska B, Galldiks N, Soffietti R, Kim MM, et al. Response assessment in neuro-oncology working group and European Association for Neuro-Oncology recommendations for the clinical use of PET imaging in gliomas. *Neuro-Oncology*. **2016**;*18*(9):1199–208.
16. Kondo A, Ishii H, Aoki S, Suzuki M, Nagasawa H, Kubota K, et al. Phase IIa clinical study of [^{18}F]fluciclovine: efficacy and safety of a new PET tracer for brain tumors. *Ann Nucl Med*. **2016**;*30*(9):608–18.
17. Filss CP, Galldiks N, Stoffels G, Sabel M, Wittsack HJ, Turowski B, et al. Comparison of ^{18}F-FET PET and perfusion-weighted MR imaging: a PET/MR imaging hybrid study in patients with brain tumors. *J Nucl Med*. **2014**;*55*(4):540–5.
18. Piroth MD, Holy R, Pinkawa M, Stoffels G, Kaiser HJ, Galldiks N, et al. Prognostic impact of postoperative, pre-irradiation ^{18}F-fluoroethyl-l-tyrosine uptake in glioblastoma patients treated with radiochemotherapy. *Radiother Oncol*. **2011**;*99*(2):218–24.
19. la Fougère C, Suchorska B, Bartenstein P, Kreth F-W, Tonn J-C. Molecular imaging of gliomas with PET: opportunities and limitations. *Neuro-Oncology*. **2011**;*13*(8):806–19.
20. Tsuyuguchi N, Takami T, Sunada I, Iwai Y, Yamanaka K, Tanaka K, et al. Methionine positron emission tomography for differentiation of recurrent brain tumor and radiation necrosis after stereotactic radiosurgery —In malignant glioma—. *Ann Nucl Med*. **2004**;*18*(4):291–6.
21. Lodge MA, Holdhoff M, Leal JP, Bag AK, Nabors LB, Mintz A, et al. Repeatability of ^{18}F-FLT PET in a multicenter study of patients with high-grade glioma. *J Nucl Med*. **2017**;*58*(3):393–8.
22. Pafundi DH, Laack NN, Youland RS, Parney IF, Lowe VJ, Giannini C, et al. Biopsy validation of ^{18}F-DOPA PET and biodistribution in gliomas for neurosurgical planning and radiotherapy target delineation: results of a prospective pilot study. *Neuro-Oncology*. **2013**;*15*(8):1058–67.
23. Bangiyev L, Rossi Espagnet MC, Young R, Shepherd T, Knopp E, Friedman K, et al. Adult brain tumor imaging: state of the art. *Semin Roentgenol*. **2014**;*49*(1):39–52.
24. Díez Valle R, Tejada Solis S, Idoate Gastearena MA. García de Eulate, R.; Domínguez Echávarri, P.; Aristu Mendiroz, J., Surgery guided by 5-aminolevulinic fluorescence in glioblastoma: volumetric analysis of extent of resection in single-center experience. *J. Neurooncol.* **2011**;*102*(1):105–13.
25. Schucht P, Beck J, Abu-Isa J, Andereggen L, Murek M, Seidel K, et al. Gross total resection rates in contemporary glioblastoma surgery: results of an institutional protocol combining 5-aminolevulinic acid intraoperative fluorescence imaging and brain mapping. *Neurosurgery*. **2012**;*71*(5):927–36.
26. Stummer W, Stocker S, Wagner S, Stepp H, Fritsch C, Goetz C, et al. Intraoperative detection of malignant gliomas by 5-aminolevulinic acid-induced porphyrin fluorescence. *Neurosurgery*. **1998**;*42*(3):518–25 discussion 525-6.
27. Tonn JC, Stummer W. Fluorescence-guided resection of malignant gliomas using 5-aminolevulinic acid: practical use, risks, and pitfalls. *Clin Neurosurg*. **2008**;*55*:20–6.
28. FDA Briefing Information for the May 10, 2017 Meeting of the Medical Imaging Drugs Advisory Committee: NDA 208630 5-ALA (5-aminolevulinic acid HCl). https://www.fda.gov/AdvisoryCommittees/CommitteesMeetingMaterials/Drugs/MedicalImagingDrugsAdvisoryCommittee/ucm557135.htm ().
29. Liu JT, Meza D, Sanai N. Trends in fluorescence image-guided surgery for gliomas. *Neurosurgery*. **2014**;*75*(1):61–71.
30. Belykh E; Martirosyan NL; Yagmurlu K; Miller EJ; Eschbacher JM; Izadyyazdanabadi M; Bardonova LA; Byvaltsev VA; Nakaji P; Preul MC. Intraoperative fluorescence imaging for personalized brain tumor resection: current state and future directions. *Front Surg*. **2016;** *3*:(55).
31. Zhang RR, Schroeder AB, Grudzinski JJ, Rosenthal EL, Warram JM, Pinchuk AN, et al. Beyond the margins: real-time detection of cancer using targeted fluorophores. *Nat Rev Clin Oncol*. **2017**;*14*(6):347–64.
32. Huang R, Vider J, Kovar JL, Olive DM, Mellinghoff IK, Mayer-Kuckuk P, et al. Integrin $\alpha_v\beta_3$-Targeted IRDye 800CW Near-infrared imaging of glioblastoma. *Clin Cancer Res*. **2012**;*18*(20):5731–40.
33. de Souza ALR, Marra K, Gunn J, Samkoe KS, Hoopes PJ, Feldwisch J, et al. Fluorescent affibody molecule administered in vivo at a microdose level labels EGFR expressing glioma tumor regions. *Mol Imaging Biol*. **2017**;*19*(1):41–8.
34. Miller SE, Tummers WS, Teraphongphom N, van den Berg NS, Hasan A, Ertsey RD, et al. First-in-human intraoperative near-infrared fluorescence imaging of glioblastoma using cetuximab-IRDye800. *J Neuro-Oncol*. **2018**;*139*(1):135–43.
35. Cepeda MA, Evered CL, Pelling JJH, Damjanovski S. Inhibition of MT1-MMP proteolytic function and ERK1/2 signalling influences cell migration and invasion through changes in MMP-2 and MMP-9 levels. *J Cell Commun Signal*. **2017**;*11*(2):167–79.
36. Atkinson JM, Falconer RA, Edwards DR, Pennington CJ, Siller CS, Shnyder SD, et al. Development of a novel tumor-targeted vascular disrupting agent activated by membrane-type matrix metalloproteinases. *Cancer Res*. **2010**;*70*(17):6902–12.
37. Ansari C, Tikhomirov GA, Hong SH, Falconer RA, Loadman PM, Gill JH, et al. Development of novel tumor-targeted theranostic nanoparticles activated by membrane-type matrix metalloproteinases for combined cancer magnetic resonance imaging and therapy. *Small*. **2014**;*10*(3):566–75.
38. Mohanty S, Chen Z, Li K, Morais GR, Klockow J, Yerneni K, et al. A novel theranostic strategy for MMP-14-expressing glioblastomas impacts survival. *Mol Cancer Ther*. **2017**;*16*(9):1909–21.
39. Peng X, Chen H, Draney DR, Volcheck W, Schutz-Geschwender A, Olive DM. A nonfluorescent, broad-range quencher dye for Förster resonance energy transfer assays. *Anal Biochem*. **2009**;*388*(2):220–8.
40. Simard B, Tomanek B, van Veggel FC, Abulrob A. Optimal dye-quencher pairs for the design of an "activatable" nanoprobe for optical imaging. *Photochem Photobiol Sci*. **2013**;*12*(10):1824–9.
41. Zhu L, Wang H, Wang L, Wang Y, Jiang K, Li C, et al. High-affinity peptide against MT1-MMP for in vivo tumor imaging. *J Control Release*. **2011**;*150*(3):248–55.
42. Kondo N, Temma T, Shimizu Y, Ono M, Saji H. Radioiodinated peptidic imaging probes for *in vivo* detection of membrane type-1 matrix metalloproteinase in cancers. *Biol Pharm Bull*. **2015**;*38*(9):1375–82.
43. Min K, Ji B, Zhao M, Ji T, Chen B, Fang X, et al. Development of a radiolabeled peptide-based probe targeting MT1-MMP for breast cancer detection. *PLoS One*. **2015**;*10*(10):e0139471.
44. Gill JH, Loadman PM, Shnyder SD, Cooper P, Atkinson JM, Ribeiro Morais G, et al. Tumor-targeted prodrug ICT2588 demonstrates therapeutic activity against solid tumors and reduced potential for cardiovascular toxicity. *Mol Pharm*. **2014**;*11*(4):1294–300.
45. Snyman C, Niesler CU. MMP-14 in skeletal muscle repair. *J Muscle Res Cell Motil*. **2015**;*36*(3):215–25.
46. Giannini C, Sarkaria JN, Saito A, Uhm JH, Galanis E, Carlson BL, et al. Patient tumor EGFR and PDGFRA gene amplifications retained in an invasive intracranial xenograft model of glioblastoma multiforme. *Neuro-Oncology*. **2005**;*7*(2):164–76.
47. Oliva CR, Nozell SE, Diers A, McClugage SG 3rd, Sarkaria JN, Markert JM, et al. Acquisition of temozolomide chemoresistance in gliomas leads to remodeling of mitochondrial electron transport chain. *J Biol Chem*. **2010**;*285*(51):39759–67.

48. Bourboulia D, Stetler-Stevenson WG. Matrix metalloproteinases (MMPs) and tissue inhibitors of metalloproteinases (TIMPs): positive and negative regulators in tumor cell adhesion. *Semin Cancer Biol*. **2010**;*20*(3):161–8.
49. Ulasov I, Yi R, Guo D, Sarvaiya P, Cobbs C. The emerging role of MMP14 in brain tumorigenesis and future therapeutics. *Biochimi Biophysic Acta*. **2014**;*1846*(1):113–20.
50. Devy L, Huang L, Naa L, Yanamandra N, Pieters H, Frans N, et al. Selective inhibition of matrix metalloproteinase-14 blocks tumor growth, invasion, and angiogenesis. *Cancer Res*. **2009**;*69*(4):1517–26.
51. Markovic DS, Vinnakota K, Chirasani S, Synowitz M, Raguet H, Stock K, et al. Gliomas induce and exploit microglial MT1-MMP expression for tumor expansion. *Proc Natl Acad Sci U S A*. **2009**;*106*(30):12530–5.
52. Markovic DS, Vinnakota K, van Rooijen N, Kiwit J, Synowitz M, Glass R, et al. Minocycline reduces glioma expansion and invasion by attenuating microglial MT1-MMP expression. *Brain Behav Immun*. **2011**;*25*(4):624–8.
53. Charles NA, Holland EC, Gilbertson R, Glass R, Kettenmann H. The brain tumor microenvironment. *Glia*. **2011**;*59*(8):1169–80.
54. McGowan PM, Duffy MJ. Matrix metalloproteinase expression and outcome in patients with breast cancer: analysis of a published database. *Ann Oncol*. **2008**;*19*(9):1566–72.
55. Määttä M, Soini Y, Liakka A, Autio-Harmainen H. Differential expression of matrix metalloproteinase (MMP)-2, MMP-9, and membrane type 1-MMP in hepatocellular and pancreatic adenocarcinoma: implications for tumor progression and clinical prognosis. *Clin Cancer Res*. **2000**;*6*(7):2726–34.
56. Hofmann UB, Westphal JR, Zendman AJ, Becker JC, Ruiter DJ, van Muijen GN. Expression and activation of matrix metalloproteinase-2 (MMP-2) and its co-localization with membrane-type 1 matrix metalloproteinase (MT1-MMP) correlate with melanoma progression. *J Pathol*. **2000**;*191*(3):245–56.
57. Imanishi Y, Fujii M, Tokumaru Y, Tomita T, Kanke M, Kanzaki J, et al. Clinical significance of expression of membrane type 1 matrix metalloproteinase and matrix metalloproteinase-2 in human head and neck squamous cell carcinoma. *Hum Pathol*. **2000**;*31*(8):895–904.
58. Huang M, Xiong C, Lu W, Zhang R, Zhou M, Huang Q, et al. Dual-modality micro-positron emission tomography/computed tomography and near-infrared fluorescence imaging of EphB4 in orthotopic glioblastoma xenograft models. *Mol Imaging Biol*. **2014**;*16*(1):74–84.
59. Li C, Wang W, Wu Q, Ke S, Houston J, Sevick-Muraca E, et al. Dual optical and nuclear imaging in human melanoma xenografts using a single targeted imaging probe. *Nucl Med Biol*. **2006**;*33*(3):349–58.
60. Sampath L, Kwon S, Ke S, Wang W, Schiff R, Mawad ME, et al. Dual-labeled trastuzumab-based imaging agent for the detection of human epidermal growth factor receptor 2 overexpression in breast cancer. *J Nucl Med*. **2007**;*48*(9):1501–10.
61. Kimura RH, Miao Z, Cheng Z, Gambhir SS, Cochran JR. A dual-labeled knottin peptide for PET and near-infrared fluorescence imaging of integrin expression in living subjects. *Bioconjug Chem*. **2010**;*21*(3):436–44.
62. Olson ES, Jiang T, Aguilera TA, Nguyen QT, Ellies LG, Scadeng M, et al. Activatable cell penetrating peptides linked to nanoparticles as dual probes for in vivo fluorescence and MR imaging of proteases. *Proc Natl Acad Sci U S A*. **2010**;*107*(9):4311–6.
63. Elliott JT, Marra K, Evans LT, Davis SC, Samkoe KS, Feldwisch J, et al. Simultaneous *in vivo* fluorescent markers for perfusion, protoporphyrin metabolism, and EGFR expression for optically guided identification of orthotopic glioma. *Clin Cancer Res*. **2017**;*23*(9):2203–12.
64. Zhu L, Zhang F, Ma Y, Liu G, Kim K, Fang X, et al. In vivo optical imaging of membrane-type matrix metalloproteinase (MT-MMP) activity. *Mol Pharm*. **2011**;*8*(6):2331–8.
65. Gao S, Zhang L, Wang G, Yang K, Chen M, Tian R, et al. Hybrid graphene/Au activatable theranostic agent for multimodalities imaging guided enhanced photothermal therapy. *Biomaterials*. **2016**;*79*:36–45.
66. Li D, Zhang J, Chi C, Xiao X, Wang J, Lang L, et al. First-in-human study of PET and optical dual-modality image-guided surgery in glioblastoma using ^{68}Ga-IRDye800CW-BBN. *Theranostics*. **2018**;*8*(9):2508–20.
67. Ribeiro de Souza AL, Marra K, Gunn J, Samkoe KS, Hull S, Paulsen KD, et al. Optimizing glioma detection using an EGFR-targeted fluorescent affibody. *Photochem Photobiol*. **2018**;*94*(6):1167–71.
68. Acerbi F, Broggi M, Schebesch K-M, Höhne J, Cavallo C, De Laurentis C, et al. Fluorescein-guided surgery for resection of high-grade gliomas: a multicentric prospective phase II study (FLUOGLIO). *Clin Cancer Res*. **2018**;*24*(1):52–61.
69. Suchorska B, Jansen NL, Linn J, Kretzschmar H, Janssen H, Eigenbrod S, et al. Biological tumor volume in ^{18}FET-PET before radiochemotherapy correlates with survival in GBM. *Neurology*. **2015**;*84*(7):710–9.
70. Verger A, Filss CP, Lohmann P, Stoffels G, Sabel M, Wittsack HJ, et al. Comparison of ^{18}F-FET PET and perfusion-weighted MRI for glioma grading: a hybrid PET/MR study. *Eur J Nucl Med Mol Imaging*. **2017**;*44*(13):2257–65.
71. Dunet V, Pomoni A, Hottinger A, Nicod-Lalonde M, Prior JO. Performance of ^{18}F-FET versus ^{18}F-FDG-PET for the diagnosis and grading of brain tumors: systematic review and meta-analysis. *Neuro-Oncology*. **2016**;*18*(3):426–34.
72. Yoo MY, Paeng JC, Cheon GJ, Lee DS, Chung JK, Kim EE, et al. Prognostic value of metabolic tumor volume on ^{11}C-methionine PET in predicting progression-free survival in high-grade glioma. *Nucl Med Mol Imaging*. **2015**;*49*(4):291–7.
73. Doi Y, Kanagawa M, Maya Y, Tanaka A, Oka S, Nakata N, et al. Evaluation of trans-1-amino-3-^{18}F-fluorocyclobutanecarboxylic acid accumulation in low-grade glioma in chemically induced rat models: PET and autoradiography compared with morphological images and histopathological findings. *Nucl Med Biol*. **2015**;*42*(8):664–72.
74. Yang Y, Hernandez R, Rao J, Yin L, Qu Y, Wu J, et al. Targeting CD146 with a ^{64}Cu-labeled antibody enables in vivo immunoPET imaging of high-grade gliomas. *Proc Natl Acad Sci U S A*. **2015**;*112*(47):E6525–34.
75. Merrell MA, Ilvesaro JM, Lehtonen N, Sorsa T, Gehrs B, Rosenthal E, et al. Toll-like receptor 9 agonists promote cellular invasion by increasing matrix metalloproteinase activity. *Mol Cancer Res*. **2006**;*4*(7):437–47.